CONSOLIDATED UNDRAINED SHEARING RESPONSE OF HYDROPHOBIC
SANDS

A THESIS SUBMITTED TO
THE GRADUATE SCHOOL OF NATURAL AND APPLIED SCIENCES
OF
MIDDLE EAST TECHNICAL UNIVERSITY

BY

HÜSEYİN MELİH TATAR

IN PARTIAL FULFILLMENT OF THE REQUIREMENTS
FOR
THE DEGREE OF MASTER OF SCIENCE
IN
CIVIL ENGINEERING

MARCH 2018

Approval of the thesis:

CONSOLIDATED UNDRAINED SHEARING RESPONSE OF HYDROPHOBIC SANDS

submitted by **HÜSEYİN MELİH TATAR** in partial fulfillment of the requirements for the degree of **Master of Science in Civil Engineering Department, Middle East Technical University** by,

Prof. Dr. Gülbin DURAL ÜNVER   _____
Dean, Graduate School of **Natural and Applied Sciences**

Prof. Dr. İsmail Özgür YAMAN   _____
Head of Department, **Civil Engineering**

Prof. Dr. Kemal Önder ÇETİN   _____
Supervisor, **Civil Engineering Dept., METU**

Examining Committee Members:

Prof. Dr. Erdal ÇOKÇA   _____
Civil Engineering Dept., METU

Prof. Dr. Kemal Önder ÇETİN   _____
Civil Engineering Dept., METU

Assoc. Prof. Dr. Zeynep GÜLERCE   _____
Civil Engineering Dept., METU

Asst. Prof. Dr. Nejan Huvaj SARIHAN   _____
Civil Engineering Dept., METU

Assoc. Prof. Dr. Berna UNUTMAZ   _____
Civil Engineering Dept., Hacettepe University

Date: 02.03.2018

I hereby declare that all information in this document has been obtained and presented in accordance with academic rules and ethical conduct. I also declare that, as required by these rules and conduct, I have fully cited and referenced all material and results that are not original to this work.

Name, Last Name: Hüseyin Melih TATAR

Signature:

ABSTRACT

CONSOLIDATED UNDRAINED SHEARING RESPONSE OF HYDROPHOBIC SANDS

TATAR, Hüseyin Melih

M.Sc., Department of Civil Engineering

Supervisor: Prof. Dr. Kemal Önder ÇETİN

March 2018, 109 pages

The geotechnical properties of hydrophilic (wettable) sands have been widely discussed in the literature. However, sands may gain hydrophobic (non-wettable) property after certain processes. Available studies regarding the response of hydrophobic sands mostly focused on its environmental and hydrological aspects. The current state of knowledge about the geotechnical aspects of hydrophobic sands is quite limited and consists of the results of a limited number of direct shear tests. To close this gap, a comparative laboratory testing program consisting of 18 static strain-controlled consolidated undrained triaxial shear tests was designed. Tests were performed on fully saturated hydrophilic and hydrophobic reconstituted Kızılırmak sand samples of different relative densities with pore water measurements. Additionally, soil classification tests including specific gravity (G_S), minimum void ratio (e_{min}) and maximum void ratio (e_{max}) determination and sieve analysis were performed. Hydrophobic samples were prepared by using varying amounts of WD-40 lubricant. The effects of hydrophobic agent was examined by comparing the stress – excess pore water pressure - strain responses of hydrophobic sand samples with

those of conventional (hydrophilic) sand samples. Test results revealed that addition of hydrophobic agent increases the dilatancy of sands at low confining stresses (~100kPa) by decreasing the excess pore water pressure generation. At higher confining stresses (~400kPa) this effect is less pronounced. Moreover, the addition of hydrophobic agent does not significantly and systematically change the shear strength of sand samples independent of their initial relative density and confining stress levels.

Keywords: Sand, CU triaxial shear test, hydrophobicity, WD-40 lubricant, dilatancy, density, effective stress, critical state, stress − strain response.

ÖZ

ISLANMAYAN (HİDROFOBİK) KUMLARIN KONSOLİDASYONLU DRENAJSIZ KAYMA DAVRANIŞI

TATAR, Hüseyin Melih

Yüksek Lisans, İnşaat Mühendisliği Bölümü

Tez Yöneticisi: Prof. Dr. Kemal Önder ÇETİN

Mart 2018, 109 sayfa

Hidrofilik (ıslanabilir) kumların geoteknik özellikleri literatürde detaylıca çalışılmıştır. Ancak, kumlar belli süreçlerin sonunda hidrofobik (ıslanmaz) özellik kazanabilmektedir. Şu ana kadar hidrofobik kumların davranışı üzerinde yapılan çalışmalar, çevresel ve hidrolojik etkiler üzerine odaklanmıştır. Hidrofobik kumların geoteknik özellikleri hakkında mevcut bilgi birikimi oldukça sınırlıdır ve sadece birkaç direkt kesme deneyi sonucu içermektedir. Bu boşluğu kapatmak amacıyla 18 adet statik, gerinme kontrollü, konsolidasyonlu – drenajsız üç eksenli kayma deneyi içeren karşılaştırmalı bir deney programı hazırlanmıştır. Deneyler farklı bağıl yoğunluklarda hazırlanan doygun, hidrofilik ve hidrofobik Kızılırmak kumu numuneleri üzerinde boşluk suyu basıncı da ölçülerek gerçekleştirilmiştir. Ek olarak, özgül ağırlık (G_S), minimum boşluk oranı (e_{min}), maksimum boşluk oranı (e_{max}) ve dane boyu dağılımı gibi zemin sınıflandırma deneyleri gerçekleştirilmiştir. Hidrofobik numuneler, değişik oranlarda WD-40 yağı kullanılarak hazırlanmıştır. Hidrofobik katkı maddesinin etkileri, hidrofobik ve hidrofilik kum numunelerinin gerilme – aşırı boşluk suyu basıncı – gerinme davranışları karşılaştırılarak incelenmiştir. Deney sonuçlarından görüldüğü üzere hidrofobik katkı maddesinin

eklenmesi, düşük gerilme değerlerinde (~100kPa) aşırı boşluk suyu basıncı üretimini azaltarak numunenin genleşmesini arttırmıştır. Yüksek gerilme değerlerinde (~400kPa) bu etki azalmaktadır. Ayrıca, numunelerin ilk durumdaki bağıl sıkılık ve yanal gerilmelerinden bağımsız olarak hidrofobik katkı maddesi eklenmesinin kumların mukavemeti üzerinde ciddi ve sistematik bir etkisinin olmadığı belirlenmiştir.

Anahtar kelimeler: Kum, CU üç eksenli kayma deneyi, hidrofobiklik, WD-40 yağı, genleşme, sıkılık, efektif gerilme, kritik durum, gerilme – gerinme davranışı

To my family, for their unconditional support…

ACKNOWLEDGEMENTS

TABLE OF CONTENTS

LIST OF TABLES

TABLES

LIST OF FIGURES

FIGURES

LIST OF SYMBOLS

e	Void ratio
e_{max}	Maximum void ratio
e_{min}	Minimum void ratio
D_R	Relative density
G_S	Specific gravity
σ_1	Major principal stress
σ_3	Minor principal stress
γ	Dry density, shear strain
γ_{max}	Maximum dry density
γ_{min}	Minimum dry density
RDD	Relative dry density
ϕ_{CV}	Constant volume friction angle
ϕ_{DC}	Density component of frciton angle
τ	Shear strength
c'	Effective cohesion
σ_v'	Effective vertical stress
ϕ_μ'	Interparticle friction angle
ϕ_g'	Geometrical interference component
λ	Slope of critical state line
Γ	Critical void ratio at athmospheric pressure
V_λ	Specific volume at athmospheric pressure
ψ	Dilation angle
W	Work done by shear stress
α	Inclination of particle interlocking
β	Inclination of direction particle movement
ε_1	Strain in major principal stress direction
ε_3	Strain in minor principal stress direction
I_R	Relative dilatancy index

Q	Material constant
N$_{60}$	Corrected SPT-N blow count for enegry efficiency of 60%
(N$_1$)$_{60}$	Corrected SPT-N blow count for enegry efficiency of 60% and effective stress of 1 atm
p$_a$	Athmospheric pressure (=1 atm)
G$_0$, G$_{max}$	Maximum shear modulus
E$_0$, E$_{max}$	Maximum elastic modulus
V$_{voids}$	Volume of voids
V$_{solids}$	Volume of solids
B	Pore water pressure ratio coefficient
ΔU	Change in pore water pressure
Δσ$_3$	Change in cell pressure
H$_c$	Corrected height of specimen after consolidation
H$_0$	Initial height of specimen before consolidation
ε$_a$	Axial strain
ΔV	Volume change of specimen during consolidation
V$_0$	Initial volume of specimen before consolidation
ε$_v$	Volumetric strain
A$_c$	Corrected area of specimen after consolidation
A$_0$	Initial area of specimen before consolidation
A$_c^*$	Corrected area of specimen at any stage of shearing
ΔH	Axial deformation of specimen during shearing
σ$_d$	Deviatoric stress acting on specimen
F	Deviatoric force acting on specimen
A$_p$	Piston area
u	Pore water pressure
σ$_{cell}$	Cell pressure
p'	Mean effective stress
q	Half of deviatoric stress
σ$_c$	Condolidation pressure
τ$_{ff}$	Shear stress on the failure plane at the time of failure
σ$_{ff}$	Effective stress on the failure plane at the time of failure
u$_{ff}$	Excess pore water pressure on the failure plane at the time of failure

CHAPTER 1

INTRODUCTION

1.1. Research Statement

In the literature, there exists a vast amount of data about the engineering properties and responses of hydrophilic (wettable) sands. Their shear strength parameters, drained and undrained shearing responses at relatively dense or loose states can be conveniently assessed. However, sands may not be always found as wettable in the nature and may exhibit hydrophobic (non-wettable) properties. Within current geotechnical knowledge, unlike hydrophilic sands, there exist a limited number of sources that discuss the effects of hydrophobic agents on the geotechnical properties of sands.

Figure 1.1. Hydrophobic Sand

The general focus of available research studies regarding hydrophobic soils is in their environmental and hydrological aspects. Sands may gain hydrophobic property in various ways. A series of tests performed by Maimon et al. (2017) revealed that greywater usage for irrigation purposes to reduce fresh water consumption may cause soil hydrophobicity. In these tests, possible conditions to affect the hydrophobicity properties like persistence, rate etc. were investigated.

It is also known that providing particular chemical additives can make sands exhibit hydrophobic properties. The hydrophobic sand obtained by additives – sometimes called as smart sand or magic sand – can be used for wide range of purposes. For example, Sun et al. (2014) procured hydrophobic sand by coating pure sand with

polystyrene/pyrene/TBAHP compound and researched its usage in the detection of buried explosives.

As part of limited research studies about the geotechnical properties of hydrophobic sand, Kim et al. (2013) and Byun and Lee (2012) performed direct shear tests on chemically treated sands. The results of direct shear tests performed on hydrophobic sands were compared with those of hydrophilic sands.

The aim of this research study is to investigate the effects of addition of hydrophobic agent on the stress − strain − excess pore water pressure responses sand samples prepared at different relative density and stress states. For this purpose, a laboratory testing program is designed. The laboratory testing program consists of 4 different types of soil classification tests including minimum and maximum void ratio determination, sieve analysis and specific gravity determination as well as 18 static strain controlled consolidated undrained triaxial shear tests with pore water measurements. The results are compared with limited available literature and the responses of hydrophilic and hydrophobic sands are comparatively discussed.

1.2. Research Objectives

The research objectives of this thesis study are defined as to investigate;

1.   The effects of hydrophobicity on the strength of relatively
   i.   "dense" sands and,
   ii.   "loose" sands.
2.   The effect of hydrophobicity on the straining response of relatively
   i.   "dense" sands and,
   ii.   "loose" sands.

1.3. Scope of the Thesis

As summarized in the research statement and research objectives, the main focus of this thesis study is to contribute to the current state of knowledge about consolidated undrained shearing response of hydrophobic sands. Following this brief introduction, in Chapter 2, literature review focusing on straining response of hydrophilic sands under monotonic loading is presented. Data compiled from limited sources about hydrophobic sands is also discussed in this chapter.

In Chapter 3, laboratory testing program, test set up, sample preparation techniques and testing procedure are explained in detail. Individual test results are also presented in this chapter.

Chapter 4 is dedicated to the interpretation of test results. The results of hydrophilic sand samples were compared with those of hydrophilic sand samples and the effects of hydrophobicity on overall behavior is discussed.

In Chapter 5, a summary of the study and main outcomes are presented and suggestions for future studies are listed.

CHAPTER 2

LITERATURE REVIEW

2.1. Introduction

In this chapter, straining response of hydrophilic sands under monotonic loading with factors affecting this response and shear strength and stiffness estimations of sands are described in detail. The main factors affecting the straining response are initial density and stress states of the sample. Their effects are discussed by applying to the valuable experimental studies performed by several researchers. Moreover, critical state concept that takes an important place in the geotechnical engineering field to understand the response of sands is introduced. After that, behaviour, strength and stiffness estimations of sands with respect to initial density and confining stress states are examined. Finally, limited available data about straining response of hydrophobic sandy soils is summarized.

2.2. Straining Response of Hydrophilic Sandy Soils Under Monotonic Loading

Due to their porous structure, sandy soils allow pore water movement between grains. Therefore, in case of a loading, excess pore water dissipates quickly and all the load is transferred to soil particles. During this process, the rate of loading must permit excess pore water to dissipate within an acceptable time interval (i.e. construction of a foundation). This process is simulated in the laboratory by loading the specimen in drained conditions. In some cases (i.e. earthquake), rate of loading is so rapid that excess pore pressure cannot dissipate quickly and soil behaves in an

undrained manner. This situation can also be modelled in laboratory by preventing water entrance and exit from inside of specimen during monotonic loading.

As a result of the experimental studies in the literature, it can be inferred that under drained loading conditions dense sands absorb water and dilate after a slight dissipation of water and contraction of sample at the initial stage of the test, whereas loose sands dissipate water and contract. In a triaxial compression test on a fully saturated sand, sand grains and pore water are considered to be incompressible and thus, in case of undrained loading, volume of the specimen remains constant while elastic and plastic deformations are taking place. Conformably with drained loading, under undrained loading conditions dense sands generate negative excess pore water pressure and tend to dilate by absorbing water and loose sands generate positive excess pore water pressure and tend to decrease its' volume by dissipating water.

The overall response of sands under drained and undrained loading are given in Figure 2.1. As revealed by this figure, depending on the relative density state and confining stresses, samples exhibit a fundamentally different shear stress-strain as well as volumetric straining or excess pore pressure responses. A proper assessment of shearing responses requires the estimation of initial stress and density states as well as shear strength and stiffness parameters.
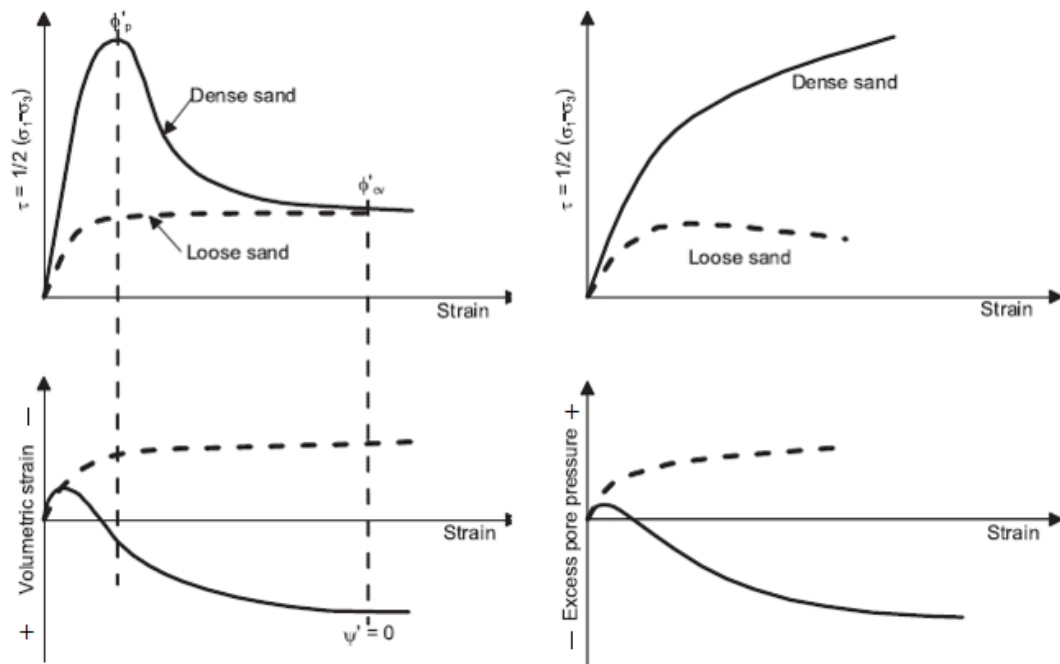
Figure 2.1. Typical Straining Responses of Hydrophilic Sands Under Drained and Undrained Loading (From Andersen and Schjetne, 2013)

2.2.1. Factors Affecting the Shearing Response

2.2.1.1. Relative Density

The density and stress states of soils govern their strength and stiffness characteristics. In most of the correlations proposed to estimate the strength, as given in Equation 2.1, the level of compaction of sandy soils is specified by relative density (D_R):

$$D_R(\%) = \frac{e_{max}-e}{e_{max}-e_{min}} \cdot 100 \qquad (2.1)$$

where e_{max} denotes the maximum void ratio, e_{min} denotes the minimum void ratio and e denotes the sample's void ratio. In theory, e_{max} and e_{min} correspond to void ratio values of the loosest and densest states, respectively, that can be found in nature. However, in practice, e_{max} and e_{min} corresponds to void ratio values of the

7

loosest and densest states estimated by following certain procedures (Bardet, 1997). The main reason of this choice is that D_R concept provides a practical basis to prepare samples in the laboratory with the limitation of eliminating the depositional and geological factors.

The relationship between density and response of sands is investigated by many researchers. It is known that denser sands have higher peak strengths as revealed by a general trend observed during the tests.

The experimental study carried out by Cornforth (1973) was one of the most detailed studies on the density – response relationship of sands, although it has one fundamental deficiency like correlating the response only to density by ignoring the effects of initial stress. Within the scope of the study, drained plain strain and triaxial compression tests were performed on sand samples prepared at different initial densities. The main findings of the tests are illustrated in Figure 2.2:
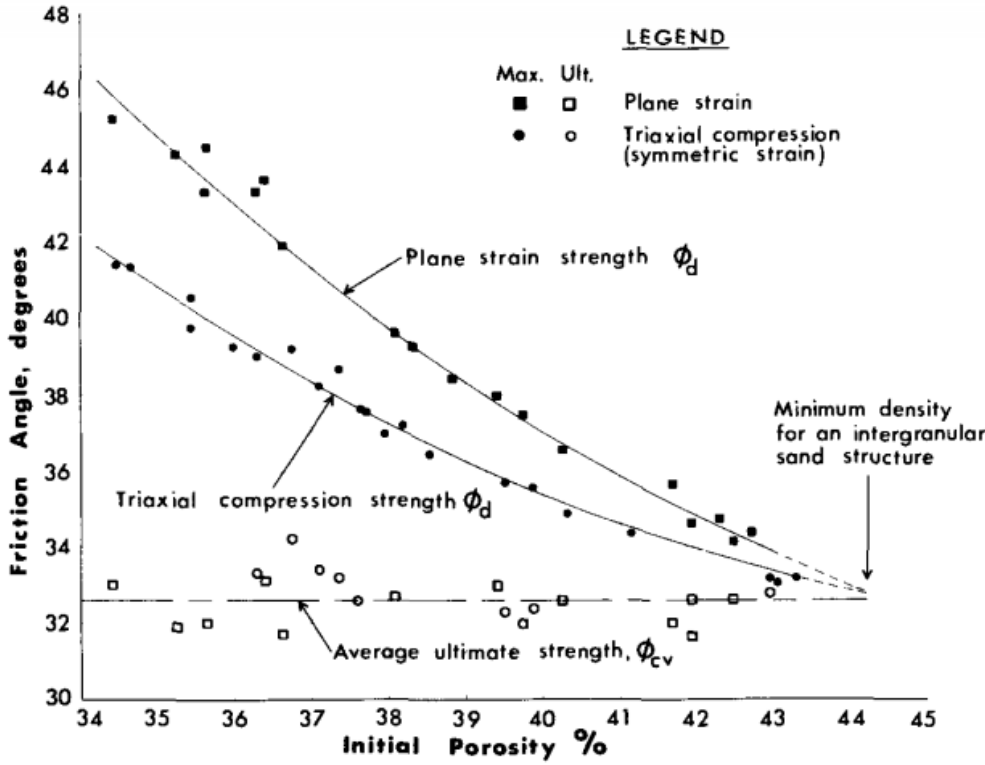
Figure 2.2. Strength – Density Relationships (Cornforth, 1973)

8

Cornforth (1973) concluded that the shear strength of the specimen in plain strain is higher than the shear strength in triaxial (symmetric strain) for a constant density state. The differences in these strength levels increases as the density of the sample increases.

In the tests performed on Brestad sand, it was observed that after the failure shearing continues with no volume change of the specimen under large strains, all samples reached to the similar ultimate strength value. Moreover, as shown in Figure 2.3., maximum dilation rates are obtained near failure strains and approaches zero as the ultimate strength mobilizes. This observation was independent of the initial density state and test type, whether plain strain or triaxial test was used.
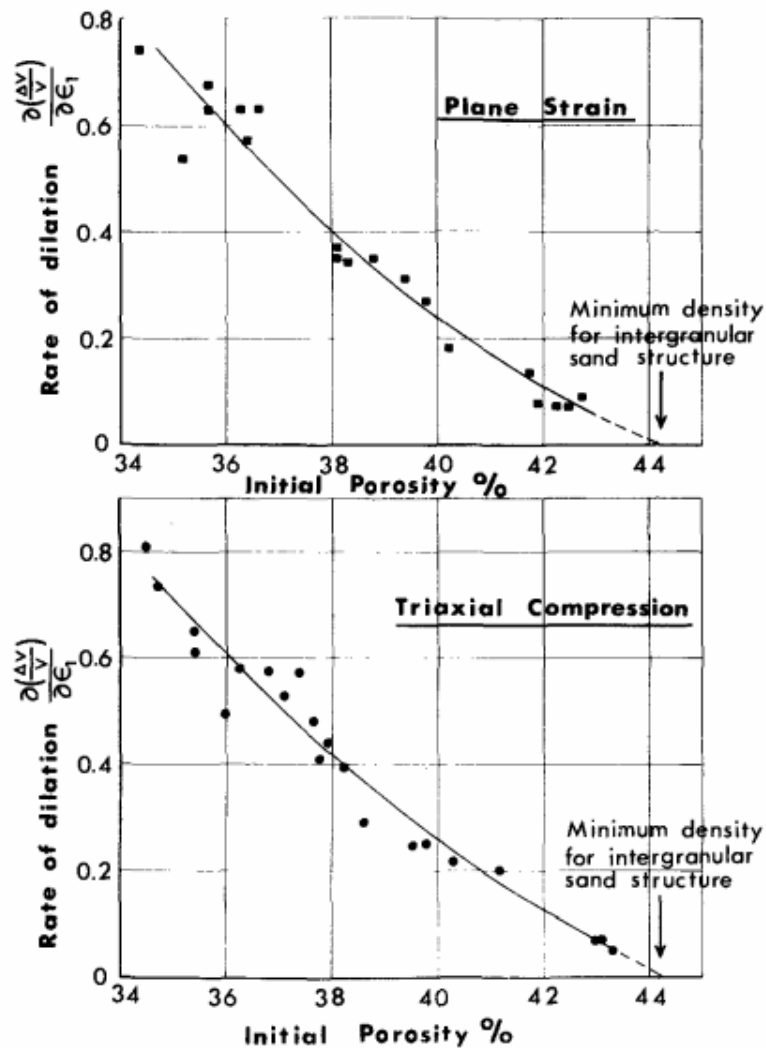
Figure 2.3. Dilation Rates (Cornforth, 1973)

Cornforth (1973) relates the density to the shear strength by proposing a dimensionless factor named as density factor which is the ratio of peak strength to ultimate strength obtained at any density state:

$$density\ factor = \frac{(\frac{\sigma_1-\sigma_3}{\sigma_3})_{maximum}}{(\frac{\sigma_1-\sigma_3}{\sigma_3})_{ultimate}} \qquad (2.2)$$

where σ_1 denotes the major principal stress and σ_3 denotes the minor principal stress. In his work, Cornforth preferred to specify the level of compaction of sandy soils as a function of dry densities. The relative dry density is defined as:

$$RDD(\%) = \frac{\gamma-\gamma_{min}}{\gamma_{max}-\gamma_{min}}.100 \qquad (2.3)$$

where γ is the dry unit weight of sand in its natural state and the relationship between relative density (D_R) and relative dry density (RDD) is:

$$RDD = D_R \cdot (\frac{\gamma}{\gamma_{max}}) \qquad (2.4)$$
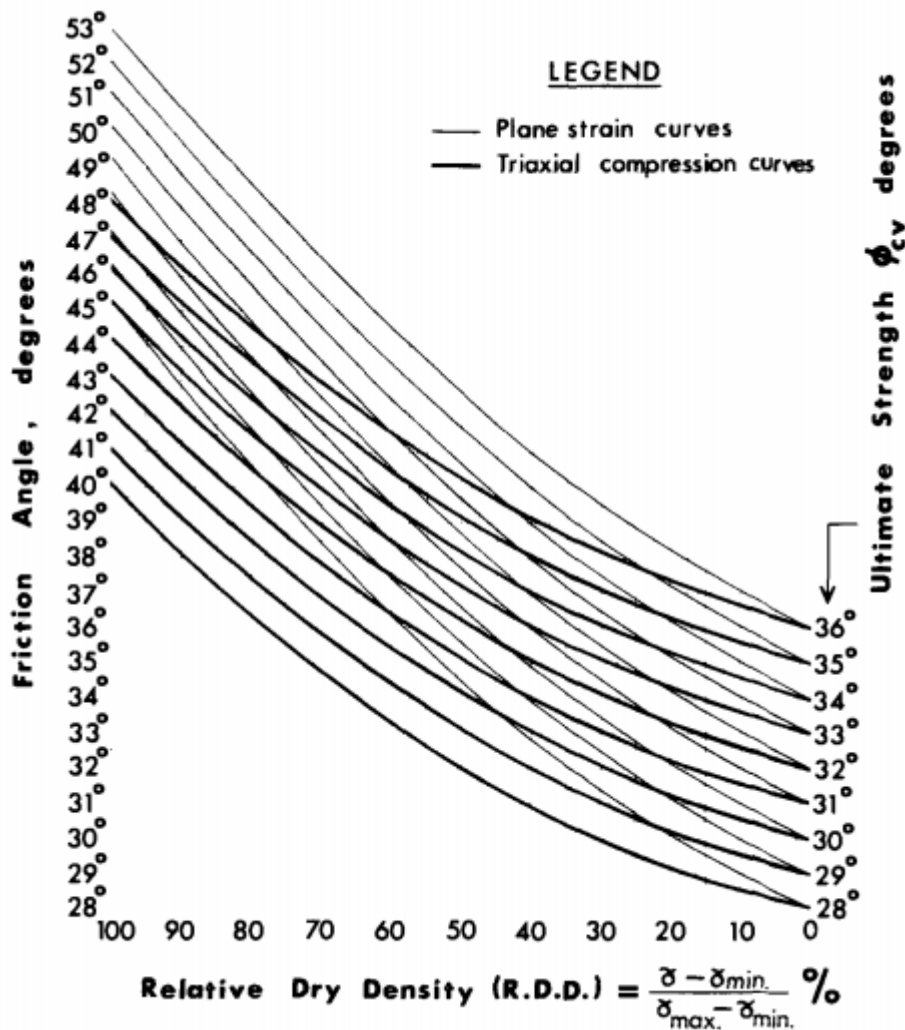
Figure 2.4. Strength – Density Relationship of Soils Having Different Ultimate Strength based on Density Factor = 2.0 (Cornforth, 1973)

Test results of sands having different ultimate strengths (constant volume friction angles varying between 28° and 36°) show that the increase in the strength of a soil added to ultimate strength for a certain density factor is independent of the constant volume strength of the soil and as the density factor increases, the increase in the strength also increases.

As an interpretation of the results, Cornforth described the peak (failure) strength of a sand at which the dilation rate is maximum as the sum of ultimate strength and density component:

$$\phi = \phi_{CV} + \phi_{DC} \tag{2.5}$$

where ϕ_{CV} denotes the ultimate (constant volume) strength and ϕ_{DC} denotes the density component of the strength. In Equation 2.5, ϕ_{CV} is material dependent variable and independent of initial density and ϕ_{DC} is initial density dependent variable and independent of the ultimate (constant volume) strength of the sand, in other words independent of the sand minerology. The contribution of the density to the ultimate strength of the sand is summarized in Figure 2.5. Assuming that ultimate (constant volume) strength is the same with the angle of repose for any type of sand, peak (failure) strength can be predicted just by determining the density state of the sand.
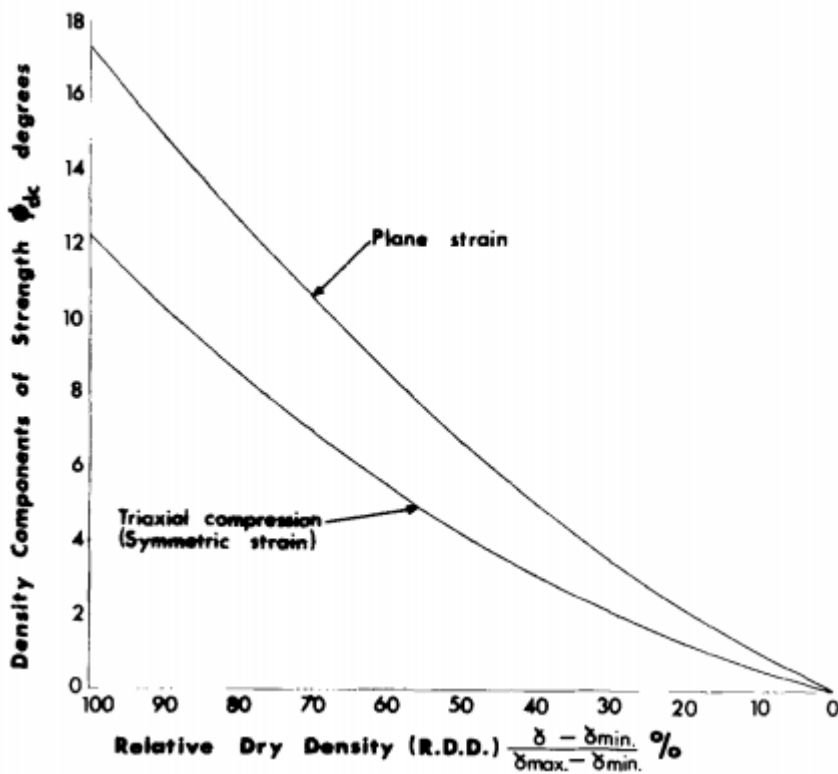
Figure 2.5. Density Component of the Peak Strength (Cornforth, 1973)

The fundamental deficiency of the Cornforth's study was the fact that the increase in strength of the sand above constant volume strength was related to not only the density state but also effective stress state that the sand experiences. In other words, a

true identification of the factors affecting the increase in shear strength requires the assessment of not only density component but also effective stress. As Houlsby (1991) stated, the straining response of sands can be modeled correctly just by clearly understanding the relationship between peak and constant volume strength, density and effective stress states of sands.

2.2.1.2. Effective Stress

Stress level is another determinant on the straining response of sands. In Mohr-Coulomb failure criterion, shear strength of soil is defined as the sum of cohesive and frictional forces between soil particles (Equation 2.6).

$$\tau = c' + \sigma_V'.tan(\phi') \tag{2.6}$$

Considering that sands are cohesionless soils, shear strength is directly proportional to the effective stress acting on the sample as well as instantaneous friction angle. Effective stress increase on a sand sample results in an increase in total frictional forces between sand particles and correspondingly increase in shear strength. However, as the stress level that sand experience increases, amount of increase of shear strength of dense sands decreases. This phenomena addresses the "non-linear shear strength envelope" and the reason of the "instantaneous" term is illustrated in Figure 2.6.
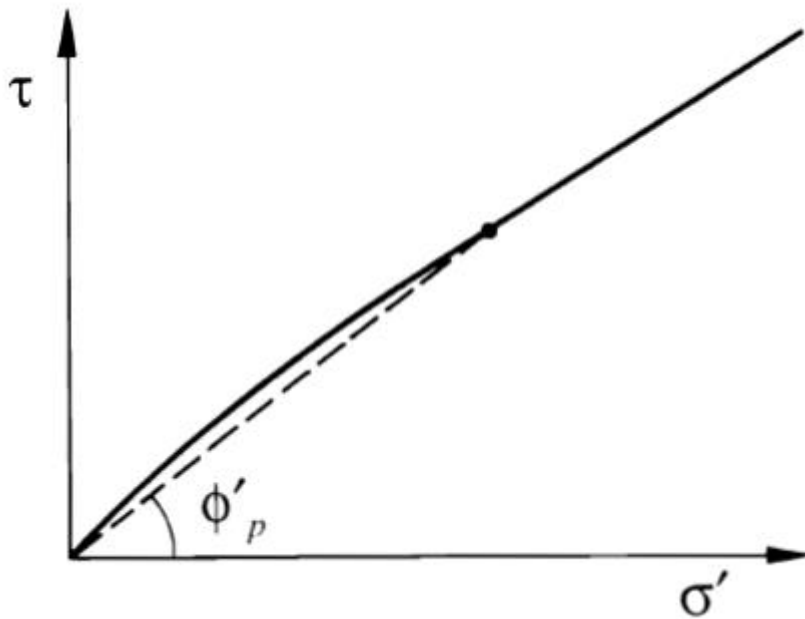
Figure 2.6. Non-linear Shear Strength Envelope of Cohesionless Soils

Non-linear shear strength envelope makes stress state an important issue while predicting the straining response and friction angle of sands. In order not to make unrealistic inferences like apparent cohesion due to nonlinearity, the mechanism behind this phenomenon must be well understood.

Rowe (1962) performed a number of triaxial tests on sands to investigate dilatancy response. During these test, it was observed that for a certain density state, shear strength envelope of loose sands follows a straight line independent of the stress state whereas the slope of the envelope of dense sands decreases as the effective stress on sand particles increases (Figure 2.7). This discrepancy was explained as the result of particle crushing at contact surfaces under high stress levels causing a decrease in interlocking of particles. Decrease of interlocking lowers dilatancy of sand and peak (failure) friction angle, that is slope of shear strength envelope, decreases progressively until ultimate (constant volume) strength mobilizes.
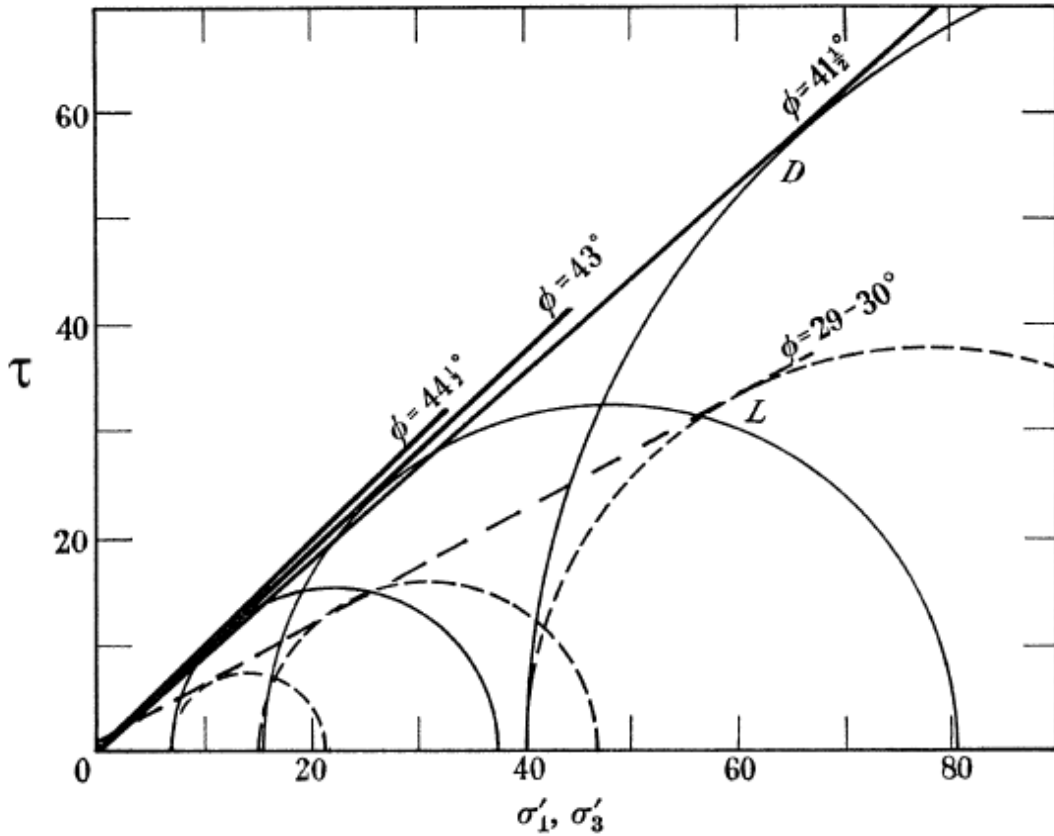
**Figure 2.7. Mohr circles of dense and loose sands at low and high stress states
(Rowe, 1962)**

Terzaghi et al (1996) explained the mechanism behind the non-linear shear strength envelope in a more detailed manner. The friction angle was defined as the sum of two components:

$$\phi' = \phi'_\mu + \phi'_g \tag{2.7}$$

where ϕ'_μ denotes the interparticle friction angle related to sand minerology like Rowe (1962) called and ϕ'_g denotes the geometrical interference component. In dense sands, particles subjected to shearing try to push the adjacent particles into directions different than shear forces act in order to slide in the direction of the shear. This geometrical interference causes material to dilate and mobilizes additional strength to ϕ'_μ component. As the confining stress increases, particle movement becomes more difficult and particle crushing occurs. As a result of this behavior,

general particle movement tends to be aligned with the direction of the shear forces and contribution of the geometrical interference decreases. This decrease causes the nonlinearity of the strength envelope.

Similar results are also observed in the triaxial tests performed by Barden et al. (1969). Three samples of River Welland Sand prepared at the same density and sheared under different confining pressure levels. At higher confining pressures, lower peak strength values obtained as a result of the decrease in the dilation rate of sand as the confining stress increases. From Figure 2.8, it can be clearly seen that the sand at a certain density can exhibit both "dense" material and "loose" material responses given in Figure 2.1, just based on confining pressure. An initially dense material may behave like a loose material under high stresses.
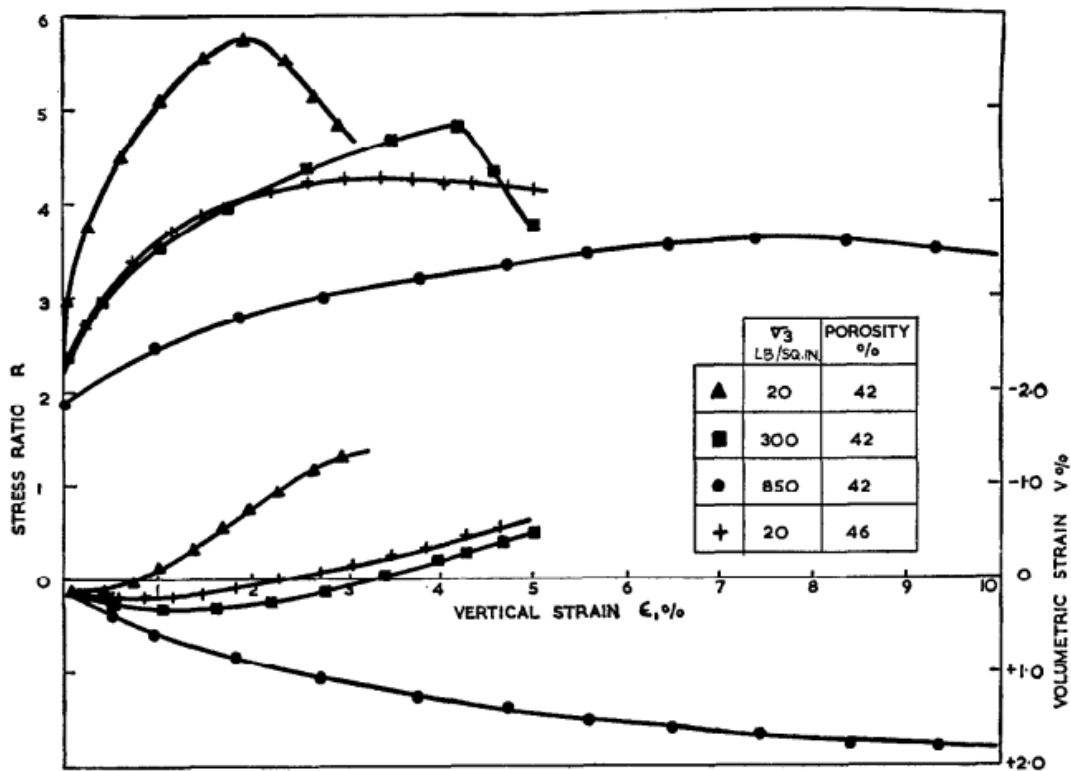
Figure 2.8. Stress – strain behavior of River Welland sand under different confining pressure levels (Barden et al, 1969)

2.2.1.3. Critical State Concept

Sands subjected to shearing begin to contract or dilate based on their initial density and stress state. As the shearing continues, sand samples turn into a form in which no volume or effective stress change occur under shearing. The void ratio obtained at this phase is named as critical void ratio. The form of a sand at critical void ratio is identified as frictional fluid by Schofield and Wroth (1968).

The critical void ratio is defined for drained and undrained loading conditions by Roscoe (1958) as below:

- In drained tests, dense sands suck water into pores and loose sands remove water from pores under shearing and correspondingly, void ratio changes. The critical void ratio is defined as the void ratio at the ultimate state in which shearing proceeds with no void ratio changes.
- In undrained tests, assuming sand grains and pore water are incompressible, volume of specimen remains constant. Dense sands tend to suck water into pores and generate negative pore pressure and loose sands tend to remove water from pores and generates positive pore pressure under shearing. The critical void ratio is defined as the void ratio at the ultimate state in which shearing proceeds with no effective stress change. This means that the initial void ratio which remains constant during shearing, becomes the critical void ratio.

The critical void ratio is independent of the initial void ratio, in other words independent of initial density, for a certain effective stress level. A number of simple shear tests was performed on steel balls by Wroth and Bassett (1958). When the results were plotted on a single graph, it was observed that all samples converge to similar void ratio at large strains, regardless of the initial void ratio of the specimen and after this stage, shearing continues with no void ratio change (Figure 2.9).
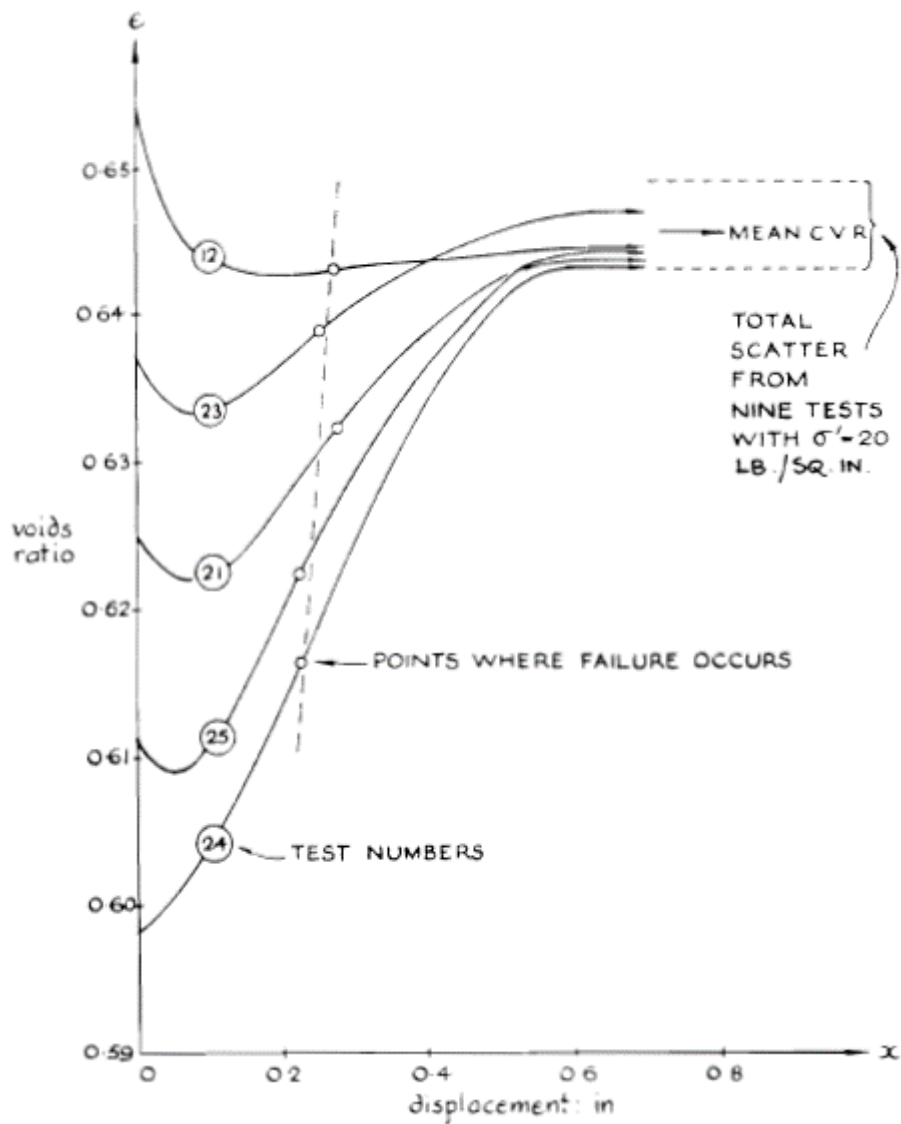
Figure 2.9. Void ratio – shear displacement relationship for simple shear test performed on steel balls (from Wroth, 1958)

Stroud (1971) also performed simple shear tests on sand at varying effective stresses. When the critical void ratio values for each effective stress level were plotted on a single graph, a straight line was obtained. This line, later named as critical state line, demonstrates that critical void ratio decreases as the effective stress level increases (Figure 2.10).
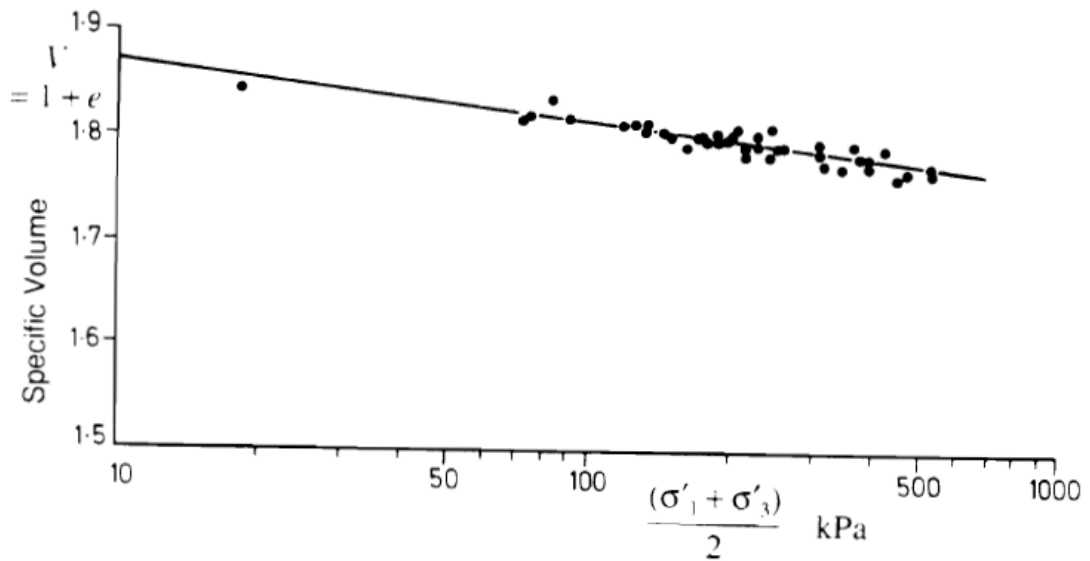
Figure 2.10. Critical State Line for simple shear tests performed on sand (after Stroud, 1971)

The dependence of critical void ratio to the effective stress, oblige to use critical state line instead of critical void ratio. Schofield and Wroth (1968) associated specific volume and effective stress and named sands as wet or dry by specifying their position with respect to the critical state. The upper-right side of the critical state was defined as wet since a loose sand sample removes pore water it contains and makes its environment wet. The lower-left side of the critical state was defined as dry since a dense sand sample absorbs water into pores it contains and makes its environment dry.

19
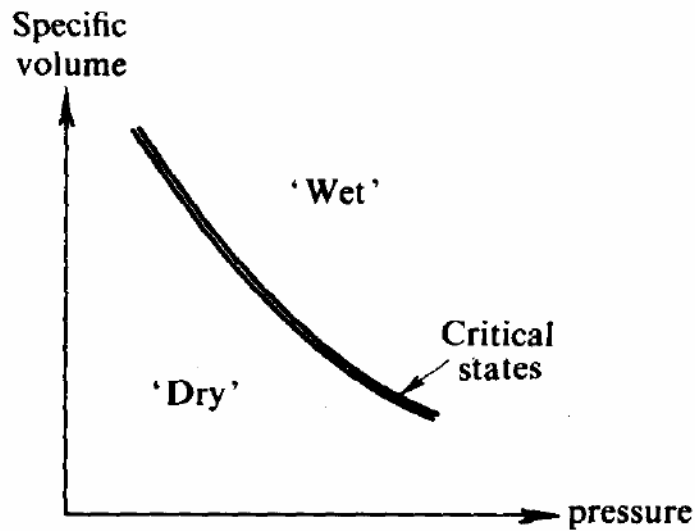
Figure 2.11. Critical State (Schofield and Wroth, 1968)

Critical state is one the major concepts that must be well understood in order to predict soil behavior successfully. All sands reach the same yield surface during continuous yielding. This yield surface is defined as critical state line and it is a combination of critical void ratio and effective stress. The initial position of a sand with respect to critical state line determines its response.

Figure 2.12 presents a brief summary of the critical state concepts and can be used to illustrate the definition made by Roscoe (1958) for drained and undrained loading conditions:

- In drained loading; "loose" sands decrease their volume by draining water out and reach to the critical state line after contraction, similarly "dense" sands increase their volume by absorbing water and reach to the critical state line after dilation.

- In undrained loading; "dense" and "loose" responses are governed by initial density and effective stress state and loose sands and dense sands reach to the critical state line in such a way that initial void ratio, that is constant during shearing, becomes the critical void ratio with the change in effective stress they can resist.

20

In the critical state line, dilation and contraction rates are zero (Houlsby, 1991). All these responses occur while sand sample tries to reach the critical state. The distance of the initial state of a sand sample to the critical state line reveals the amount of dilation or contraction that will take place during shearing. In Figure 2.12., the slope of critical state line is defined as λ, and Γ is the value of critical void ratio at atmospheric pressure as a reference effective stress. V_λ is the specific volume of any point at atmospheric pressure and $\Gamma - V_\lambda$ difference represents the distance between initial state and critical state line.

An important point that can be inferred from Figure 2.12. is that a sand sample at a certain density, can stand on the both sides of the critical state line and can exhibit loose or dense sand behavior according to the effective stress state. An imaginary sand that having 40 SPT-N blow count can dilate under 2 story building but can contract under a 100m height dam.
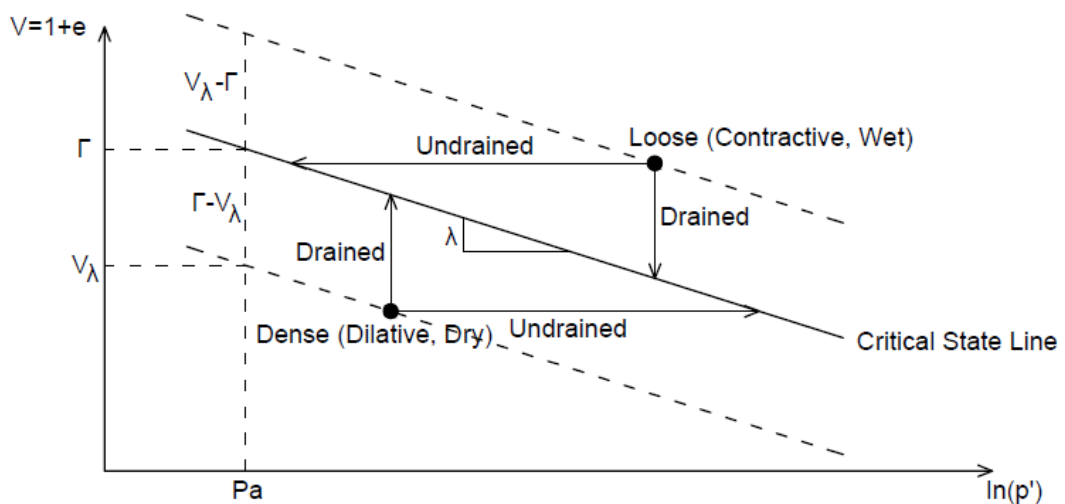
Figure 2.12. Critical State Line

21

2.2.2. Shear Strength and Stiffness Estimations

Critical state concept explains the behavior of sands from the initial phase of shearing to the large strain levels. By determining the initial state of a sand sample, its peak and critical state strength values can be predicted after assessing their dilation or contraction tendencies during shearing.

2.2.2.1. Dilation vs. Contraction

Dilation is defined as the volume increase during shearing. As stated by Terzaghi et al. (1996), sand grains in dense state and under relatively low effective stress, try to push each other when they are subjected to shear. This is due to tendency to displace in the direction of applied shear. However, pushing and interlocking cause climbing of grains over each other due to dense packing. As a result, general grain movement does not occur in the direction of applied shear and sand mass expands.

Contraction, in contrast with dilation, is defined as the volume decrease during shearing. Sand grains in loose state, move in the direction of applied shear just by pushing each other. Lack of interlocking of grains due to loose state prevents climbing of grains over each other and sand mass contracts. This process is also valid for sand grains in dense state and under relatively high effective stress. In this case, climbing of grains over each other is prevented by strong confinement due to high effective stress. Particle displacement occur with the particle crushing at the contact surfaces. As the crushing takes place continuously, general movement occur in the direction of applied shear and sand mass contracts.

The behavior of sands under shearing, whether dilative or contractive, is based on the position of initial state with respect to critical state. The amount of dilation or contraction that it will be experienced is a function of distance of initial phase to the critical state line.

For a certain granular material, all samples reach to the same yield surface, named as critical state line in the void ratio – effective stress space, obtained by determining the critical void ratio values at varying effective stresses. Along that surface, all samples have the same strength regardless of the initial state. Initial state can be called as relatively dense or relatively loose. However, an important point to prevent confusion in critical state concept is that it must be underlined that "dense" term is used for materials that will dilate to reach the critical state and "loose" term is used for materials that will contract to reach the critical state. As mentioned before, dense or loose initial state is a function of initial void ratio and effective stress together and does not correspond to a certain relative density level.

Before reaching critical state, dense samples dilate and mobilize a strength added to ultimate strength. This additional strength can be seen in a typical stress – strain plot of a granular material. The difference between the peak strength and ultimate strength is the additional strength mobilized by dilation. Unlike dense samples, loose samples does not show peak strength as initially they are weaker than the ultimate strength. Therefore the maximum strength in the stress – strain response of loose sands mobilize at the critical state.

To make a reasonable prediction of the strength of sands at any point before they reach the critical state line is vital to model the plastic deformations. Preparing loose samples in the laboratory, initially on the wet side of the critical state line, is sometimes impossible. Moreover, peak strength of loose sands mobilizes in the critical state as mentioned above, whereas peak strength of dense sands is not predictable easily due to their dilatancy component. Therefore, the research subjects of the experimental studies focused on the dilatancy of sands.

A demonstration of the relationship between friction angle and angle of dilation is provided in Figure 2.13 by Houlsby (1991). In sawtooth model, the contribution of dilatancy to peak strength is explained by applying to flow rule. In Figure 2.13 (a), a block sliding over another block on a smooth surface that has the coefficient of friction of $\tan(\phi'_{CV})$ where ϕ'_{CV} is the effective constant volume friction angle of the surface, is shown. The shear stress is expressed as;

$$\tau = \sigma'.\tan(\phi'_{CV}) \hspace{6cm} (2.8)$$

In Figure 2.13. (b), the surface between blocks is assumed to be rough as it has teeth which were inclined. The shear stresses in this case can be expressed as;

$$\tau = \sigma'.\tan(\phi') = \sigma.\tan(\phi'_{CV} + \psi) \hspace{4cm} (2.9)$$

After simplifications, Equation 2.9 gives:

$$\phi' = \phi'_{CV} + \psi \hspace{6cm} (2.10)$$

The sawtooth model does not take into consideration the failure mechanism, heat energy due to friction and principal stress and strain increment directions (Bolton, 1986), which are listed as major drawback of the model.
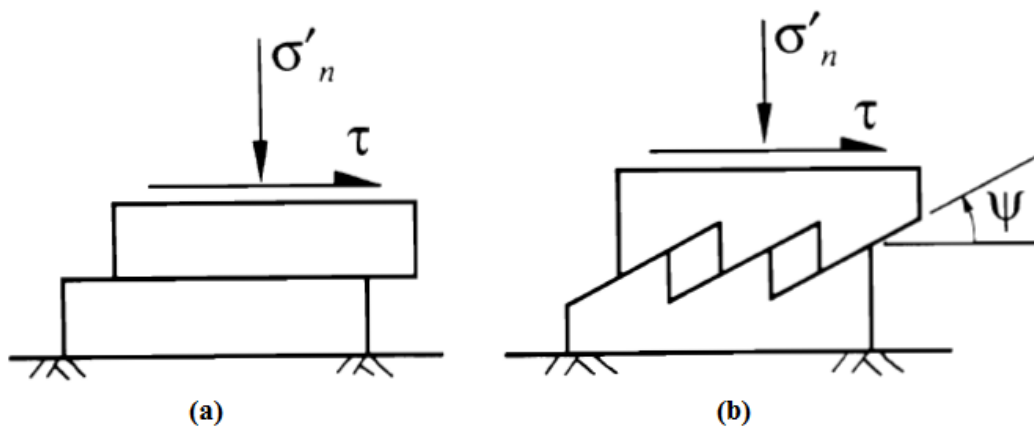
Figure 2.13. The sawtooth model for dilatancy

Taylor (1948) explained the dilatancy by energy correction. The external work done by shear stress is assumed to be dissipated in frictional soil due to dilation. Equation 2.11 represents the work done by shear stress and Equation 2.12 represents the energy dissipated internally.

$$W = \tau.\gamma \hspace{6cm} (2.11)$$

$$W = \tan(\phi'_{CV}).\sigma'_V.\gamma \hspace{5cm} (2.12)$$

Equalizing (2.11) and (2.12) gives the same result as explained in the sawtooth model:

$$\tau = \tan\left(\phi'_{CV}\right) \cdot \sigma_V' \qquad (2.13)$$
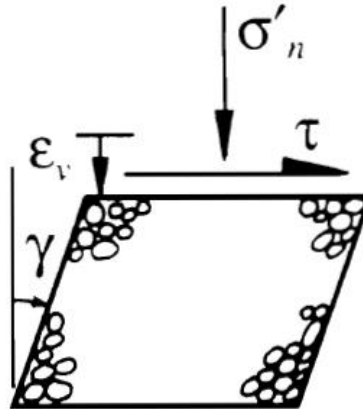
Figure 2.14. Energy Correction Analogy Proposed by Taylor (1948)

Rowe (1962) brought a new perspective to the strength – dilatancy concept by the tests performed on steel spheres packed in different geometrical arrangements. In the study, sphere assemblies given in Figure 2.15 were prepared and their strength and volume change characteristics under shearing were investigated:
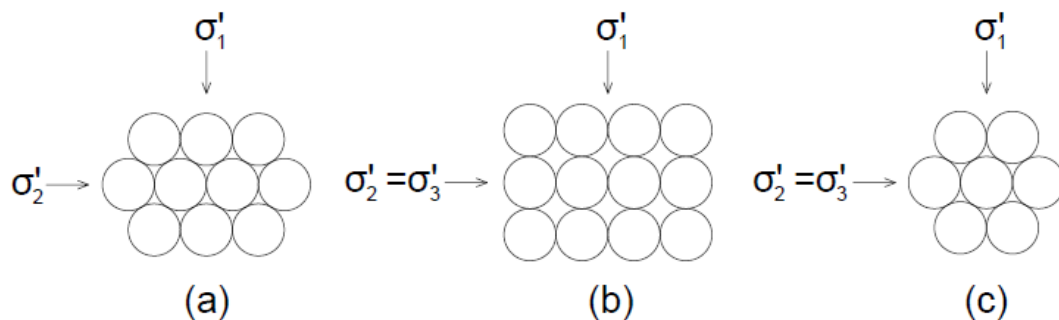
Figure 2.15. Sphere Assemblies (a) Uniform rods in a parallel stack, (b) Uniform spheres in face-centered cubic packing, (c) Uniform spheres in rhombic packing (Rowe, 1962)

25

According to test results, expressions for ratio of major principal stress to minor principal stress (Equation 2.14) and ratio of work done on the assembly by major principal stress on the assembly to the work done by assembly on the minor principal stress (Equation 2.15) were derived by Rowe as:

$$\sigma'_1 / \sigma'_3 = \tan(\alpha) \cdot \tan\left(\phi'_\mu + \beta\right) \tag{2.14}$$

$$E = \frac{\sigma'_1 \cdot \epsilon_1}{\sigma'_3 \cdot \epsilon_3} = \frac{\sigma'_1}{\sigma'_3 \cdot (1 + \frac{dV}{V\epsilon_1})} = \frac{\tan\left(\phi'_\mu + \beta\right)}{\tan(\beta)} \tag{2.15}$$

In the equations above, α denotes the inclination of imaginary plane of particle interlocking with respect to direction of minor principal stress, β denotes the inclination of the direction of movement with respect to the direction of major principal stress and ϕ'_μ denotes the interparticle friction angle. ϵ_1 and ϵ_3 correspond to strains in major and minor principal stress directions, respectively and dV/V represents the unit volume expansion during shearing.

In theory, energy ratio given in Equation 2.15 becomes 1.0 when the interparticle friction angle is zero which means that all work done by major principal stress is transmitted to minor principal stress. However, in reality, energy ratio becomes more than 1.0 because of the fact that some part of work done by major principal stress is converted to heat due to the presence of interparticle friction.
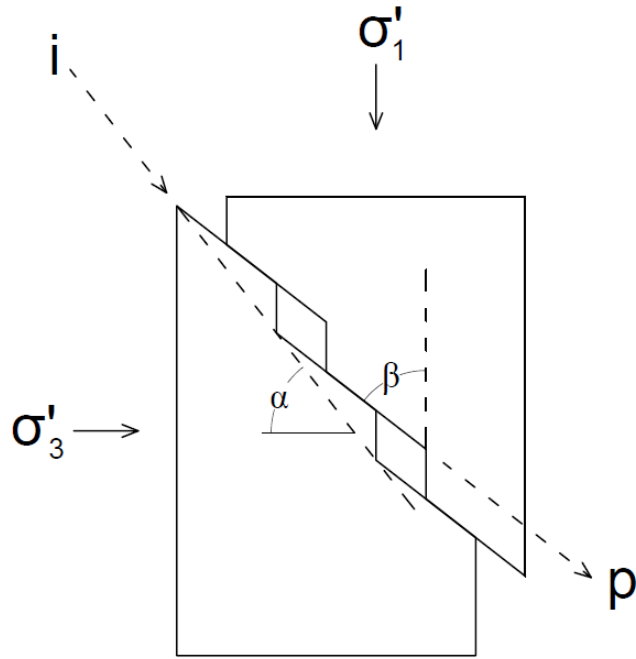
Figure 2.16. Sliding mechanism proposed by Rowe (1962)

Equations 2.14 and 2.15 are valid for any state of deformation and for any geometrical arrangement of particles. Rowe, then, assumed that these equations can also be used to explain the strength – dilatancy relationship of the sands. The sliding mechanism given in Figure 2.16 was proposed and minimum energy ratio concept was applied to eliminate the uncertainty of β due to the reorientation of particles during shearing. It was assumed that the simplest way of the reorientation of particles is minimizing the internal work done. This assumption is expressed as $dE/d\beta = 0$, which is satisfied when α and β planes are replaced with an equivalent failure plane at an inclination of $(45 - \phi_\mu/2)$ to direction of major principal plane as proposed by Mohr-Coulomb Failure Criterion and gives the fallowing relationship between stress and dilatancy of sands:

$$\frac{\sigma'_1}{\sigma'_3 .(1+\frac{dV}{V\epsilon_1})} = tan^2\left(45 + \frac{\phi'_\mu}{2}\right) \tag{2.16}$$

Bolton (1986) compared the results of sawtooth model and Rowe's stress – dilatancy relation. Comparison showed that sawtooth model overestimates the contribution of

dilatancy about 20% in proportion to Rowe's expression. Therefore, stress – dilatancy expression proposed by Rowe (1962) can also be represented as:

$$\phi' = \phi'_{CV} + 0.8\psi \tag{2.17}$$

Bolton also suggested a new empirical parameter in the light of the results of his experiments. Relative dilatancy index (I_R) relates the relative density and effective stress to the dilatancy of the sand:

$$I_R = D_R \cdot (Q - lnp') - 1 \tag{2.18}$$

where Q is material constant, D_R is relative density and p' is the mean effective stress at the failure. The suggested Q values for different materials and the contribution of dilatancy to the strength for $0 < I_R < 4$ interval are given in Table 1 and Equations 2.19 and 2.20:

Table 1. Proposed Q Values for Different Materials (Bolton, 1986)

Q	Material Type
10	Quartz and Feldspar
8	Limestone
7	Anthracite
5,5	Chalk

For plain strain;

$$\phi' - \phi'_{CV} = 0.8\psi = 5I_R^{\circ} \tag{2.19}$$

and for triaxial strain;

$$\phi' - \phi'_{CV} = 0.8\psi = 3I_R^{\circ} \tag{2.20}$$

Maximum dilatancy rate that mobilizes at the peak strength for both test types is:

$$(-\frac{d\epsilon_V}{d\epsilon_1})_{max} = 0.3I_R \tag{2.21}$$

28

2.2.2.2. Internal Friction Angle

There are various correlations in the literature for the estimation of internal friction angle of sands. Schmertmann (1978) and NAVFAC (1982) related the effective friction angle to the relative density and gradation of sandy soils and recommended the correlations given in Figure 2.17 and Figure 2.18, respectively.
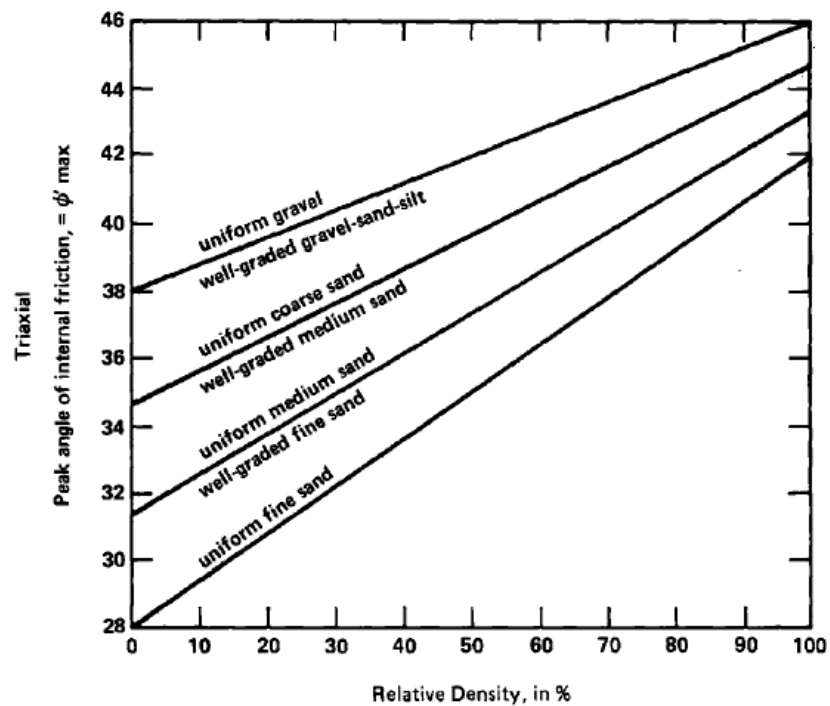
Figure 2.17. Correlation between friction angle and relative density and gradation for granular soils (Schmertmann, 1978)
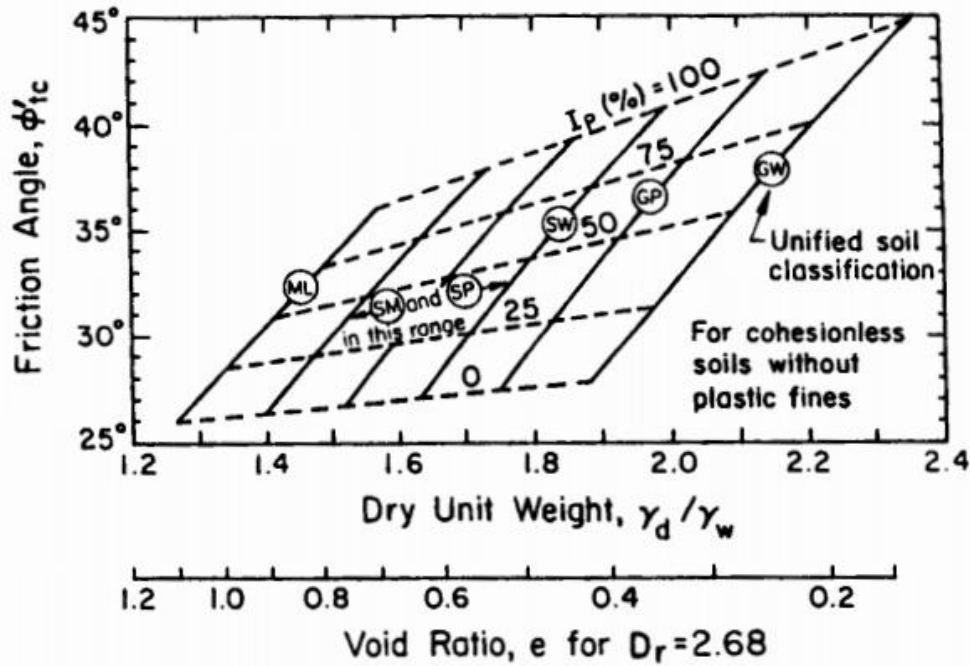
Figure 2.18. Correlation between friction angle and relative density and gradation for granular soils (Modified from NAVFAC (1982) by Lade (2001))

The limitation of these widely used correlations was that they do not reflect the effect of effective stress state on the friction angle, which is dependent on both density and effective stress state as discussed earlier.

Andersen and Schjetne (2013) compiled the data provided by Norwegian Geotechnical Institute and plotted the friction angle curves for different consolidation stress levels against relative density (Figure 2.19). The proposed empirical curves illustrate the effects of density and effective stress on the strength of sands. Friction angle increases with the increase in relative density and for a constant relative density, it decreases with increasing effective stress. Moreover, as seen in Figure 2.19, at high stress levels friction angles converge to the same value independent of the relative density.

Andersen and Schjetne (2013) also compared the curves with the proposed correlations in the literature. Bolton's expression given in the Equation 2.20 fits well with the empirical curves for $\phi'_{CV} = 33°$ for quartz. However, uniform medium sand

30

and uniform fine sand curves proposed by Schmertmann (1978) coherent with the empirical curves only by order since he correlates the gradation with the friction angle instead of effective stress.
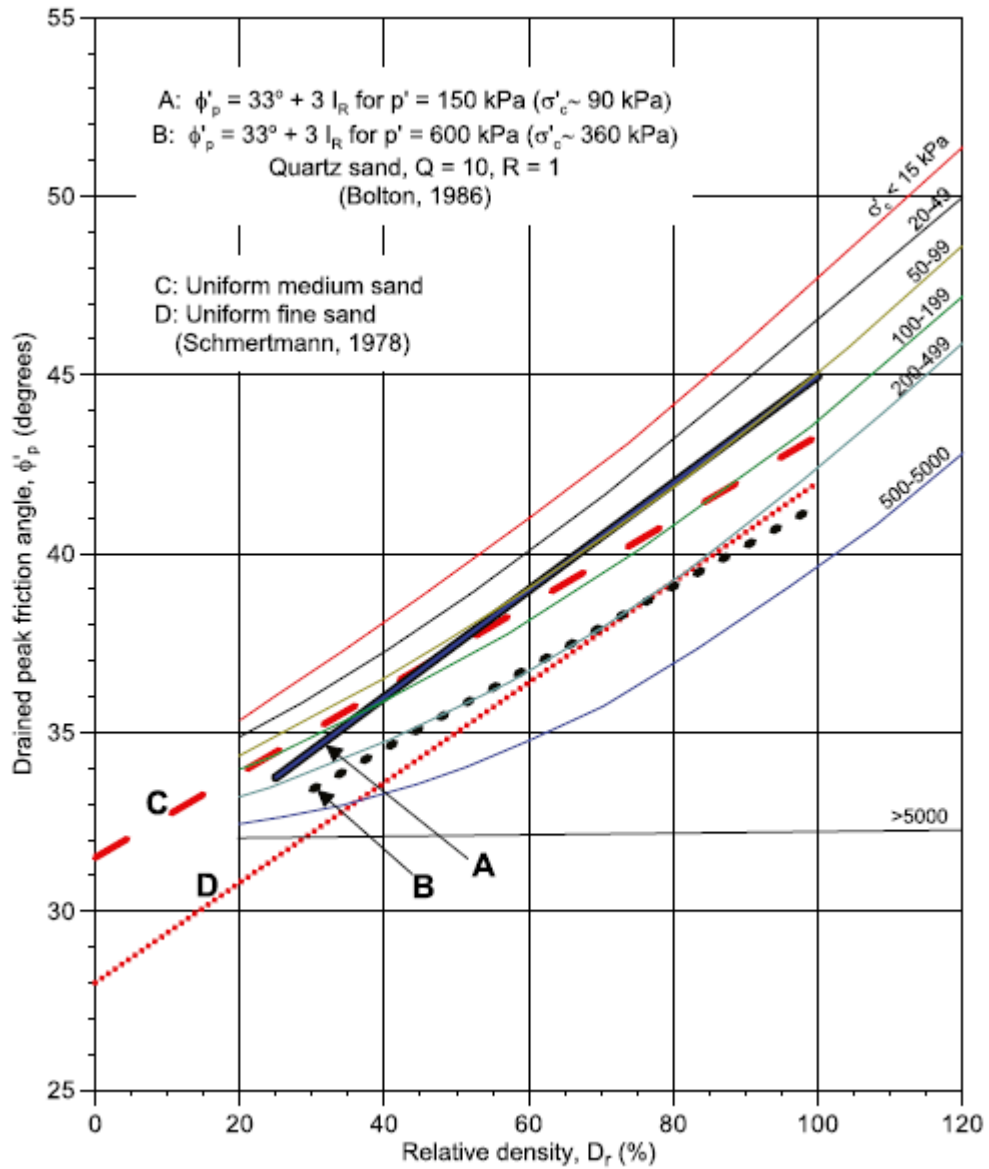
Figure 2.19. Comparison of drained peak friction angle provided from NGI database and Schmertmann (1978) and Bolton (1986) (Andersen and Schjetne, 2013)

A summary of correlations proposed by various other studies (Wolff, 1989; Kulhawy and Mayne, 1990; Hatanaka and Uchida, 1996; Mayne et al., 2001; JRA, 1996) is

provided in Table 2.2 and Figure 2.20. The effect of effective stress beside density on friction angle was introduced by correcting the SPT-N blow count for overburden pressure:

$$(N_1)_{60} = \sqrt{\frac{p_a}{\sigma'_v}} \cdot N_{60} \tag{2.22}$$

where p_a is the atmospheric pressure as a reference pressure value.

Table 2. $(N_1)_{60}$ vs ϕ Relationship (NCHRP, 2010)

No	Expression	Researcher
1	$\phi' = 54 - 27.6034e^{-0.014(N_1)_{60}}$	Kulhawy & Mayne, 1990
2	$\phi' = \sqrt{20(N_1)_{60}} + 20$ $3.5 \leq (N_1)_{60} \leq 30$	Hatanaka & Uchida, 1996
3	$\phi' = 27.1 + 0.3(N_1)_{60} - 0.00054(N_1)_{60}^2$	Wolff, 1989
4	$\phi' = \sqrt{15.4(N_1)_{60}} + 20$	Mayne et al., 2001
5	$\phi' = \sqrt{15(N_1)_{60}} + 15$ $5 < (N_1)_{60}$ and $\phi' \leq 45°$	JRA, 1996

Figure 2.20. $(N_1)_{60}$ vs ϕ' Relationship (NCHRP, 2010)

32
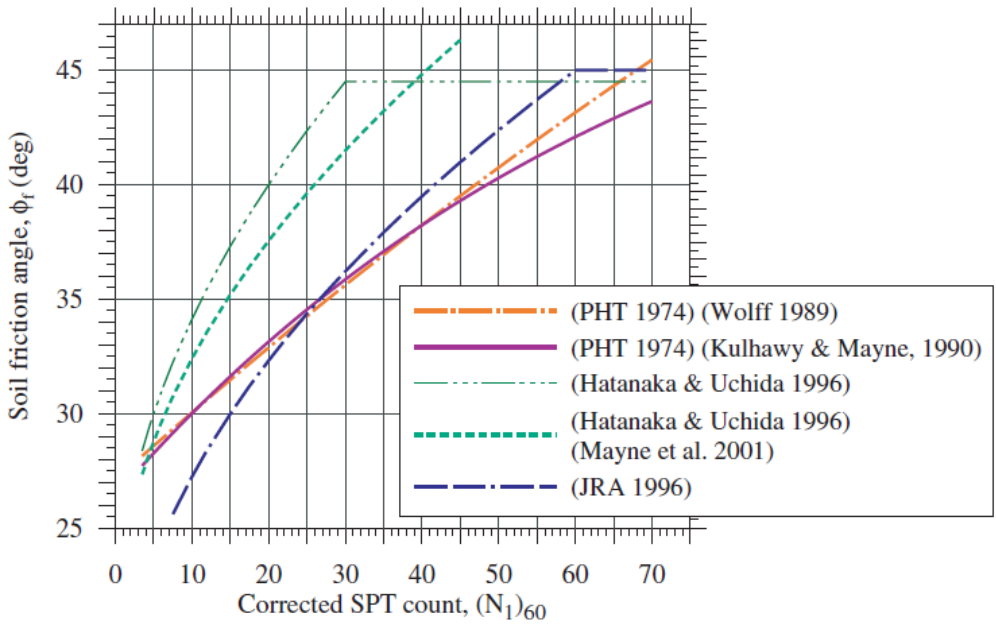
2.2.2.3. Shear and Elasticity Modulus

Estimating the stiffness of soils is one of the most difficult tasks in geotechnical engineering since the estimated and measured stiffness values are usually contradicting and this becomes a major obstacle that must be overcomed to make reliable deformation predictions during designs. With the improvements of new testing techniques and understanding the non-linear soil behavior, this task is tackled better after understanding the factors affecting it and stiffness estimations can be made with reasonable accuracy by these new relationships.

Today, it is well known that stiffness of soils is a strain dependent parameter such that at small strains it remains constant and as the strain increases, it decreases. A detailed information about strain orders is provided by Benz (2007):

- Very small strain; strain values lower than 10^{-6}. This value is also called as threshold strain, since stiffness remains constant up to it and starts to decrease at larger strains.
- Strain values between $10^{-5} - 10^{-4}$ is assumed as transition strains between small and very small strains.
- 10^{-3} is assumed as the border between small strains and large strains. This value is also strain limit of conventional testing methods like triaxial or oedometer tests.

At larger than the threshold strain, modulus decreases in a S-shape form on logarithmic scale. This decrease in stiffness with increasing strain is generally named as modulus degradation. The maximum stiffness values take place at very small strains. In the literature, these values are generally denoted as G_0 or G_{max} and E_0 or E_{max} for shear modulus and Young's modulus, respectively and named as dynamic stiffness. The modulus values obtained from conventional testing equipment correspond to large strain stiffness and named as static stiffness.
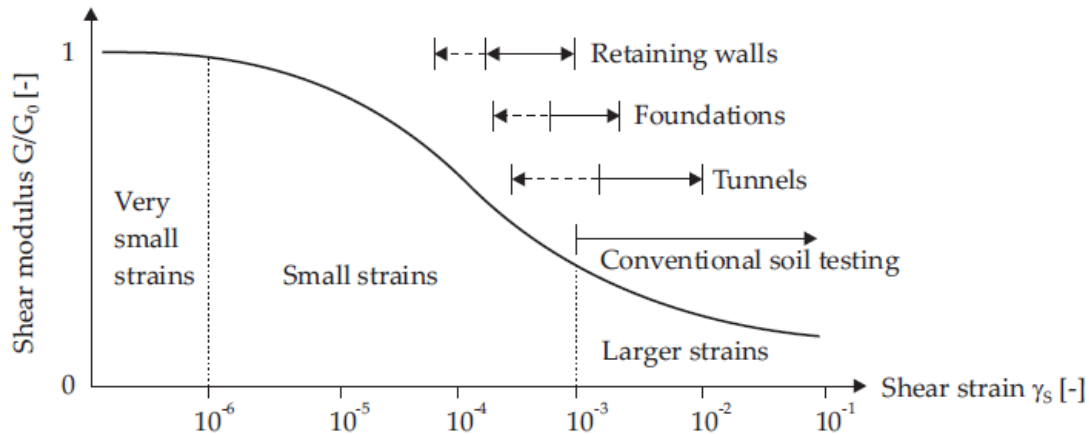
Figure 2.21. Typical stiffness – strain characteristic of soils (Benz, 2007)

As stated by Witchman and Triantafyllidis (2009), determination of G_0 and E_0 directly from field or laboratory tests is a troublesome work. Therefore, either simple relationships by using the fundamental properties of sands or correlations between static and dynamic stiffness are used in the estimations.

Benz (2007) proposed the relationship by Biarez and Hicher (1994) for the estimation of E_0 and relationship by Hardin and Black (1969) for the estimation of G_0:

$$E_0 = \frac{140}{e} \cdot \sqrt{\frac{p'}{p_{ref}}} \tag{2.23}$$

$$G_0 = 33 \frac{(2.97-e)^2}{1+e} \cdot \sqrt{\frac{p'}{p_{ref}}} \tag{2.24}$$

A correlation between stiffness values determined from conventional testing, static modulus and maximum modulus at very small strain, dynamic modulus were proposed by Alpan (1970) as given in Figure 2.22:

34
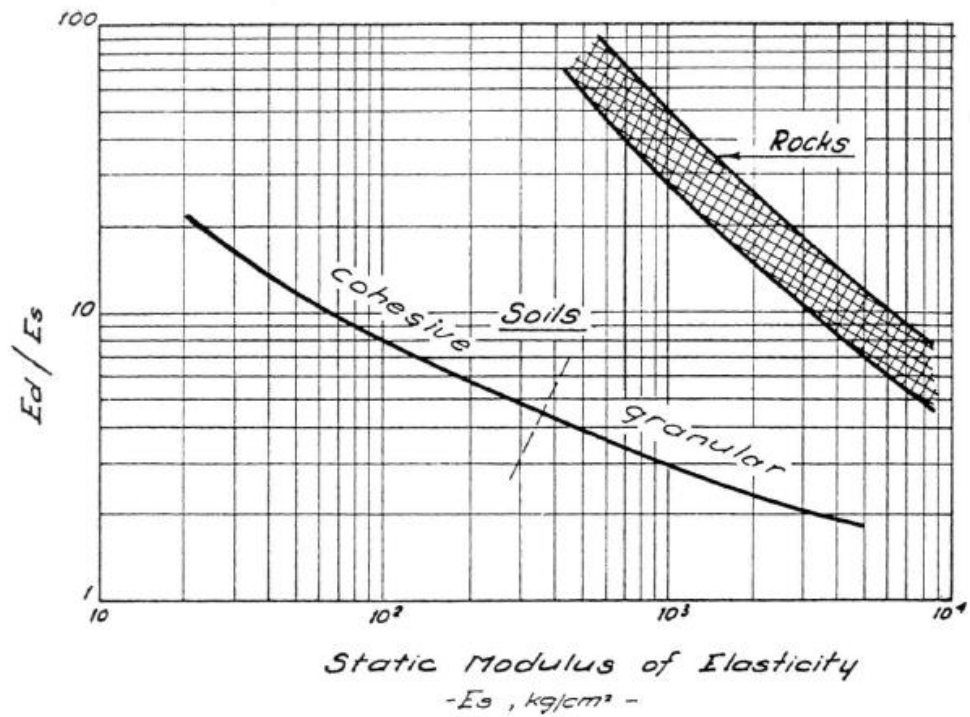
Figure 2.22. Correlation between static and dynamic stiffness proposed by Alpan (1970)

2.3. Straining Response of Hydrophobic Sandy Soils Under Monotonic Loading

A detailed survey reveals that there are almost no sources that investigated the straining response of hydrophobic sands. Majority of available studies focused on the usage of hydrophobic sands for different purposes or their effects on the environmental issues. Among the limited researches focused on the geotechnical properties of hydrophobic sands, experimental studies performed by Kim et al. (2013) and Byun and Lee (2012) are examined.

Byun and Lee investigated effect of hydrophobicity on shear strength and performed direct shear tests on glass beads and crushed sands. By using angular and sharp particles, particle shape – hydrophobicity – shear strength relationship was also observed. Hydrophobicity was provided by silica silanization reaction. Direct shear tests performed in dry condition and peak and critical state shear strengths were determined. As shown in Figure 2.23(a), hydrophobicity decreased the peak shear

strength of glass bead and crushed sand independent from the particle shape. At critical state, hydrophobicity did not affect the shear strength of glass bead whereas it caused a sum of decrease in the shear strength of crushed sand.
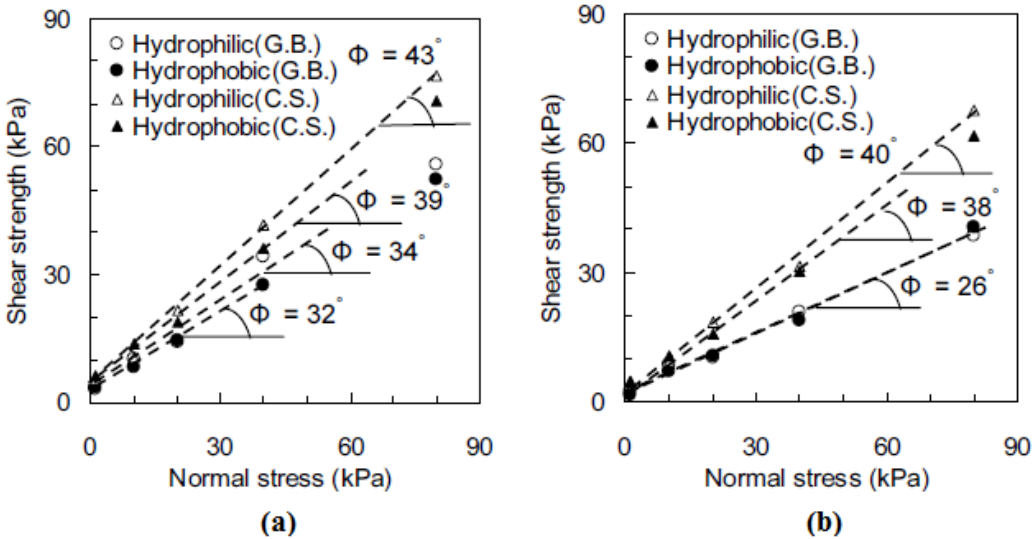
Figure 2.23. Effect of hydrophobicity on the shear strength of glass beads and crushed sands, (a) peak state; (b) critical state (G.B.: Glass bead, C.S.: Crushed Sand) (Byun and Lee, 2012)

Yang et al (2013) also performed direct shear tests on hydrophilic and hydrophobic Jumunjin sands. Hydrophobic samples were prepared by chemical treatment. Tests were performed under natural dried conditions. Test results and comparison of shear strength of hydrophilic and hydrophobic samples are given in Figure 2.24. The decrease in shear strength due to hydrophobicity was associated with surface modification of sand grains during chemical treatment.
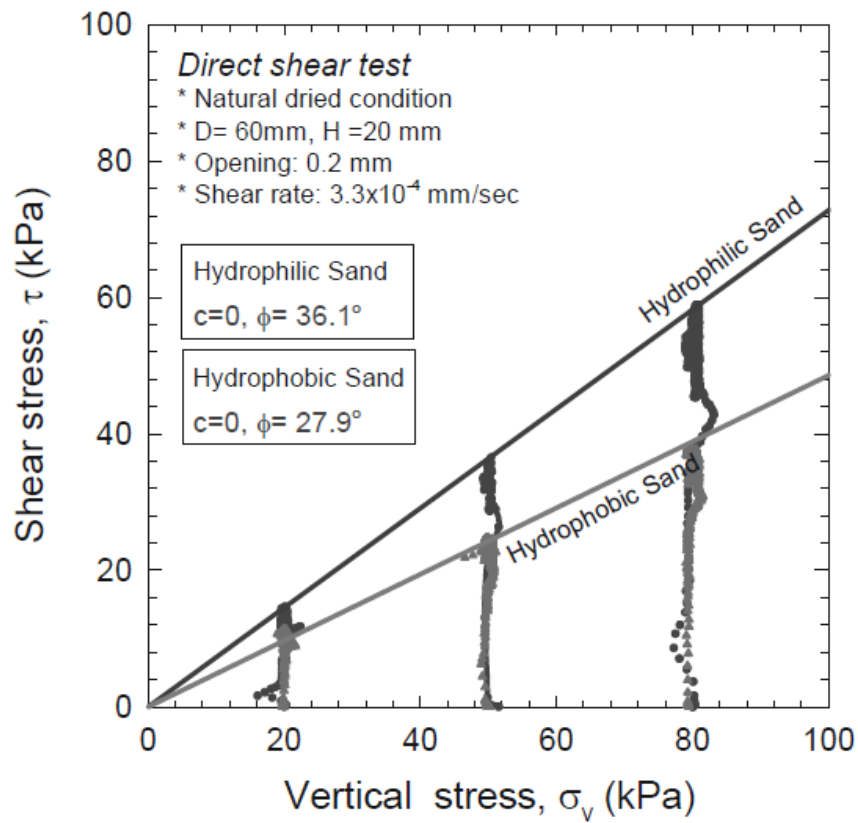
Figure 2.24. Comparison of shear strength of hydrophilic and hydrophobic sands under natural dried condition (Yang et al, 2013)

CHAPTER 3

LABORATORY TESTING PROGRAM AND PROCEDURE

3.1. Introduction

In this chapter, laboratory testing program and testing procedures are described in detail. The experimental study was carried on Kızılırmak River Sand. Laboratory testing program consists of 4 soil index tests. After the determination of fundamental soil properties, 18 monotonic strain – controlled consolidated undrained triaxial shear tests with pore water measurement were performed on relatively dense and loose reconstituted hydrophobic sand samples. In order to achieve aimed density states of samples, wet tamping and dry pluviation techniques were used.

3.2. Soil Index Testing

For the cohesionless soil used in experiments, index properties like specific gravity (G_S), minimum void ratio (e_{min}) and maximum void ratio (e_{max}) and gradation were determined.

For the determination of specific gravity (G_S), four specimens prepared and tests were performed in accordance with "Method B – Procedure for Oven-Dry Specimens" suggested by "ASTM D854-14 Standard Test Methods for Specific Gravity of Soil Solids by Water Pycnometer". The average G_S of sand is determined as 2.66, which is compatible with available literature, and individual results of all 4 specimens are presented in Appendix A.

Minimum void ratio (e_{min}) and maximum void ratio (e_{max}) were determined by following the procedure given as follows:

- e_{max} is achieved by pouring the sand into a container from the possible lowest elevation by using a funnel,
- e_{min} is achieved by compressing the soil with vibration into a container in three layers.

Measuring the volume of the container and calculating the volume of voids and volume of solids, e_{max} is determined as 0.857 and e_{min} is determined as 0.534. The details of the calculations are presented in Appendix B. Calculated e_{max} and e_{min} values were used in the determination of the required sample weight for certain relative density in the sample preparation for triaxial testing.

Gradation of the sand was also determined by sieve analysis in accordance with "ASTM D6913/6913M-17 Standard Test Methods for Particle-Size Distribution (Gradation) of Soils Using Sieve Analysis". Grain size distribution and soil classification according to Unified Soil Classification System are given in Figure 3.1 and Table 3, respectively. Uniformity coefficient of 2.36 and curvature coefficient of 2.88 classifies the soil as poorly graded sand. Details of sieve analysis are given in Appendix C.
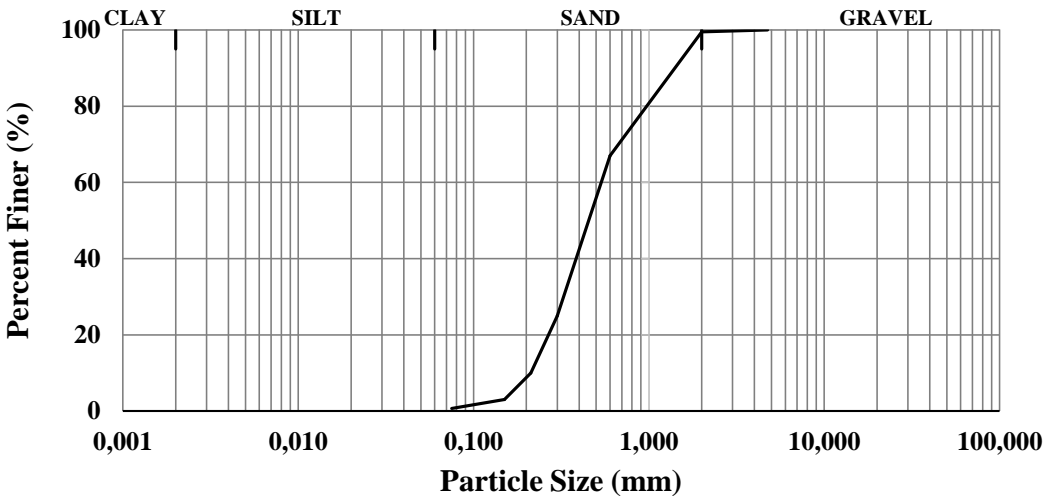
Figure 3.1. Grain size distribution of the sand used in this study

Table 3. Classification of the Sand Used in This Study

USCS:	SP
% Gravel:	0,00
% Sand:	99.31
% Fines:	0.69
D_{10} (mm):	0.22
D_{30} (mm):	0.33
D_{60} (mm):	0.52
C_u:	2.36
C_c:	2.88

Particle shape and minerology of sand were also determined. The cohesionless soil used in this study is composed of quartz, feldspar, calcite minerals and rock fragments and particle shape can be described as subangular − subrounded. Microscopic examination of sand is given in Figure 3.2:
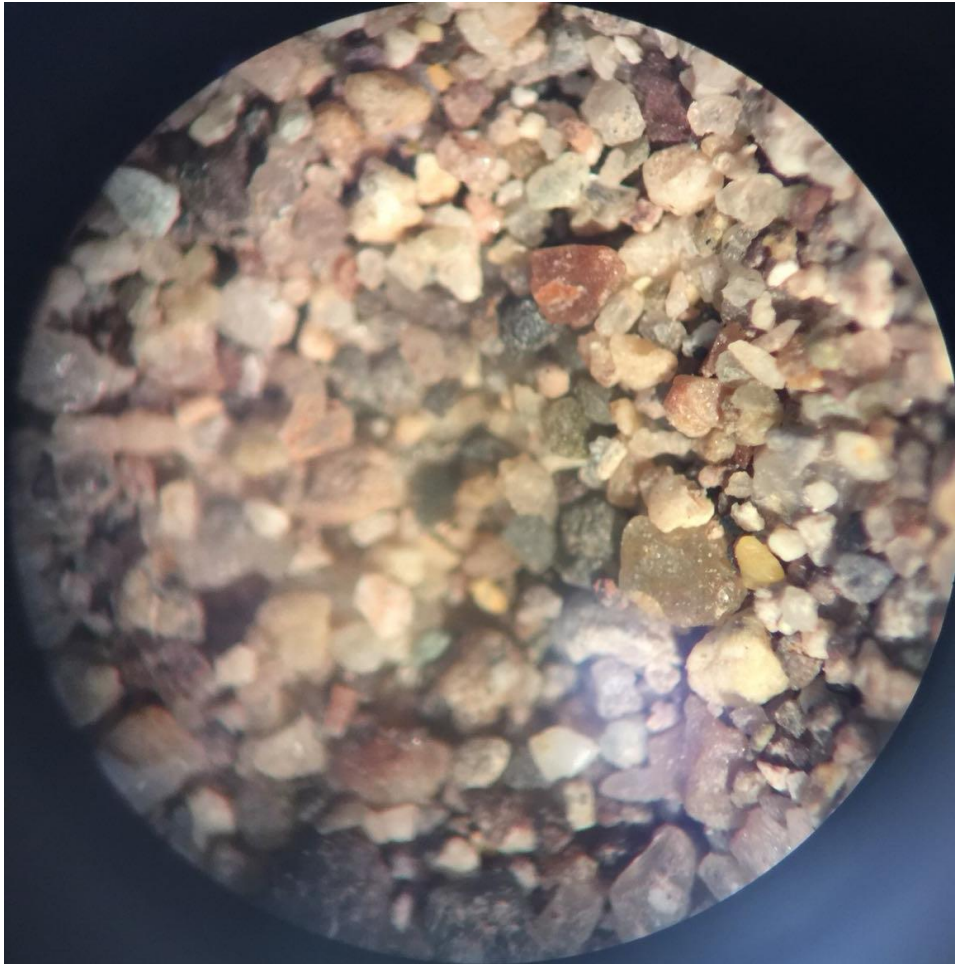
Figure 3.2. Microscopic examination of the sand used in this study

3.3. Triaxial Testing

The scope of this experimental study is to investigate the effect of hydrophobicity on the straining response of sandy soils. For this aim, an extensive and comparative laboratory testing program consisting of 18 static (monotonic) strain – controlled consolidated undrained triaxial shear tests with pore water measurement was designed. Although it was proposed for cohesive soils, "ASTM D4767-11 Standard Test Methods for Consolidated Undrained Triaxial Compression Test for Cohesive Soils" was applied as an advisor for triaxial testing.

Hydrophobic samples were prepared by adding WD-40 lubricant into the sand. In order to check the hydrophobicity, WD-40 was added to the sand and the mixture was blended in a bowl until it becomes homogeneous. After that, a pit was opened at the middle of mixture such that the bottom of bowl become visible. Then, water was added into the pit. After waiting about 15 minutes, it was observed that the water surface remain constant which means that no water leakage occurred through the pores between sand particles.

Properties and image of lubricant provided by manufacturer are given in Table 4 and Figure 3.3 and, respectively.

Table 4. Properties of the WD-40 Lubricant Used in This Study

Color:	Light (or pale) amber
Specific Gravity:	0.80 – 0.82
Freeze Point:	-63 °C
Boiling Point:	183 – 187 °C
Kinematic Viscosity:	2.79 – 2.96 cSt (0.00000279 – 0.00000296 m^2/sn)
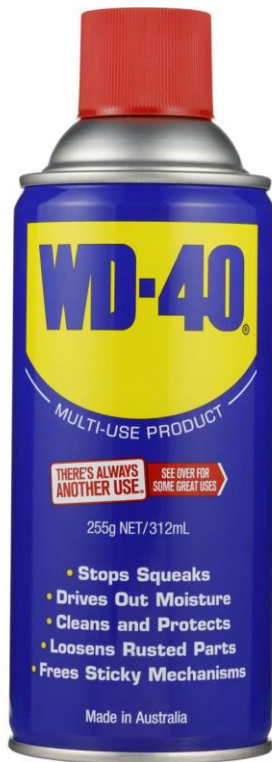
Figure 3.3. WD-40 lubricant used in this study

Microscopic examination of hydrophobic sand is also given in Figure 3.4:
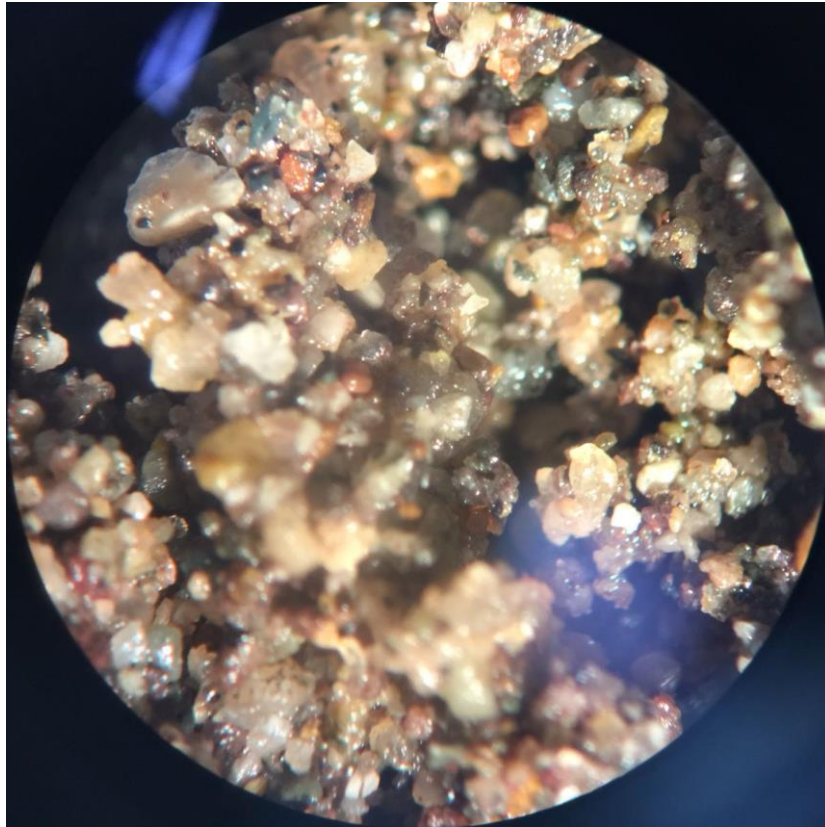
Figure 3.4. Microscopic examination of the hydrophobic sand prepared in this study

To accomplish the aims of the study, following points were considered while preparing the triaxial testing program:

- The effect of hydrophobicity on relatively dense and relatively loose samples' straining response
- The effect of hydrophobicity on relatively dense and relatively loose samples' strength

Testing program consisting of 18 static strain controlled consolidated undrained triaxial shear tests with pore water measurement is given in Table 5. 9 tests were performed on relatively dense specimens and 9 tests were performed on relatively loose specimens. 80% relative density for relatively dense specimens and 40% relative density for relatively loose specimens were specified as target density states. To be able to compare the results of hydrophobic specimens with those of

hydrophilic specimens, 6 of 18 tests were performed on pure (hydphilic) sand samples with no WD-40. In order to observe the effect of the level of hydrophobicity, 6 of 18 tests were performed on specimens prepared with the addition of 1% WD-40 by mass and 6 of 18 tests were performed on specimens with the addition of 2% WD-40 by mass.

Table 5. Triaxial Testing Program

	TEST NAME / CONSOLIDATION PRESSURE / WD-40		
	STXD_01 / 100kPa / 0%	STXD_02 / 200kPa / 0%	STXD_03 / 400kPa / 0%
$D_R = 80\%$	STXD_04 / 100kPa / 1%	STXD_05 / 200kPa / 1%	STXD_06 / 400kPa / 1%
	STXD_07 / 100kPa / 2%	STXD_08 / 200kPa / 2%	STXD_09 / 400kPa / 2%
	STXL_01 / 100kPa / 0%	STXL_02 / 200kPa / 0%	STXL_03 / 400kPa / 0%
$D_R = 40\%$	STXL_04 / 100kPa / 1%	STXL_05 / 200kPa / 1%	STXL_06 / 400kPa / 1%
	STXL_07 / 100kPa / 2%	STXL_08 / 200kPa / 2%	STXL_09 / 400kPa / 2%

3.3.1. Sample Preparation

Undisturbed samples of cohesive soils can be obtained easily for laboratory testing by the conventional sampling methods. However, acquiring undisturbed sand samples requires special techniques. Freezing method is generally used to obtain undisturbed samples of granular soils, but the cost of this technique restricts its usage only for special projects with high budgets. Additionally, sample disturbance after thawing is inevitable. Therefore, alternative methods have been applied for the preparation of reconstituted sand samples in the laboratory. Pluviation and tamping are the most widely used techniques in preparing reconstituted samples.

In pluviation method, soil is dropped from a particular height into a mould. Unsurprisingly, obtained relative density increases up to a certain height as the drop height increases. Lo Presti et al. (1992) defines the major advantage of this technique as being able to obtain samples at uniform densities with negligible crushing and reasonable segregation of particle sizes.

In tamping method, soil is placed into a mould in layers and each layer are tamped by a number of blows. To obtain uniform samples, it is key to apply the same energy to all layers without causing particle crushing. Otherwise, non-uniform samples with local weak zones may be obtained and this may lead to unrealistic results in triaxial testing. Raghunandan et al. (2012) prepared reconstituted sand samples with dry and wet tamping methods and digital images of the samples were taken with help of microscope. In Figure 3.5 (a) and (b), the borders between neighbor layers are clearly seen. In case of unequal energy transfer through soil layers, this borders may act as plastic joints and may cause stress localization during deviatoric loading.
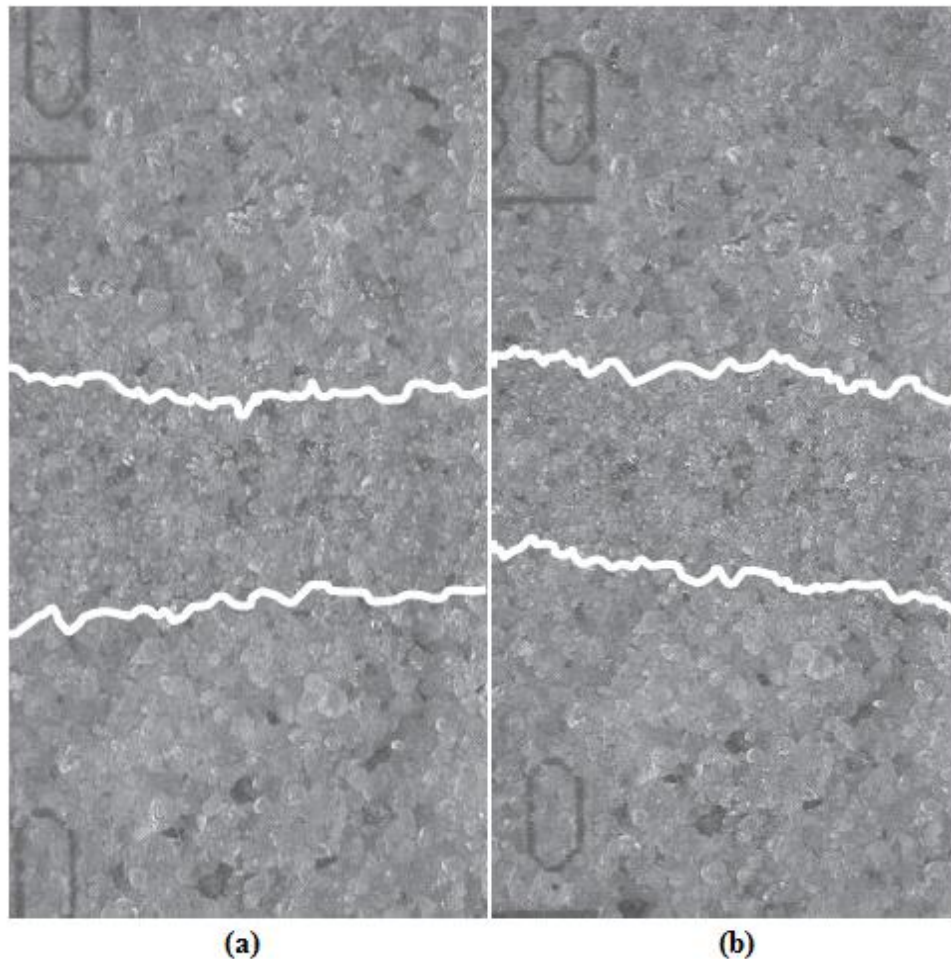

Figure 3.5. Borders between layers in (a) dry tamping and (b) wet tamping (Raghunandan et al., 2012)

Dry pluviation and wet tamping methods were used as the sample preparation technique in this study. Samples with 38mm diameter and 76mm height were prepared. In dry pluviation, oven-dried sand particles were pluviated into the mould by a funnel. By taking the limitations of triaxial test equipment into consideration, drop heights varying from 10 – 25cm were used. Sand is pluviated in 5 layers and drop heights were rearranged for each layer such that the same energy amount was delivered to each layer. In wet tamping, trials were performed at 5% water content. In order to avoid any inhomogeneous zone and stress localization, soil is placed into the mould in 10 layers. By using a tamp of 25mm diameter, blows varying 3 – 13 in number applied to each layer and the utmost attention was paid to deliver the same amount of energy. Obtained void ratio and relative density values by using both methods are given in Figure 3.6 to and Figure 3.9:
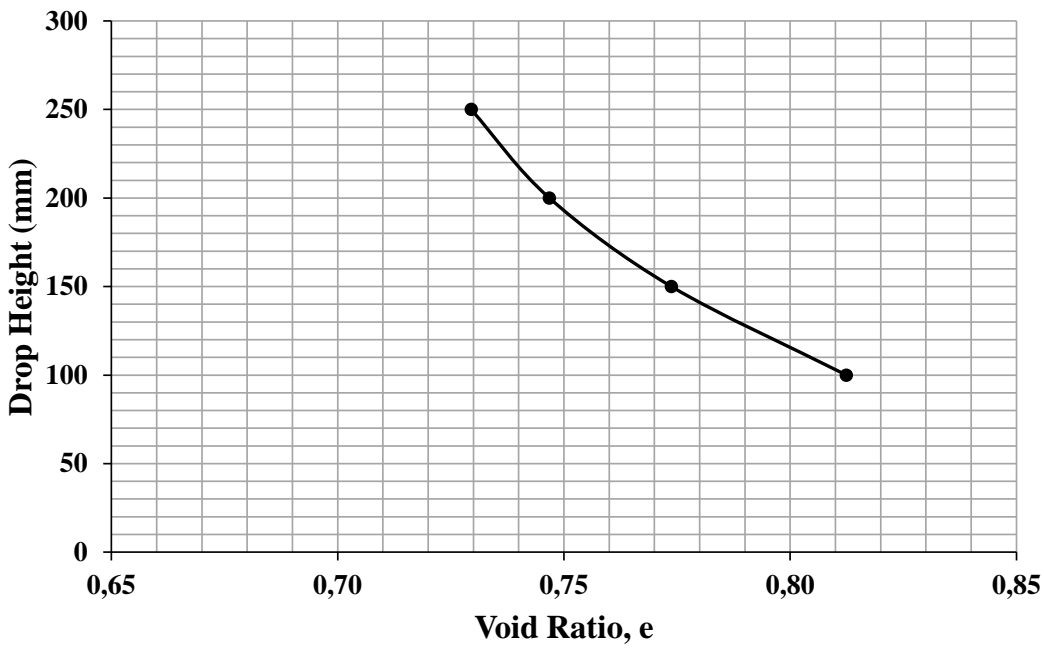

Figure 3.6. Void ratio vs. drop height relationship of reconstituted samples prepared with dry pluviation
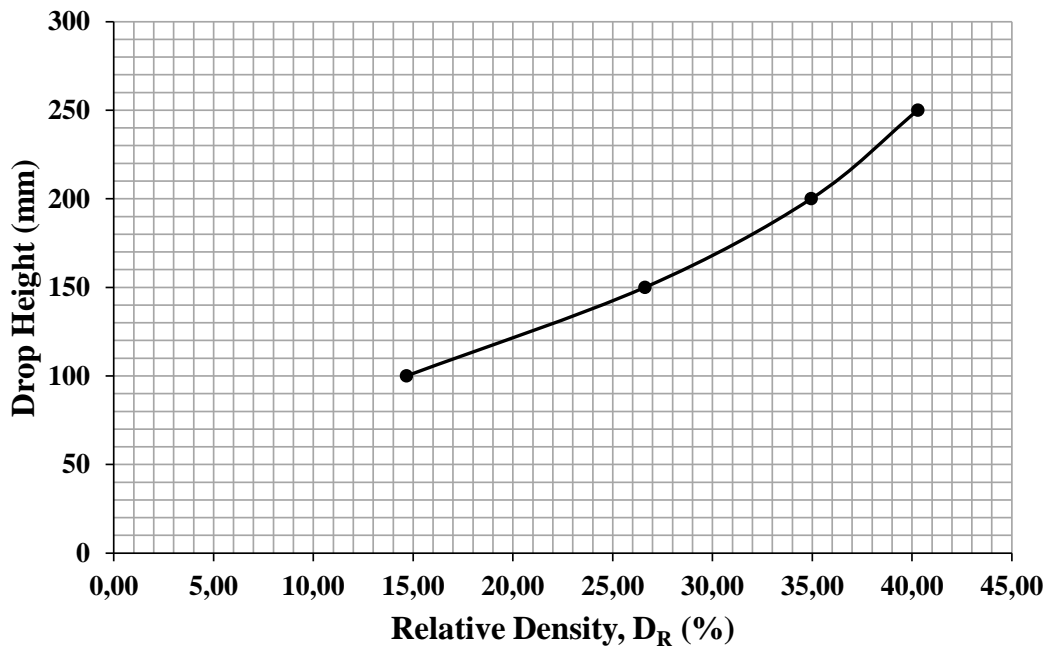
48

Figure 3.7. Relative density vs. drop height relationship of reconstituted samples prepared with dry pluviation
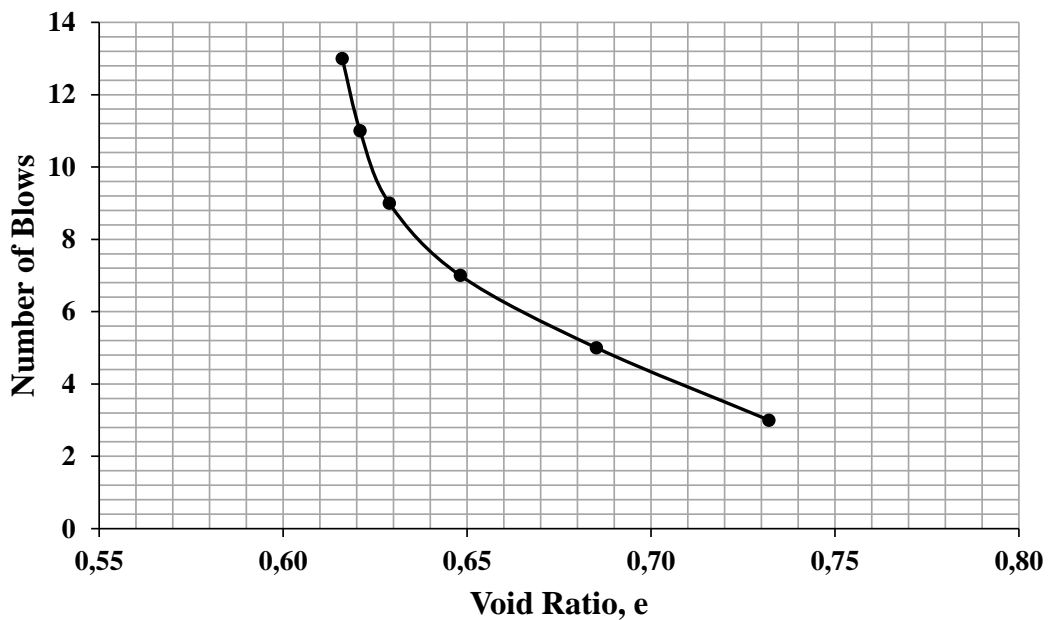
Figure 3.8. Void ratio vs. blow count relationship of reconstituted samples prepared with wet tamping
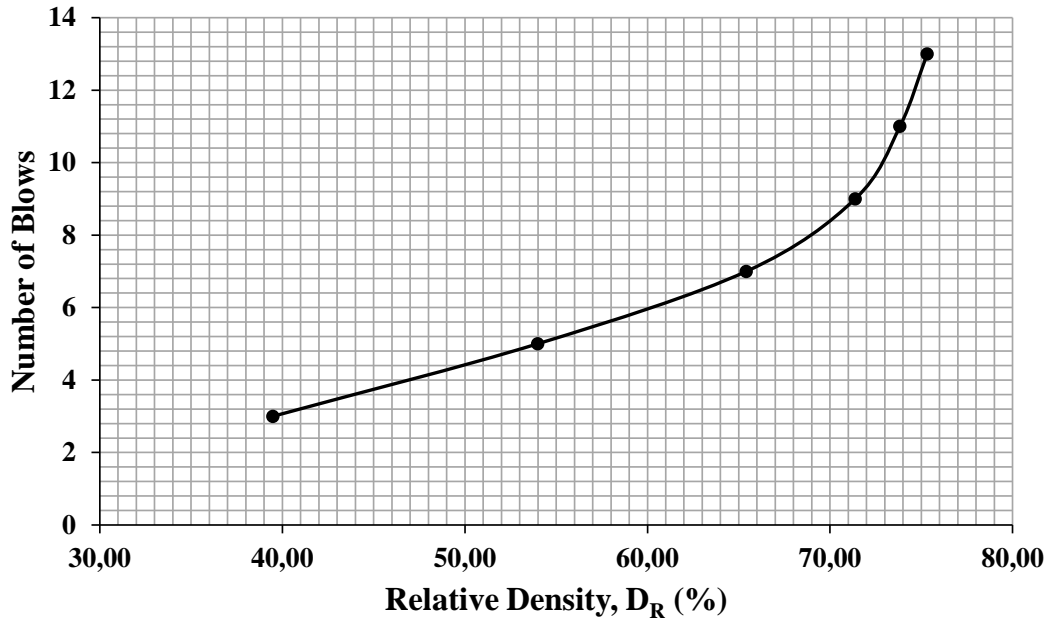
Figure 3.9. Relative density vs. blow count relationship of reconstituted samples prepared with wet tamping

Specimens at 40% relative density can be obtained by 250mm drop height in dry pluviation or by 3 blows in wet tamping. Considering the ease of operation, wet tamping method was chosen for the preparation of loose specimens.

Specimens at 80% relative density could not be obtained by dry pluviation with reasonable drop heights. In wet tamping method, 13 blows with a tamp of 25mm diameter produced 75% relative density specimens. To achieve 80% relative density, 15-20 blows per each of 10 layer with a tamp of 15mm diameter were applied.

All specimens were prepared at 5% water content and the required weight of sand to provide the target densities are determined by using fundamental formulations of soil mechanics. For a certain relative density, corresponding void ratio (e) is defined as:

$$e = e_{max} - D_R \cdot (e_{max} - e_{min}) \tag{3.1}$$

The definition of void ratio is as follows:

$$e = \frac{V_{voids}}{V_{solids}} \tag{3.2}$$

Rearranging Equation 3.2 with the volume of the specimen (V) is equal to the sum of V_{voids} and V_{solids} gives:

$$V_{solids} = \frac{V}{1+e}$$ (3.3)

Required weight of sand to provide the target density is calculated as:

$$W_{solids} = G_S.\frac{V}{1+e}$$ (3.4)

3.3.2. Monotonic Triaxial Testing

3.3.2.1. Apparatus

All static triaxial tests were performed by using the VJ TECH triaxial testing system given in Figure 3.10. System includes the following components:

- A triaxial cell to mould the specimen and apply cell pressure
- A cell pressure unit with pressure transducer to apply and measure the cell pressure throughout the test
- A back pressure unit with to apply back pressure and pressure transducers to measure the back pressure and volume change of the specimen throughout the test
- A load cell to measure the deviatoric load acting on the specimen
- A linear variable displacement transducer (LVDT) to measure the axial deformation of the specimen
- A data logger to monitor the deviatoric load and axial deformation
- A loading unit
- A computer to use the Clisp software

Figure 3.10. Triaxial testing system used in this study

3.3.2.2. Setup of the Specimen

Before beginning to each test, triaxial cell unit was cleaned with a brush to provide water tightness during the test due to any remaining soil particles from previous tests. Moreover, cell pressure, back pressure, pore pressure and top cap valves were also controlled against clogging.

Membrane and O-rings were placed on the mould. Providing that all valves are open and no leakage will occur, mould with membrane and O-rings was placed on the pedestal and specimen was started to be reconstituted. Vacuum pressure was applied to the membrane during reconstitution in order to provide a smooth surface inside the membrane. A filter paper was also placed between the inner surface of the mould and membrane to prevent the membrane from blocking the pores of mould where vacuum pressure is applied.

First pre-boiled porous disc with a circular filter paper was placed at the bottom of the mould and a little de-aired water was dripped to make saturation easier. After that, sand was tamped in layers to the target relative density. Second pre-boiled porous disc with another circular filter paper was placed on the top of the specimen and top cap was placed. Before removing the mould from the specimen, vacuum pressure was shifted from mould to the back pressure valve so that sand specimen remains tight. The 80kPa capacity of the vacuum used in this study was smaller than the pre-determined consolidation pressures, which are 100kPa, 200kPa and 400kPa, and over consolidation of the specimens before shearing was not occurred without needing to use pressure regulator.

Before placing the triaxial cell, the weight of sand used and height and diameter of the specimen were measured to calculate the initial relative density of the specimen. Height and diameter of the specimen were measured three times by using a digital vernier caliper and average values were used in the calculations. Moreover, the inclination of the top cap was checked by using a water gage and stress localization was prevented by providing horizontal top cap such that deviatoric load will be applied only in axial direction and second order moments will not mobilize.

Triaxial cell was placed and filled with water until bleeding was observed from the hole in the top of triaxial cell. The hole was closed with a bolt and 20kPa cell pressure was applied. After that, the 80kPa vacuum pressure inside the specimen was eliminated with de-aired water. For this purpose, a hose filled with de-aired water was connected between back pressure valve and a container filled with de-aired water. Then, back pressure valve was opened and -80kPa pressure was confirmed by pore pressure transducer, which will drop down to zero as the de-aired water filled the pores.

3.3.2.3. Back Pressure Saturation and Consolidation

Saturation of the specimen before consolidation was achieved by back pressure saturation. As the -80kPa vacuum pressure was eliminated and 20kPa cell pressure

was applied to the specimen, back pressure was applied with 100kPa increments. Before each increment, cell pressure was also increased 100kPa so that back pressure was not greater than cell pressure at any step of saturation process. The degree of saturation of the specimen was determined by calculating the B value, which is defined as the ratio of pore pressure increase and cell pressure increase:

$$B = \frac{\Delta u}{\Delta \sigma_3} \tag{3.5}$$

After each 100kPa back pressure increment and about 5 minutes waiting to let the air bubbles inside pores dissolve in the pore water, back pressure valve was closed, pore water pressure was recorded and cell pressure was increased to 20kPa. At the moment that cell pressure on the specimen reached to a value 20kPa higher than the initial value, pore water pressure was recorded again and B value was calculated by using the Equation 3.5. In each test, $B \approx 0.6$ was calculated initially. By applying 100kPa back pressure increments, $B \geq 0.95$ was obtained at 500kPa back pressure. In this study, specimens were considered to be saturated when $B \geq 0.95$ limit is achieved and tests were continued with the consolidation phase.

Before starting the consolidation phase, back pressure valve was closed and predetermined consolidation pressure was applied. Then, back pressure valve was opened and consolidation phase started. Consolidation of the specimen generally finished in a few minutes due to the coarse grained material used. Volume change of the specimen and pore water pressure against time were recorded during the consolidation phase. When the volume changes of the specimens stopped and no further decrease in excess pore water pressures were observed, consolidation phases were finished, total volume change of the specimens were recorded and tests were continued with the shearing phase.

3.3.2.4. Monotonic Loading

After the completion of the consolidation phase, shearing phase was started and specimens were loaded axially with 0.1mm/min strain rate. Applied deviatoric load,

axial deformation, pore water pressure and cell pressure were recorded during static loading and all tests were stopped at about 20% axial strain.

The height and volume of the specimen before loading were recalculated due to the volume change during consolidation.

$$H_c = H_0 \cdot (1 - \varepsilon_a) \tag{3.6}$$

$$\varepsilon_a = \frac{\varepsilon_v}{3} \tag{3.7}$$

$$\varepsilon_v = \frac{\Delta V}{V_0} \tag{3.8}$$

where H_0 is the height of the specimen before consolidation, H_c is the height of the specimen before shearing, ε_a is the axial strain, ε_v is the volumetric strain and ΔV is the volume change of the specimen during consolidation. Combining Equation 3.6, 3.7 and 3.8, height of the specimen before shearing is:

$$H_c = H_0 \cdot (1 - \frac{\Delta V}{3.V_0}) \tag{3.9}$$

Accordingly, area of the specimen before shearing is:

$$A_c = (V_0 - \Delta V)/H_c = A_0 \cdot \frac{1 - \varepsilon_v}{1 - \varepsilon_a} \tag{3.10}$$

where A_0 is the area of the specimen before consolidation and A_c is the area of the specimen before shearing. At any stage of shearing, corrected area of the specimen with respect to axial strain is calculated as:

$$A_c^* = \frac{A_c}{1 - \varepsilon_a} \tag{3.11}$$

where ε_a is the axial strain defined as:

$$\varepsilon_a = \frac{\Delta H}{H_c} \tag{3.12}$$

where ΔH is the axial deformation of the specimen during shearing.

After performing the necessary corrections, deviatoric stress on the specimen is calculated as:

$$\sigma_d = \frac{F}{A_c^*} \tag{3.13}$$

where σ_d is the deviatoric stress acting on the specimen, F is the deviatoric load acting on the specimen and A_c^* is the corrected area of the specimen for corresponding strain level.

In this study, correction for piston friction was not performed. The piston was oiled before tests and was able to slide by its own weight. Therefore, the effect of friction between triaxial cell and piston was ignored. However, due to the relatively high cell pressures applied in test, the effect of the ascending force that try to uplift the piston was considered and corrected deviatoric stress is calculated as:

$$\sigma_d^* = \frac{F}{A_c^*} - \sigma_3 . A_p \tag{3.14}$$

where σ_3 is cell pressure and A_p is the area of the piston.

The major effective stress (σ_1') and minor effective stress (σ_3') are defined as:

$$\sigma_1' = \sigma_{cell} + \sigma_d^* - u \tag{3.15}$$

$$\sigma_3' = \sigma_{cell} - u \tag{3.16}$$

where σ_{cell} is cell pressure and u is pore water pressure. Stress path of each test was determined by plotting mean effective stress (p') against half of deviatoric stress (q) which are defined as:

$$p' = (\sigma_1' + \sigma_3')/2 \tag{3.17}$$

$$q = (\sigma_1' - \sigma_3')/2 = \sigma_d^*/2 \tag{3.18}$$

3.3.2.5. Results

The consolidation pressure (σ_c), amount of WD-40 used in the specimen preparation, void ratio and corresponding relative density before consolidation phase ($e_{initial}$,

$D_{R, \, initial}$) and before shear phase (e_{final}, $D_{R, \, final}$), axial strain at failure ($\varepsilon_{a, \, failure}$) and calculated effective internal friction angle of each test are summarized Table 6:

Table 6. Summary of Triaxial Test Results

Test	σ_c (kPa)	WD-40 (%) by mass	$e_{initial}$	$D_{R, \, cons}$ (%)	ΔV (ml)	e_{final}	$D_{R, \, shear}$ (%)	$\varepsilon_{a, \, failure}$ (%)	ϕ' (°)
STXD_01	100	0	0,602	78,9	0,26	0,597	80,4	3,3	40,0
STXD_02	200	0	0,601	79,2	0,53	0,592	82,2	3,1	40,0
STXD_03	400	0	0,604	78,4	1,03	0,585	84,3	4,2	39,0
STXD_04	100	1	0,590	82,8	0,31	0,584	84,6	3,9	39,6
STXD_05	200	1	0,593	81,8	0,60	0,582	85,2	2,6	40,4
STXD_06	400	1	0,598	80,4	0,95	0,580	85,7	3,4	39,1
STXD_07	100	2	0,596	80,9	0,35	0,589	82,9	2,4	40,5
STXD_08	200	2	0,606	77,7	0,53	0,596	80,8	3,3	40,0
STXD_09	400	2	0,603	78,7	0,84	0,588	83,5	3,8	38,7
STXL_01	100	0	0,719	42,9	0,43	0,710	45,5	4,6	35,3
STXL_02	200	0	0,732	38,9	1,03	0,711	45,2	5,5	32,5
STXL_03	400	0	0,731	38,9	1,54	0,701	48,4	9,8	33,8
STXL_04	100	1	0,730	39,4	0,39	0,722	41,8	8,9	34,2
STXL_05	200	1	0,726	40,7	0,76	0,710	45,4	5,7	35,0
STXL_06	400	1	0,732	38,9	1,30	0,706	46,7	10,3	33,8
STXL_07	100	2	0,728	40,1	0,35	0,721	42,3	8,5	34,5
STXL_08	200	2	0,730	39,3	0,81	0,714	44,3	5,8	34,0
STXL_09	400	2	0,727	40,3	1,50	0,697	49,6	10,2	32,8

Major and minor effective stresses, excess pore water pressure and strain at the time of failure of each test are determined by applying maximum stress obliquity criterion. Individual results of each test containing half of deviatoric stress vs. axial strain, half

of deviatoric stress vs. mean effective stress, effective vertical stress vs. shear stress, excess pore water pressure vs. axial strain and stress obliquity vs. mean effective stress graphs are presented in Figures 3.11 through 3.28. In each graph, stress, strain and ratio values and Mohr circle corresponding to failure moment (maximum principal stress ratio) are sketched.
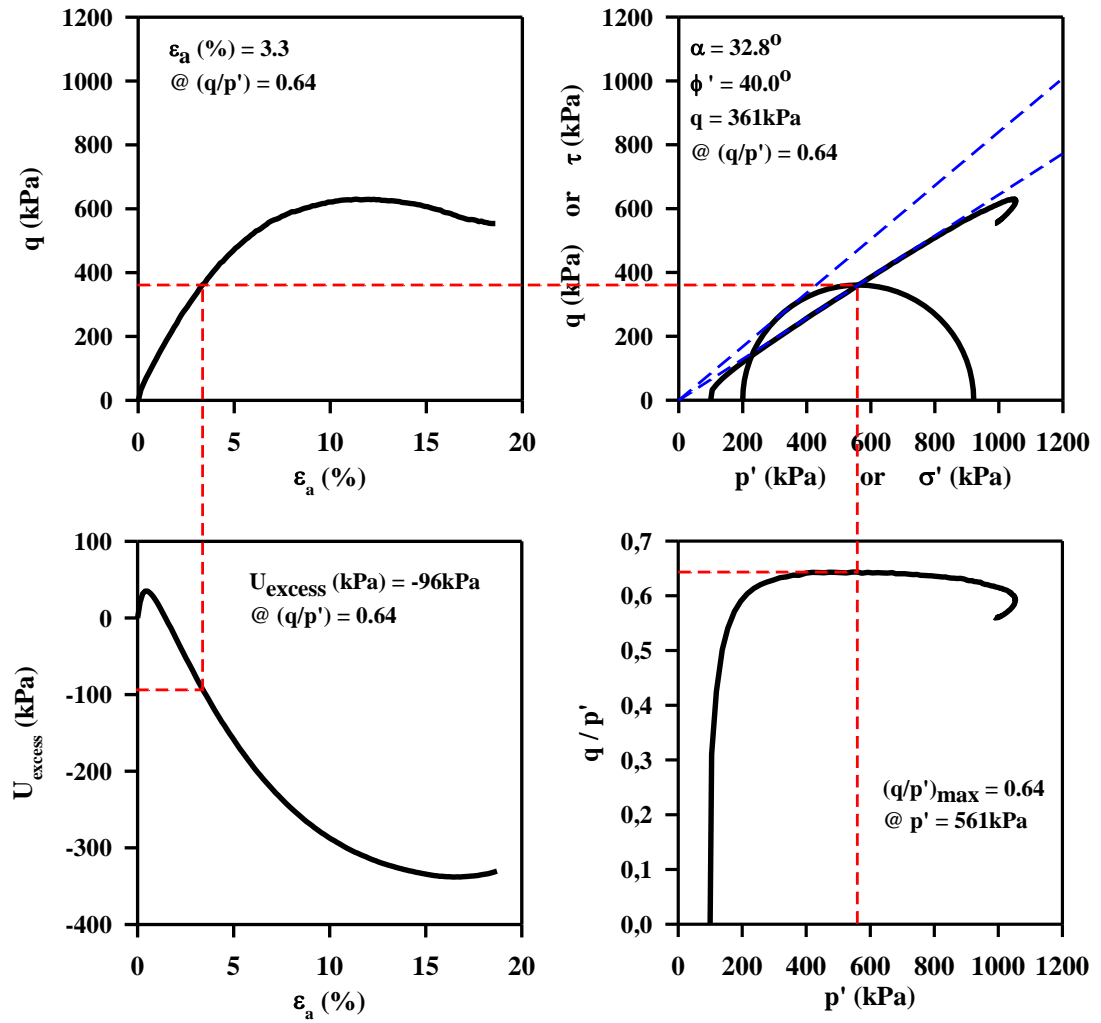
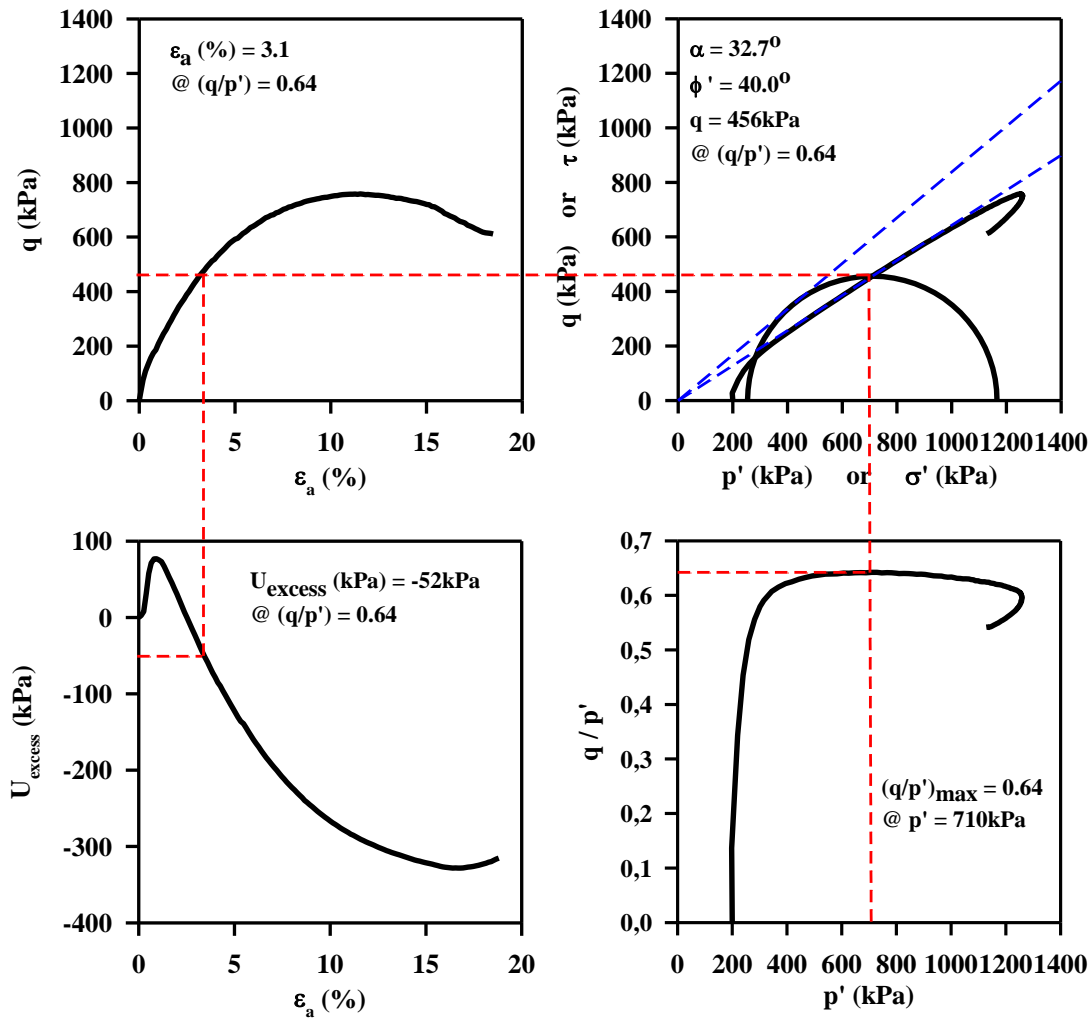**Figure 3.11. 4 Way plots of test STXD_01**
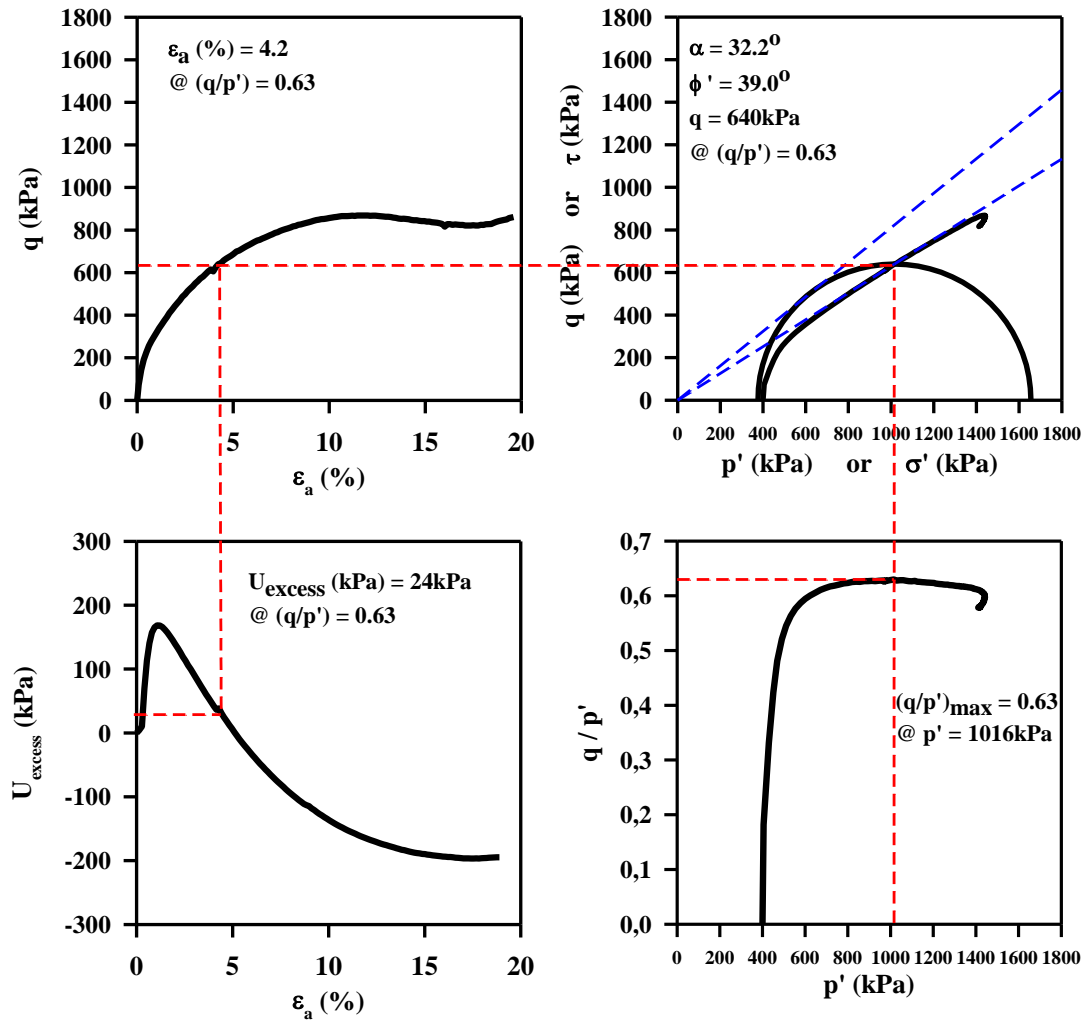
Figure 3.12. 4 Way plots of test STXD_02

Figure 3.13. 4 Way plots of test STXD_03
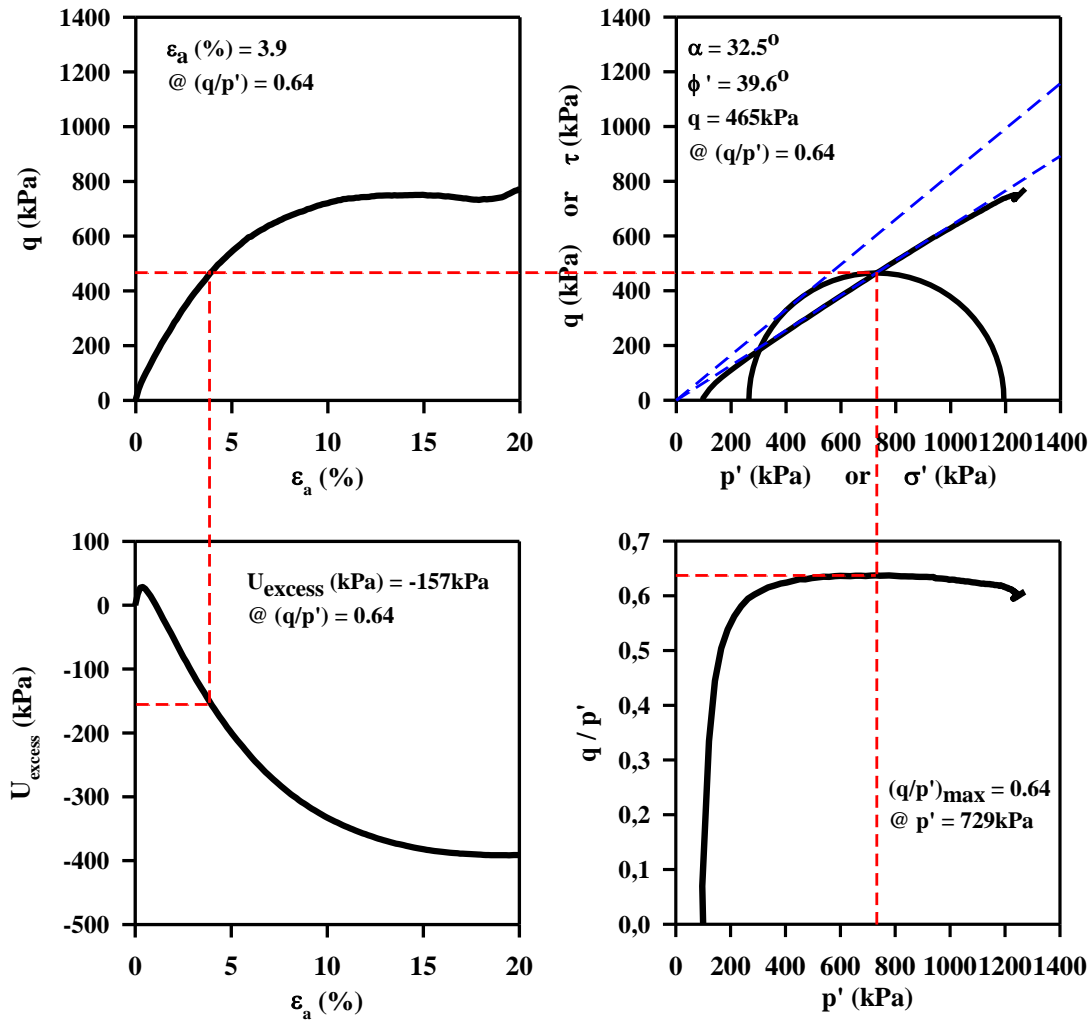
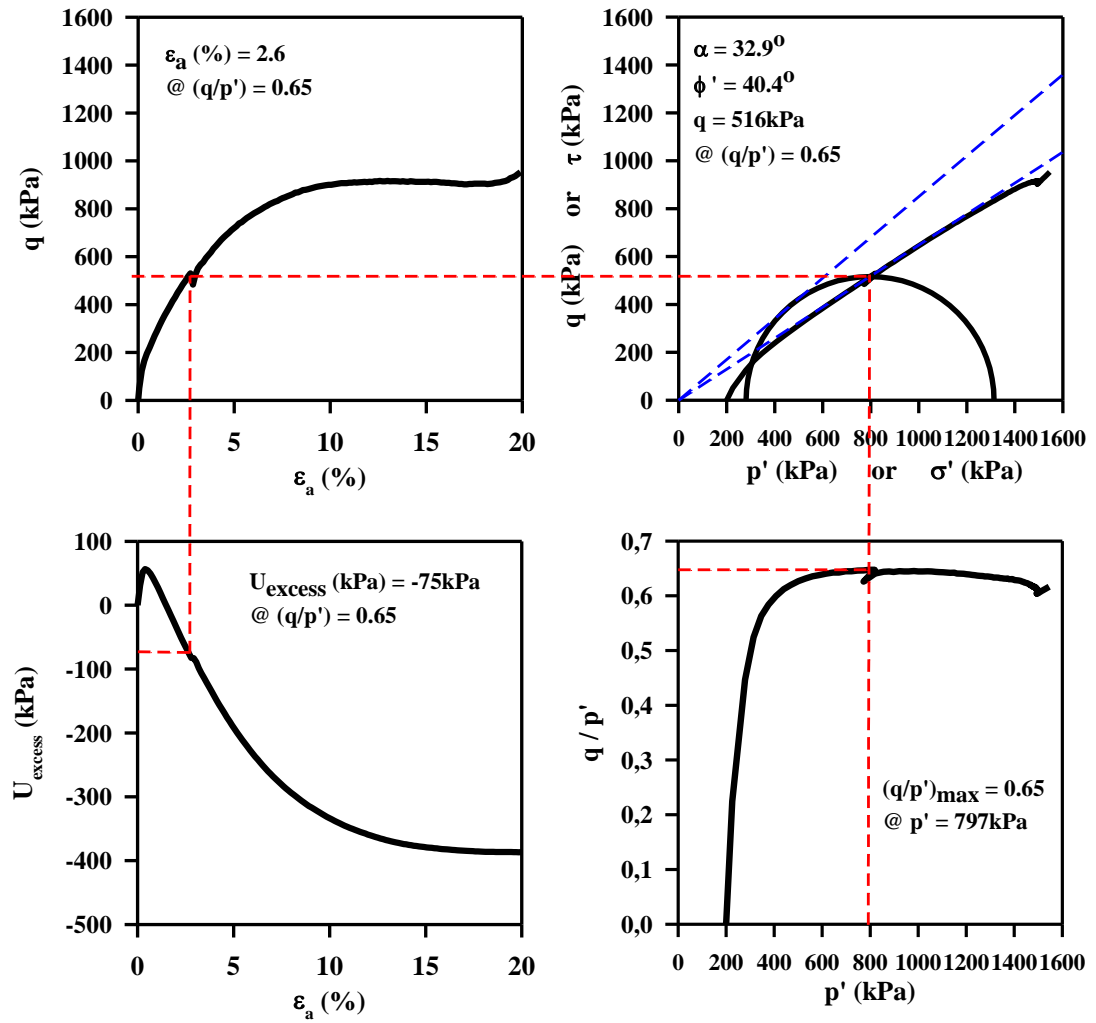**Figure 3.14. 4 Way plots of test STXD_04**

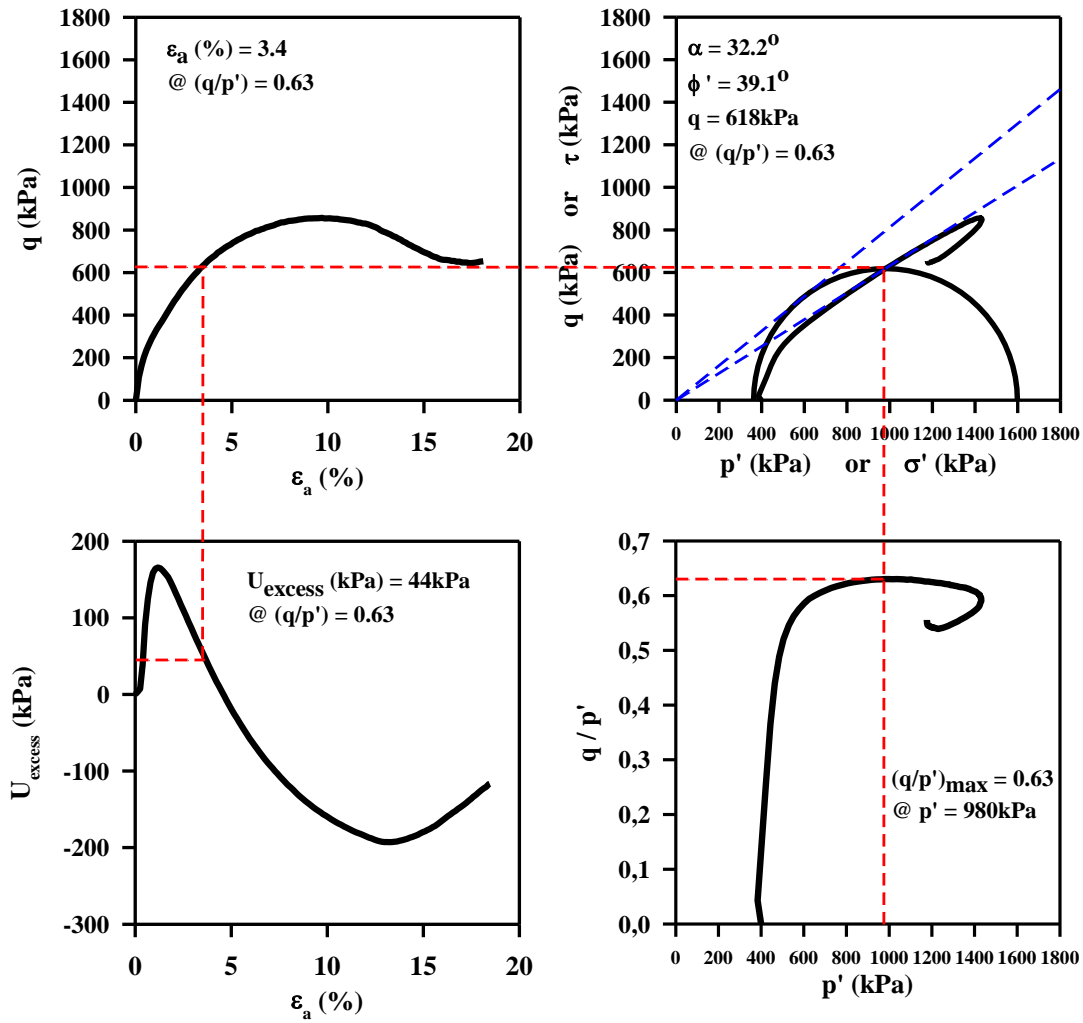**Figure 3.15. 4 Way plots of test STXD_05**

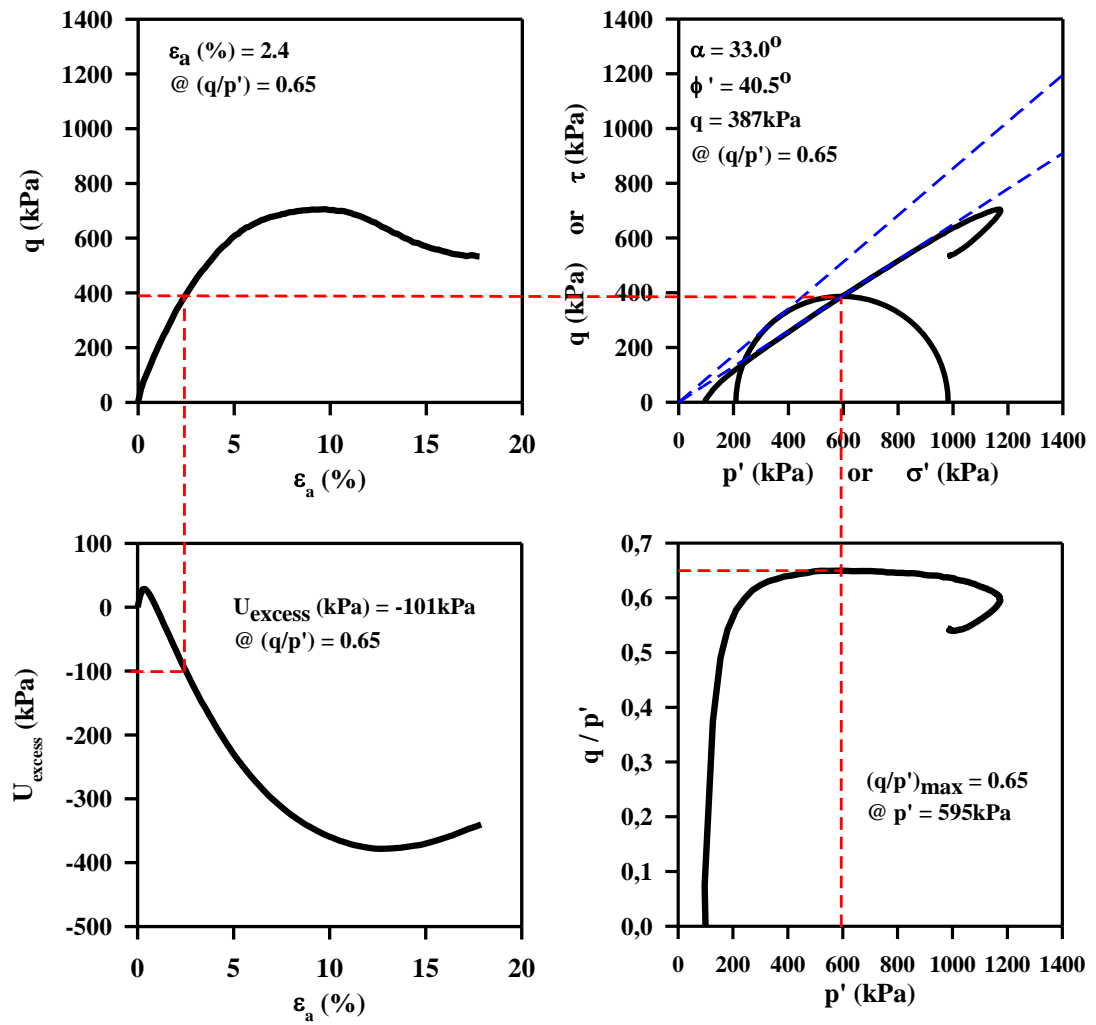**Figure 3.16. 4 Way plots of test STXD_06**

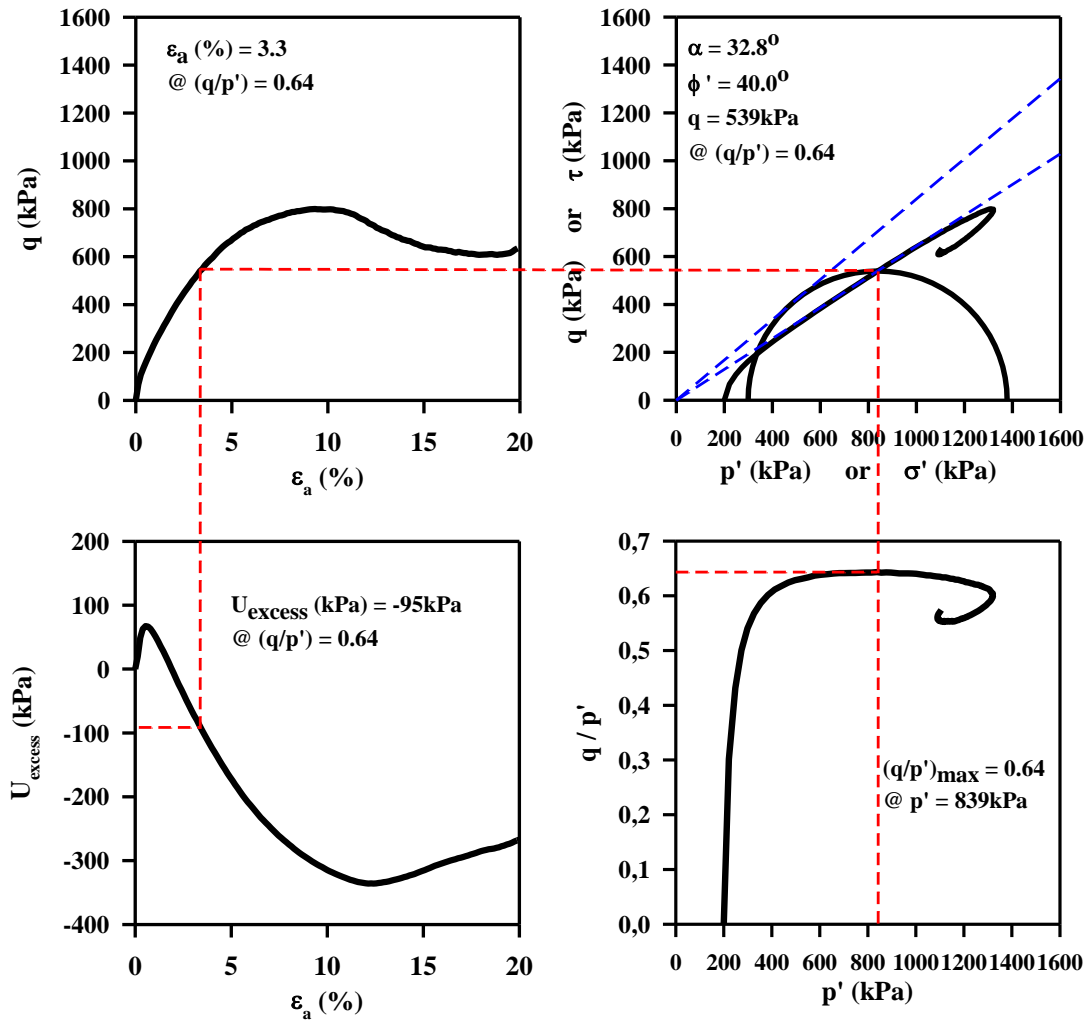**Figure 3.17. 4 Way plots of test STXD_07**

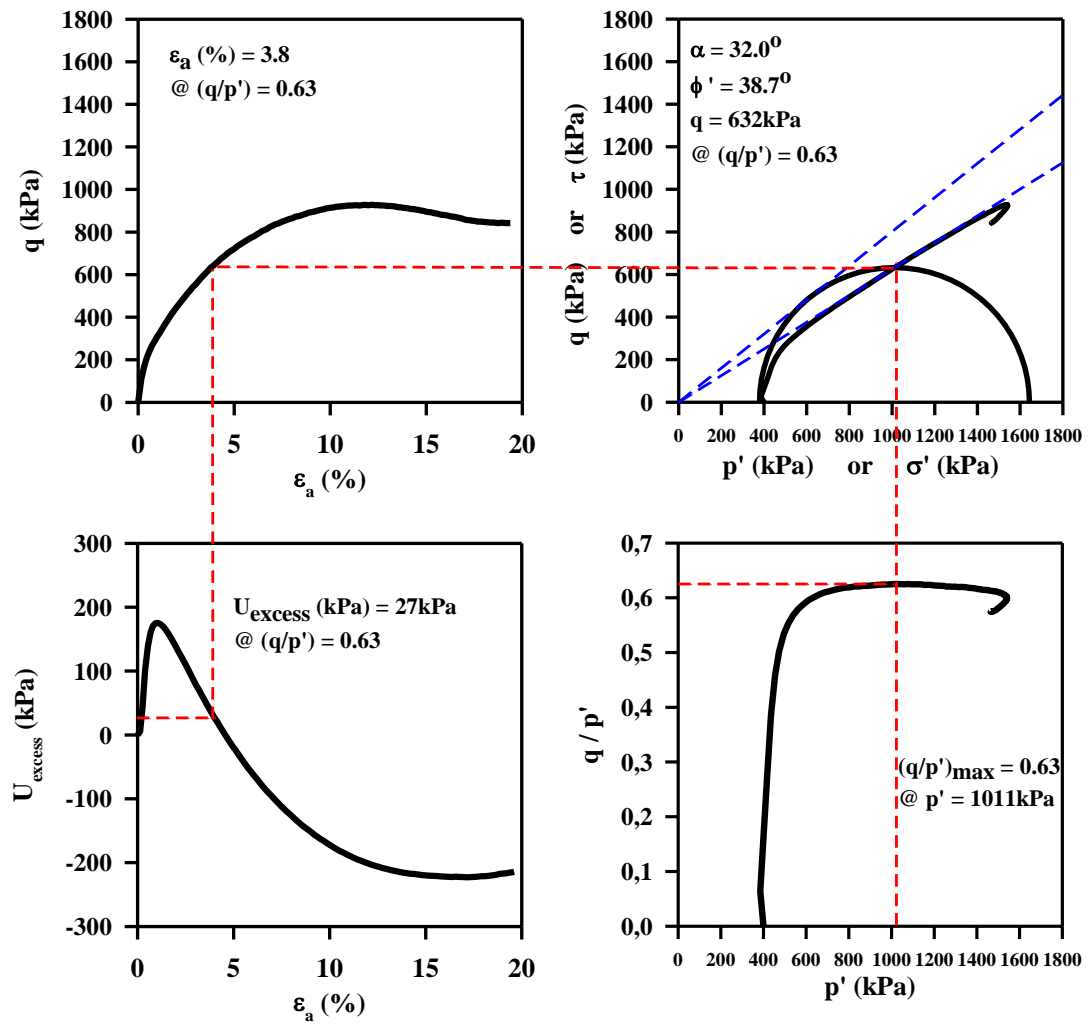**Figure 3.18. 4 Way plots of test STXD_08**
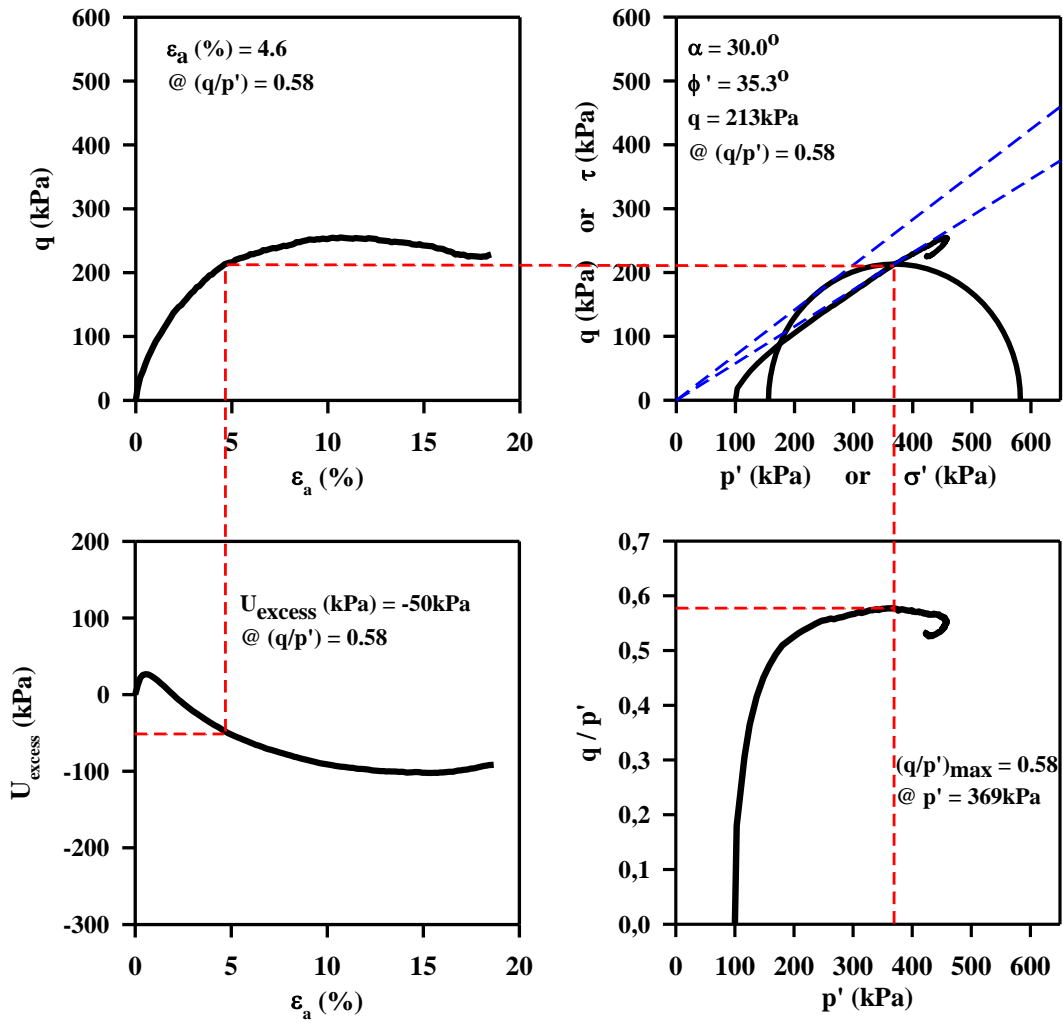
Figure 3.19. 4 Way plots of test STXD_09
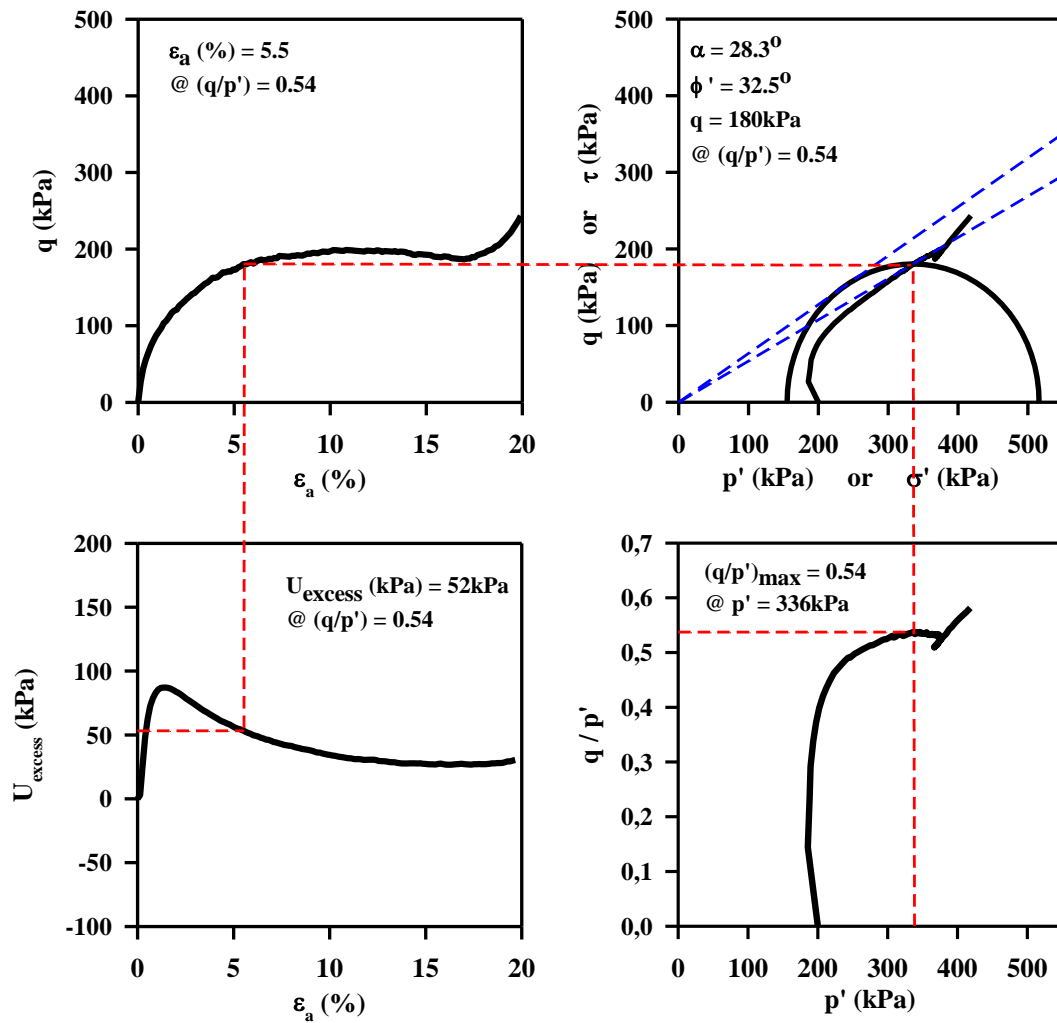
Figure 3.20. 4 Way plots of test STXL_01

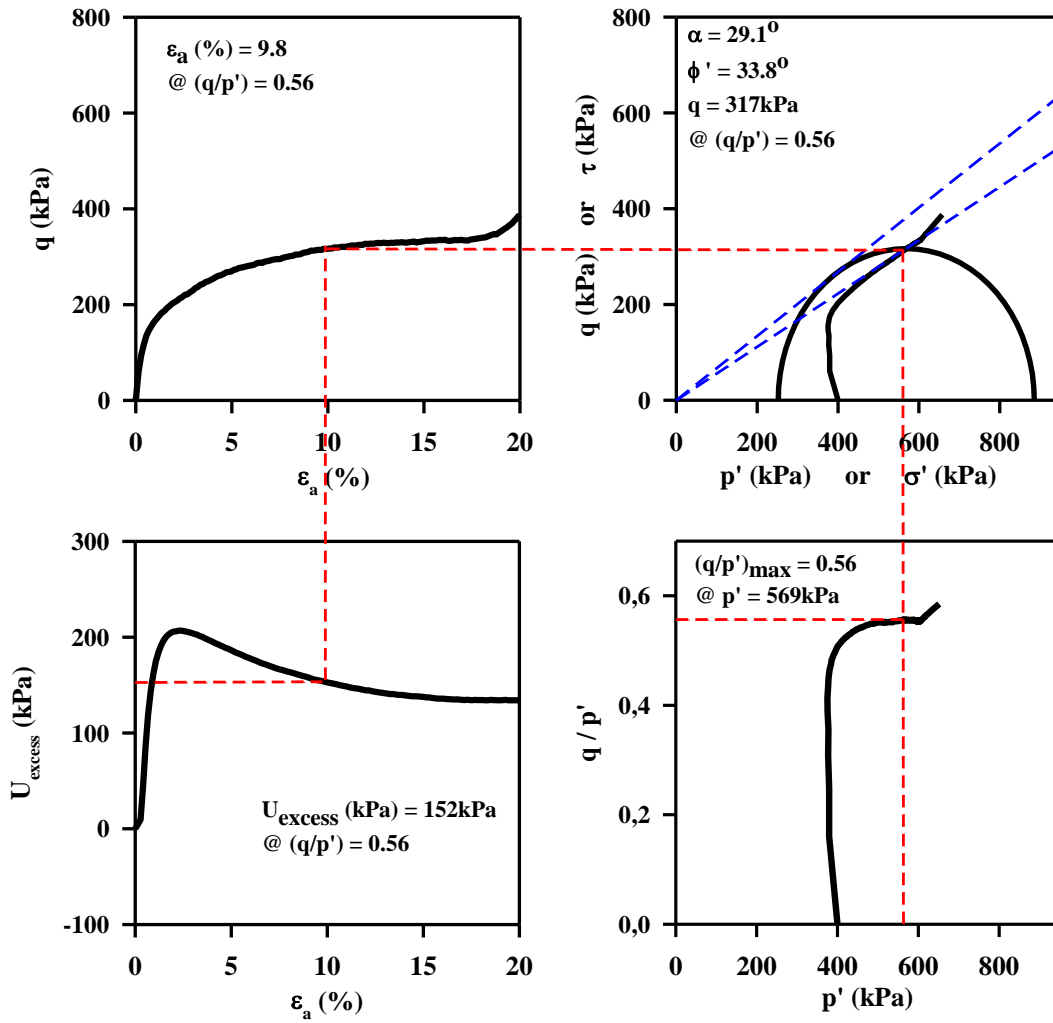**Figure 3.21. 4 Way plots of test STXL_02**

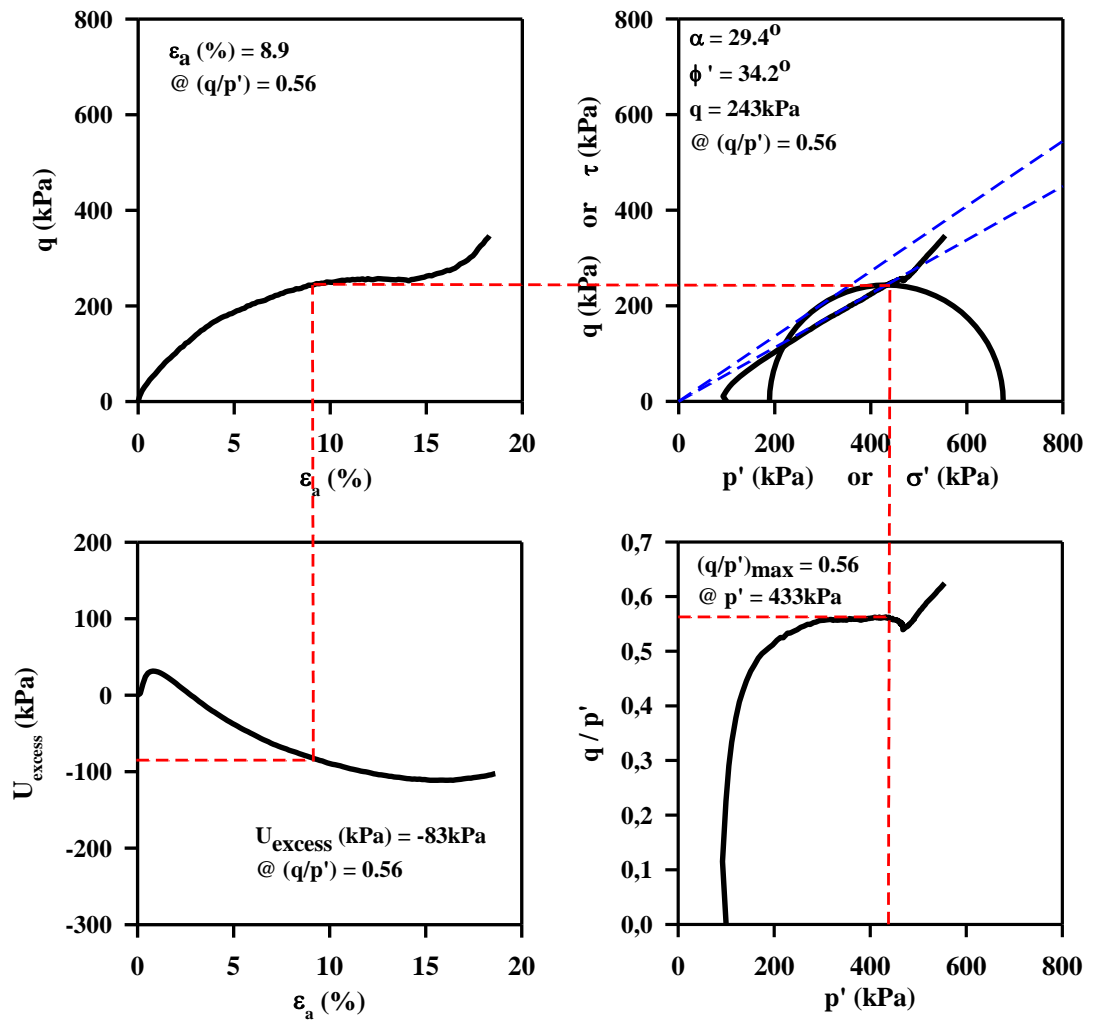**Figure 3.22. 4 Way plots of test STXL_03**

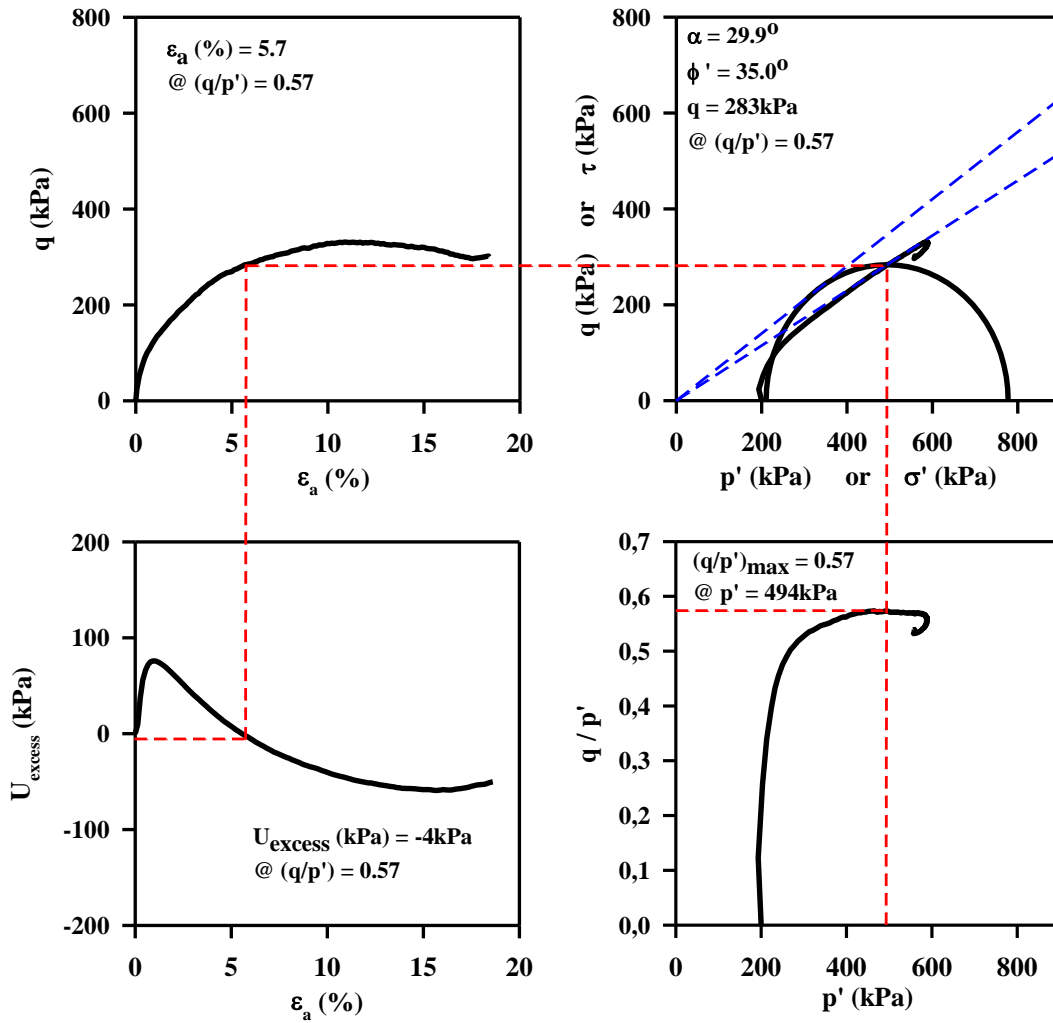**Figure 3.23. 4 Way plots of test STXL_04**

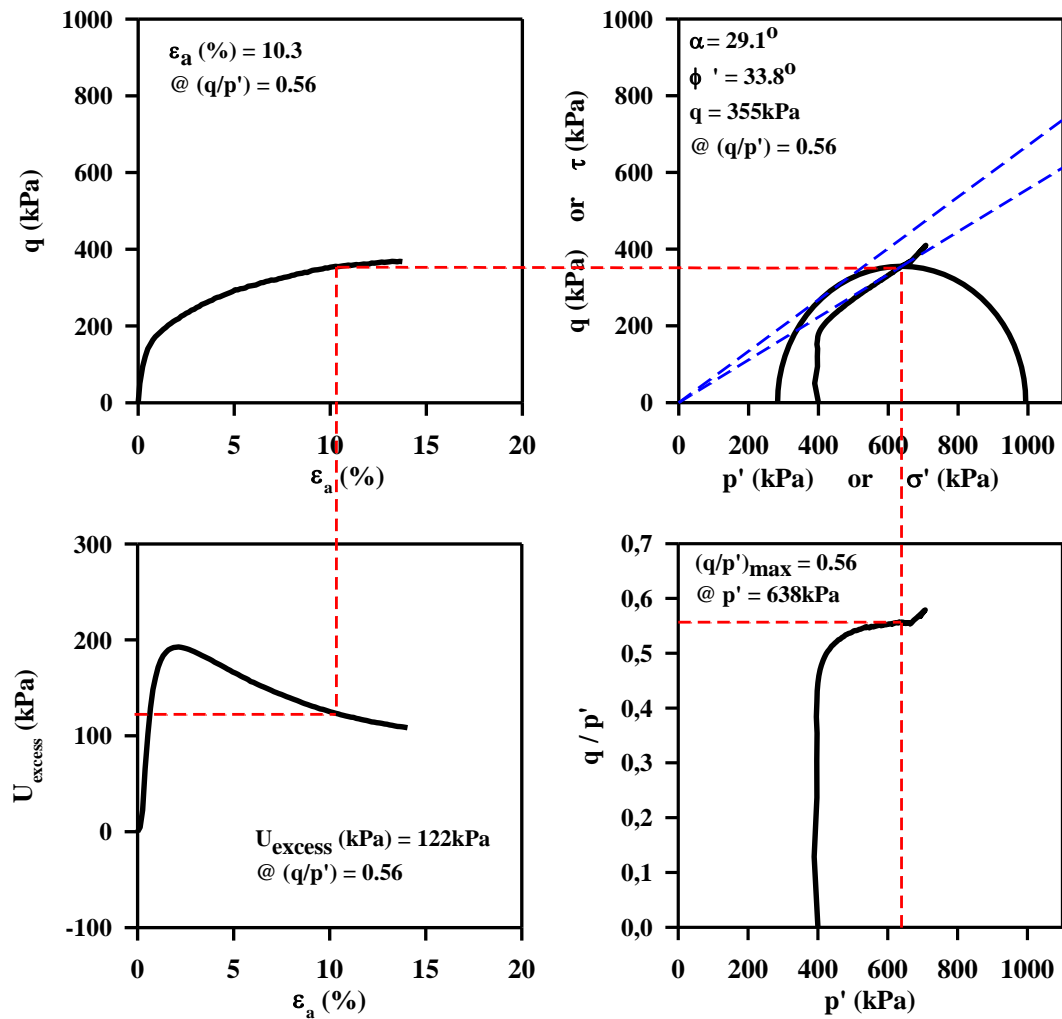**Figure 3.24. 4 Way plots of test STXL_05**
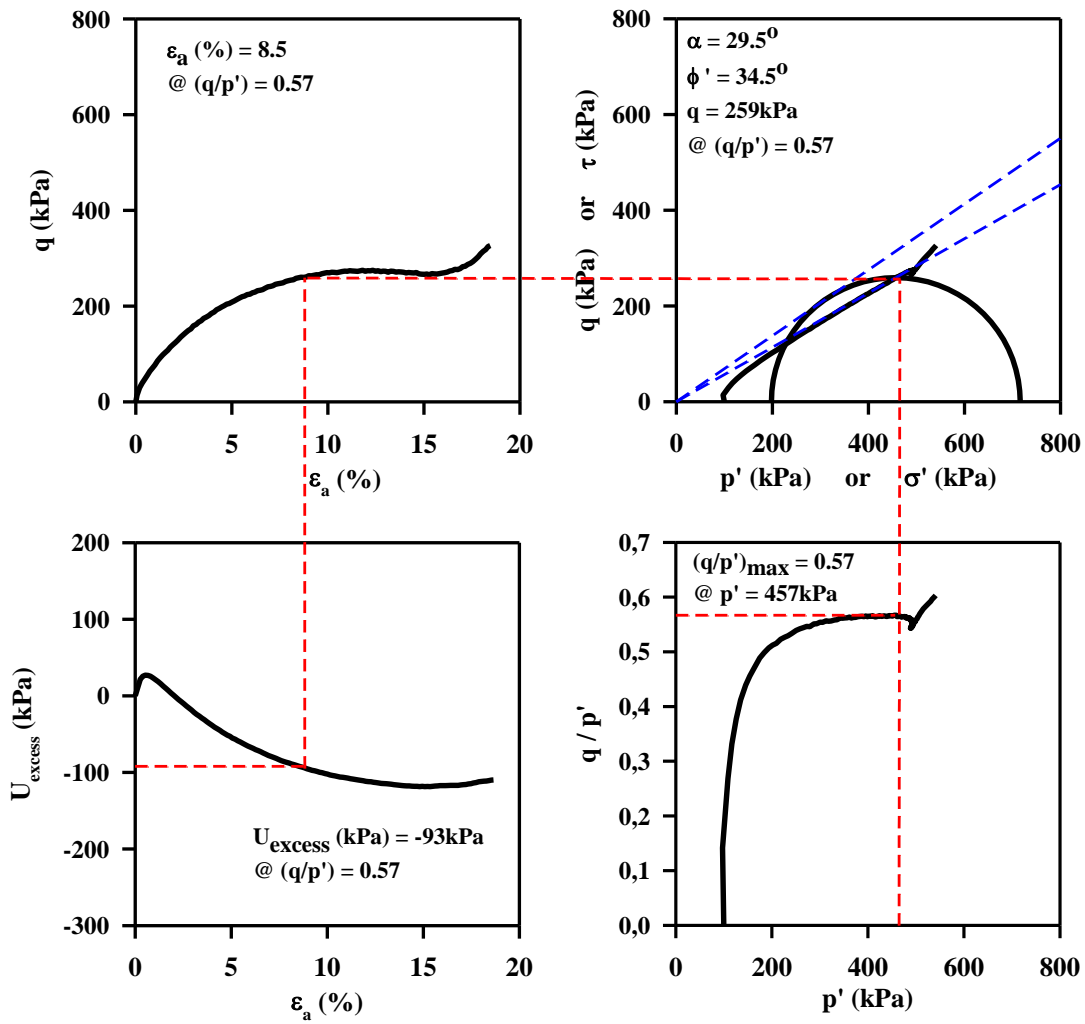
Figure 3.25. 4 Way plots of test STXL_06

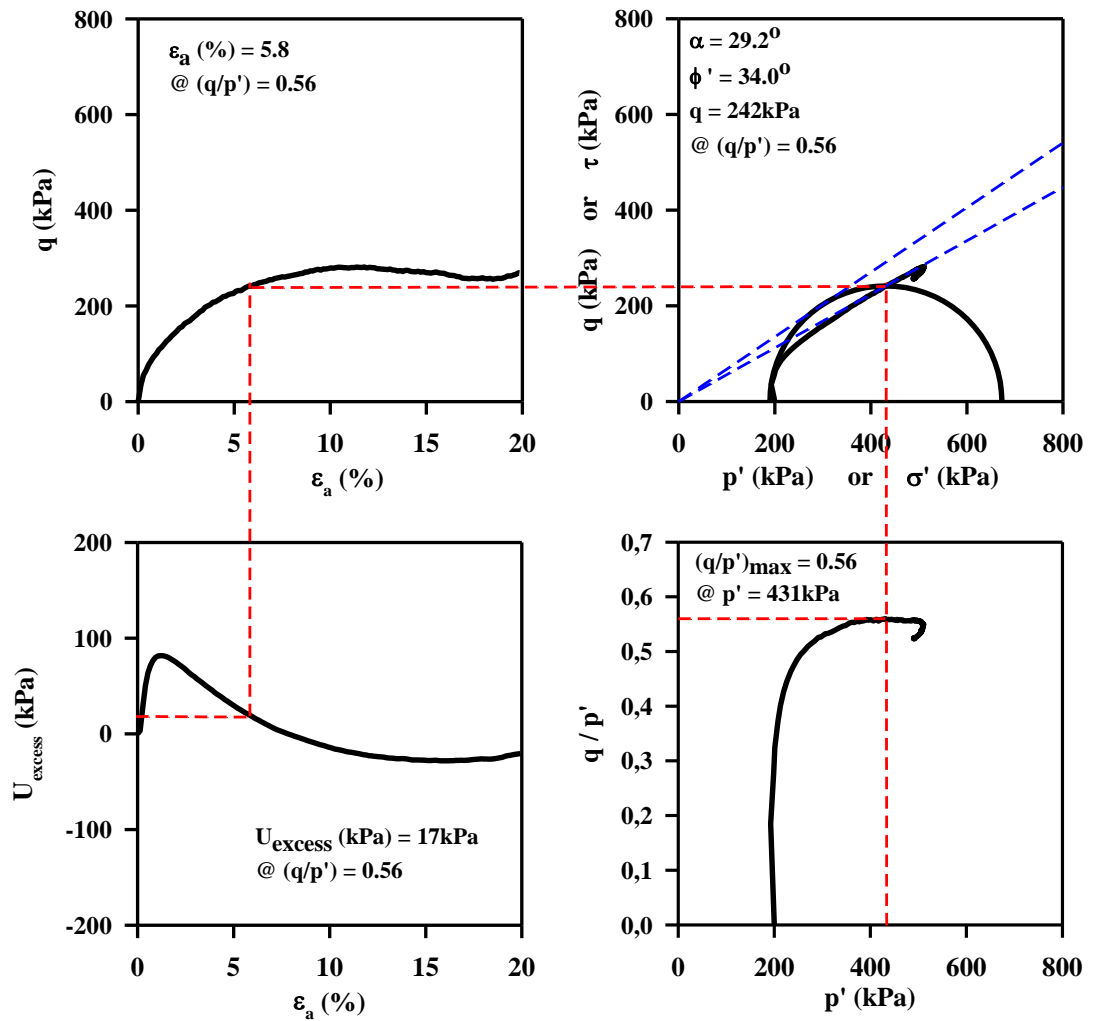**Figure 3.26. 4 Way plots of test STXL_07**
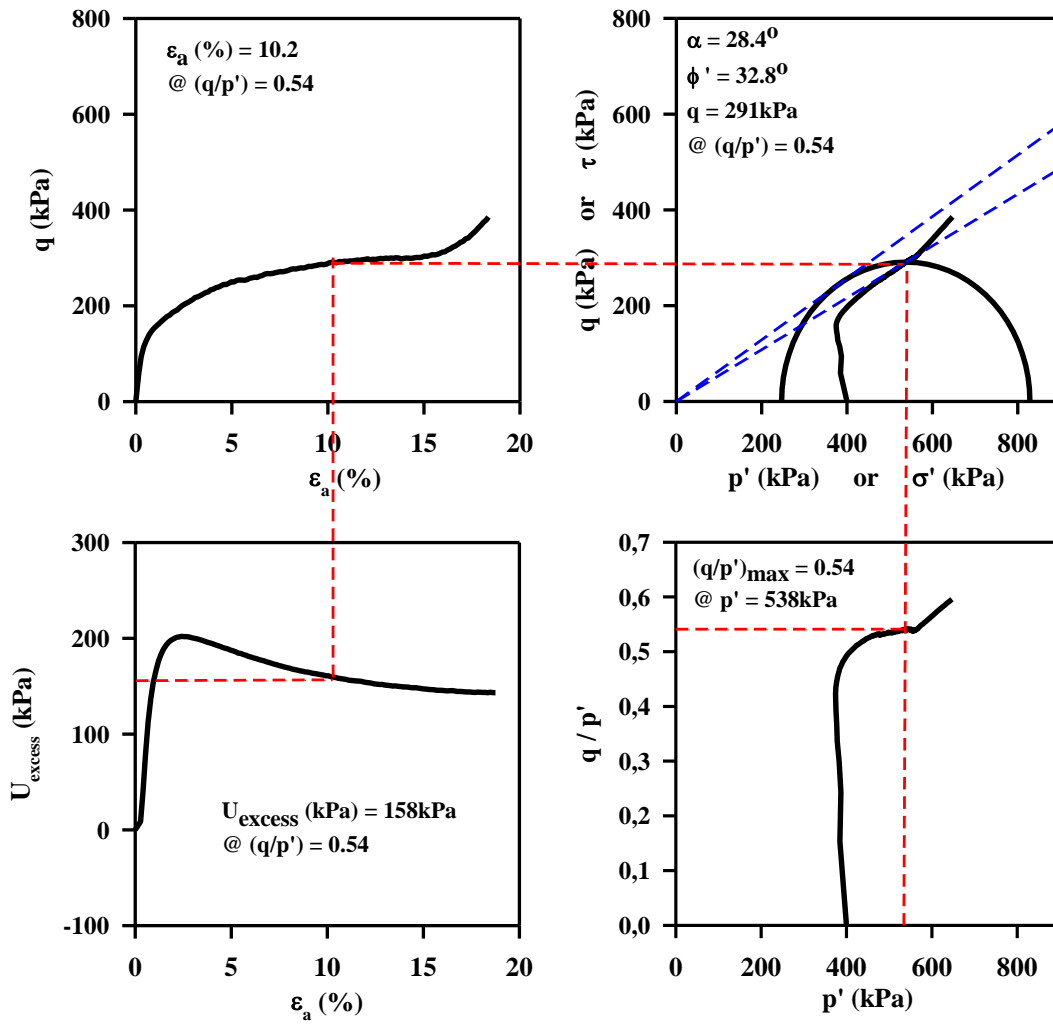
Figure 3.27. 4 Way plots of test STXL_08

Figure 3.28. 4 Way plots of test STXL_09

76

CHAPTER 4

INTERPRETATION OF RESULTS

4.1. Introduction

In this chapter, results of triaxial test were compared to determine the effect of hydrophobicity on the straining and strength responses of sands at different stress and density states. For this purpose, comparative graphs containing the Mohr Circles, half of deviatoric stress vs. axial strain and excess pore water pressure vs. axial strain data of individual tests were replotted. The main motivation behind this is to investigate the effect of hydrophobicity on the strength and straining response of relatively dense samples and relatively loose samples.

4.2. Effect of Hydrophobicity on the Strength of Relatively Dense Samples

To examine the effect hydrophobicity on the strength of relatively dense samples, Mohr circles and common shear strength envelope of samples prepared at 80% target relative density and consolidated under different pressure levels are plotted for WD-40 amount of 0%, 1% and 2%, respectively as given in Figures 4.1, 4.2 and 4.3. The comparison of shear strength envelopes reveals that effective internal friction angles of samples with different WD-40 amounts are about 39.7° and it can be inferred that hydrophobicity do not have a significant effect on the strength of sands at relatively high densities.
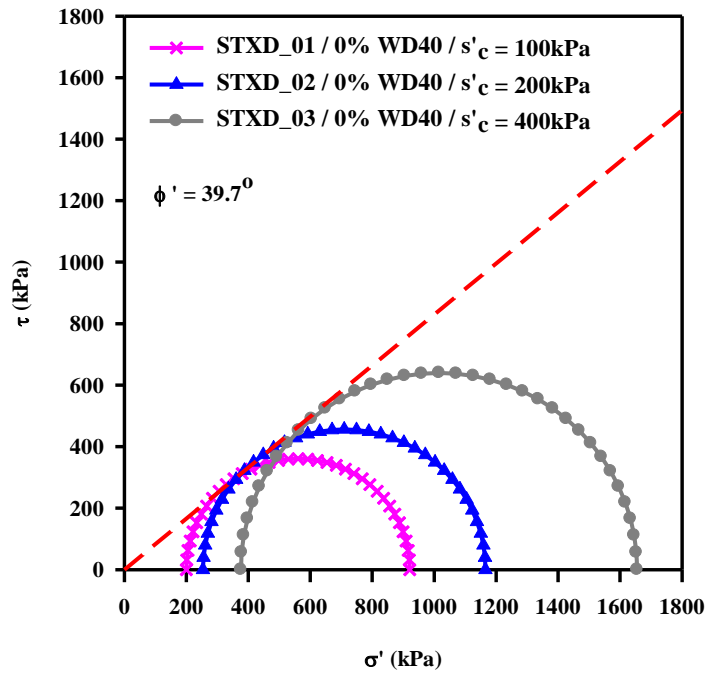
77

Figure 4.1. Mohr circles and shear strength Envelope of test STXD_01, STXD_02 and STXD_03 ($D_R \cong 80\%$)

Figure 4.2. Mohr circles and shear strength envelope of tests STXD_04, STXD_05 and STXD_06 ($D_R \cong 80\%$)

78

Figure 4.3. Mohr circles and shear strength envelope of tests STXD_07, STXD_08 and STXD_09 (D$_R$ ≅ 80%)

This observation seems inconsistent with available literature. Kim et al. (2013) and Byun and Lee (2012) stated that hydrophobic agents similar to WD-40 reduced the shear strength of sand samples in direct shear tests. However, unlike the undrained triaxial tests performed in this study, direct shear tests are drained tests. In undrained triaxial tests, hydrophobic agent decreases effective stress-based shear strength parameter (i.e.: friction angle) but increases the dilatancy (i.e.: reduces excess pore pressure), interaction of which compensates and leads to a practically unaffected shear strength. In simpler terms, decrease in shear strength parameter due to hydrophobic agent was balanced with additional strength due to increase in dilation. However, this conclusion is only valid for the type and the amount of lubricant used in this study. This response is illustrated in Equation 4.1:

$$\tau_{ff} = \sigma'_{ff}.tan\varPhi' = (\sigma - u_{ff}).tan\varPhi' \tag{4.1}$$

79

During the direct shear test, which is a drained test, effective stress remains constant. Hence, hydrophobic agent only reduces the friction which in turn lead to a reduction in shear strength.

4.3. Effect of Hydrophobicity on the Strength of Relatively Loose Samples

To examine the effect hydrophobicity on the strength of relatively loose samples, Mohr circles and common shear strength envelope of samples prepared at 40% target relative density and consolidated under different pressure levels are plotted for WD-40 amount of 0%, 1% and 2%, respectively (Figure 4.4, 4.5 and 4.6). The comparison of shear strength envelopes reveals that effective internal friction angles of samples with different WD-40 amounts are about 34° and it can be inferred that hydrophobicity again does not have a significant effect on the shear strength of sands at relatively loose densities.

Figure 4.4. Mohr circles and shear strength envelope of tests STXL_01, STXL_02 and STXL_03 ($D_R \cong 40\%$)
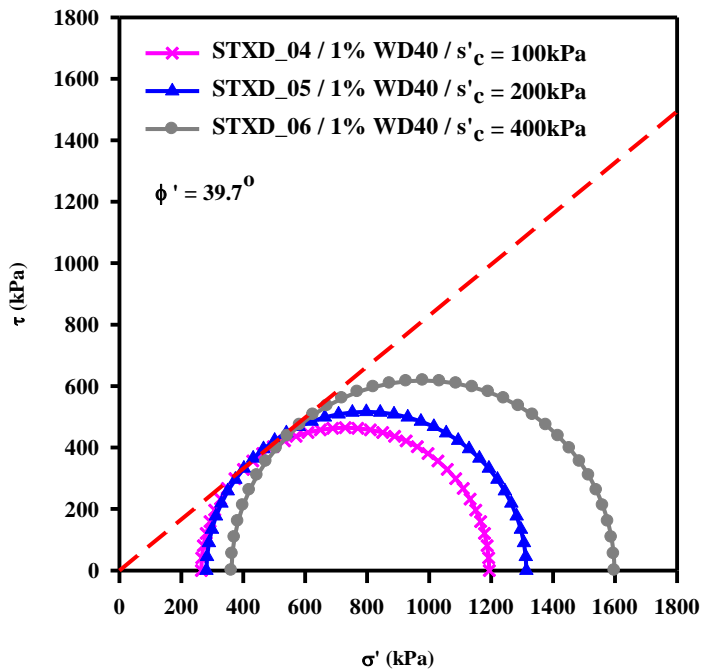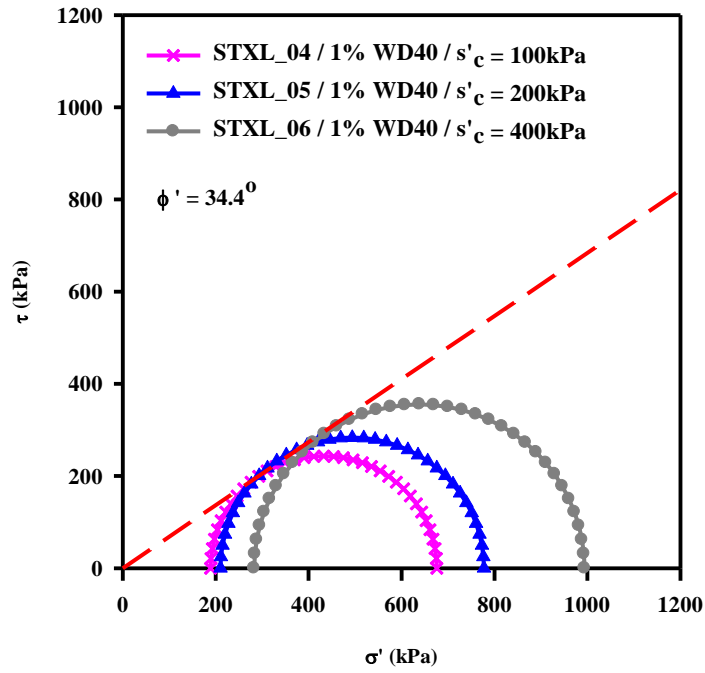
Figure 4.5. Mohr circles and shear strength envelope of tests STXL_04, STXL_05 and STXL_06 ($D_R \cong 40\%$)
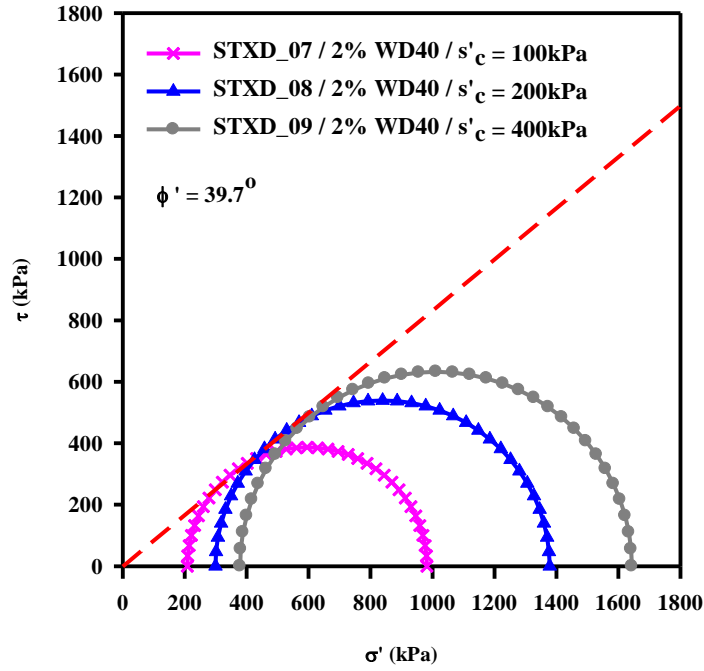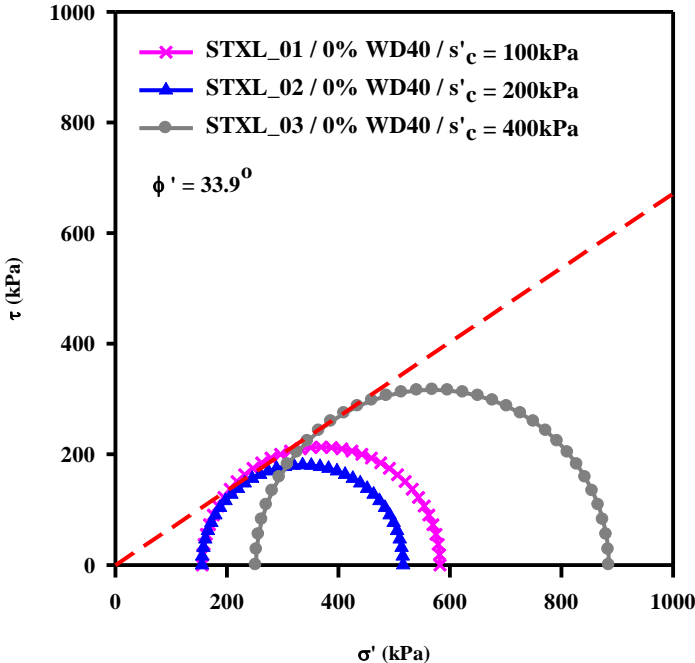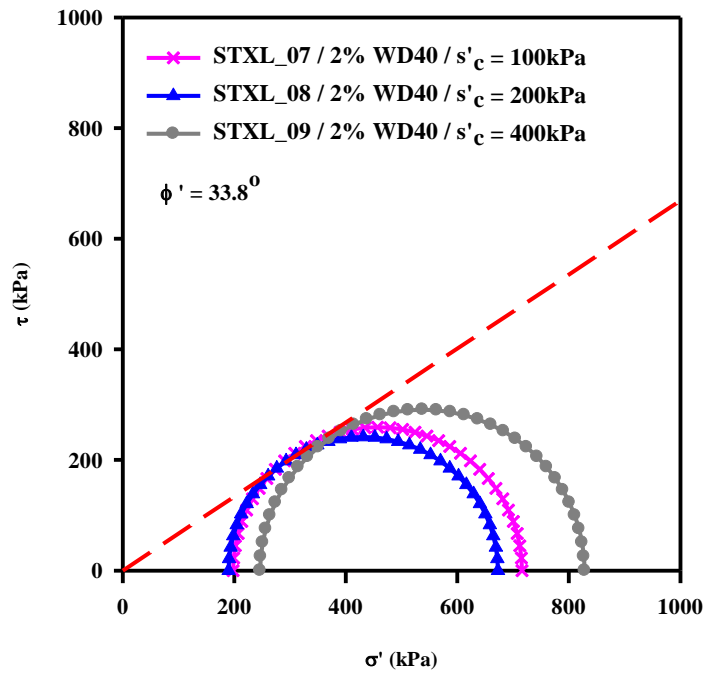

Figure 4.6. Mohr circles and shear strength envelope of tests STXL_07, STXL_08 and STXL_09 ($D_R \cong 40\%$)

4.4. Effect of Hydrophobicity on the Straining Response of Relatively Dense Samples

To examine the effect hydrophobicity on the straining response of relatively dense samples, half of deviatoric stress vs. axial strain and excess pore water pressure vs. axial strain graphs of samples prepared at 80% target relative density and consolidated under same pressure levels are plotted for WD-40 amount of 0%, 1% and 2%, respectively (Figure 4.7, 4.8 and 4.9). The comparison reveals that tendency to suck water into specimen (dilation) usually increases in the presence of WD-40 amount of 1% and reduces if this amount is increased to 2 %. It can be inferred that hydrophobicity (up to addition of 1% WD-40) increases the dilatancy of sands at relatively high densities. This effect is more pronounced at low confining pressures (~100kPa) since sample is more dilative, and decreases with increasing confining stress levels.

Figure 4.7. Comparison of responses of tests STXD_01, STXD_04 and STXD_07 ($D_R \cong 80\%$)

Figure 4.8. Comparison of responses of tests STXD_02, STXD_05 and STXD_08 ($D_R \cong 80\%$)

Figure 4.9. Comparison of responses of tests STXD_03, STXD_06 and STXD_09 (D$_R \cong$ 80%)

4.5. Effect of Hydrophobicity on the Straining Response of Relatively Loose Samples

To examine the effect hydrophobicity on the straining response of relatively loose samples, half of deviatoric stress vs. axial strain and excess pore water pressure vs. axial strain graphs of samples prepared at 40% target relative density and consolidated under same pressure levels are plotted for WD-40 amount of 0%, 1% and 2%, respectively (Figure 4.10, 4.11 and 4.12). The comparison reveals that tendency to suck water into specimen (dilation) usually increases in the presence of

WD-40 amount of 1% and reduces if this amount is increased to 2 %. It can be inferred that hydrophobicity (up to addition of 1% WD-40) increases the dilatancy of sands at relatively loose densities.

Figure 4.10. Comparison of responses of tests STXL_01, STXL_04 and STXL_07 ($D_R \cong 40\%$)

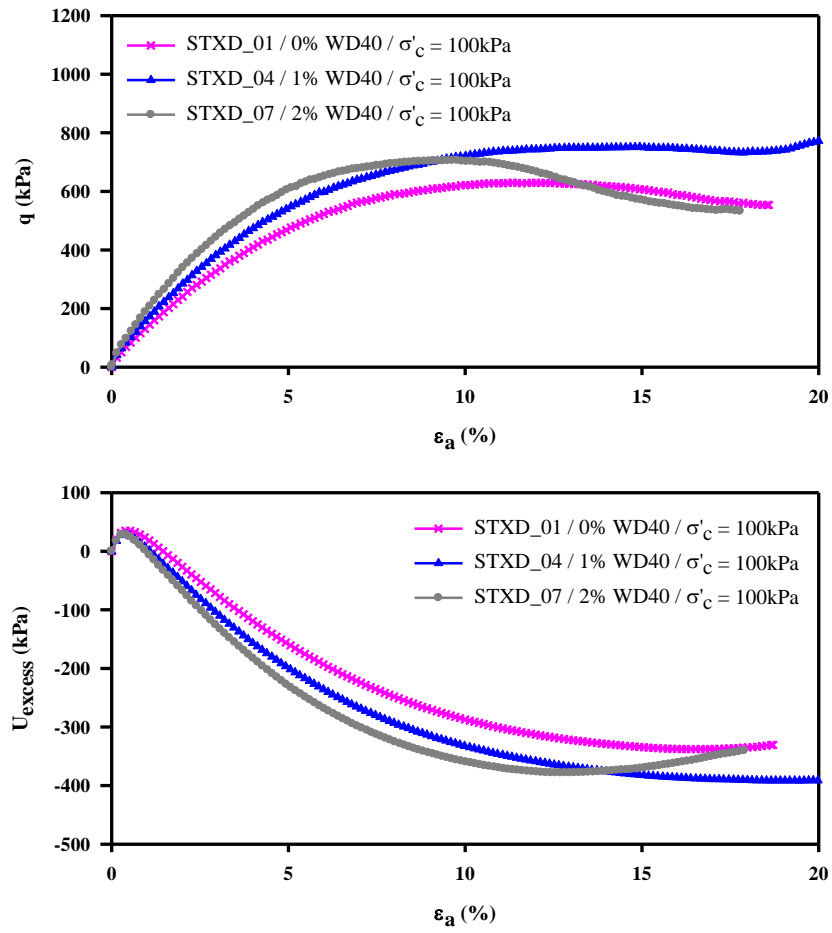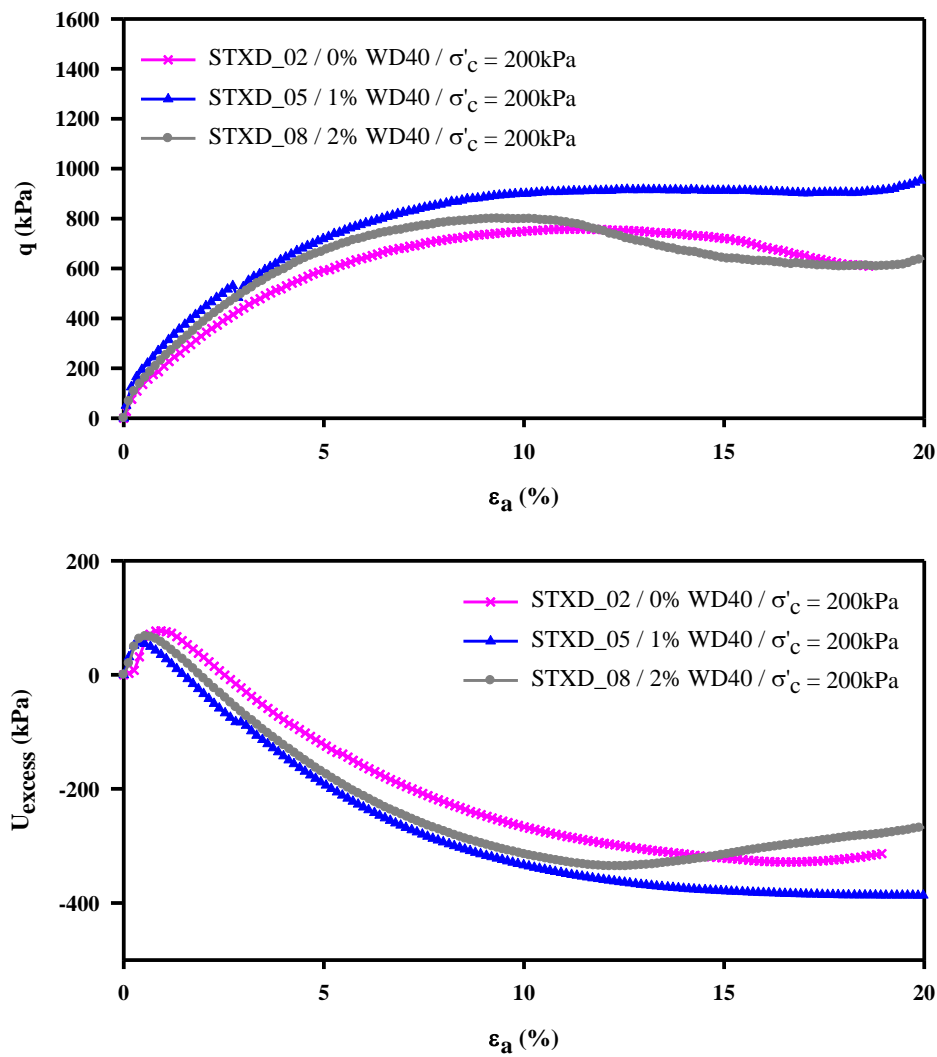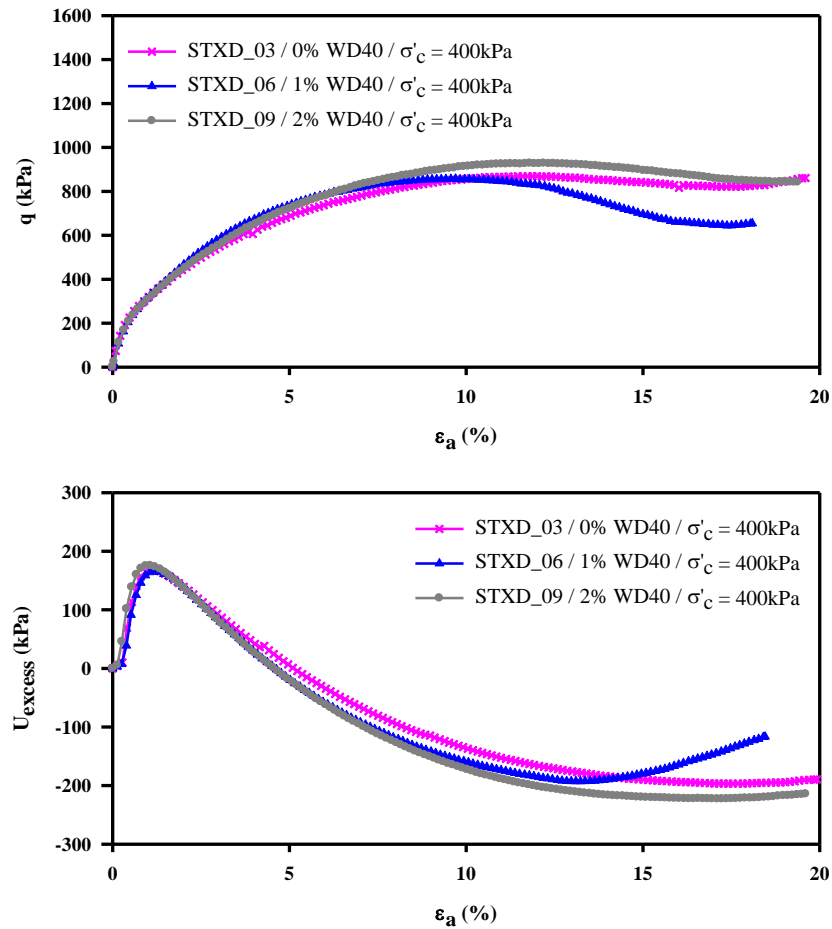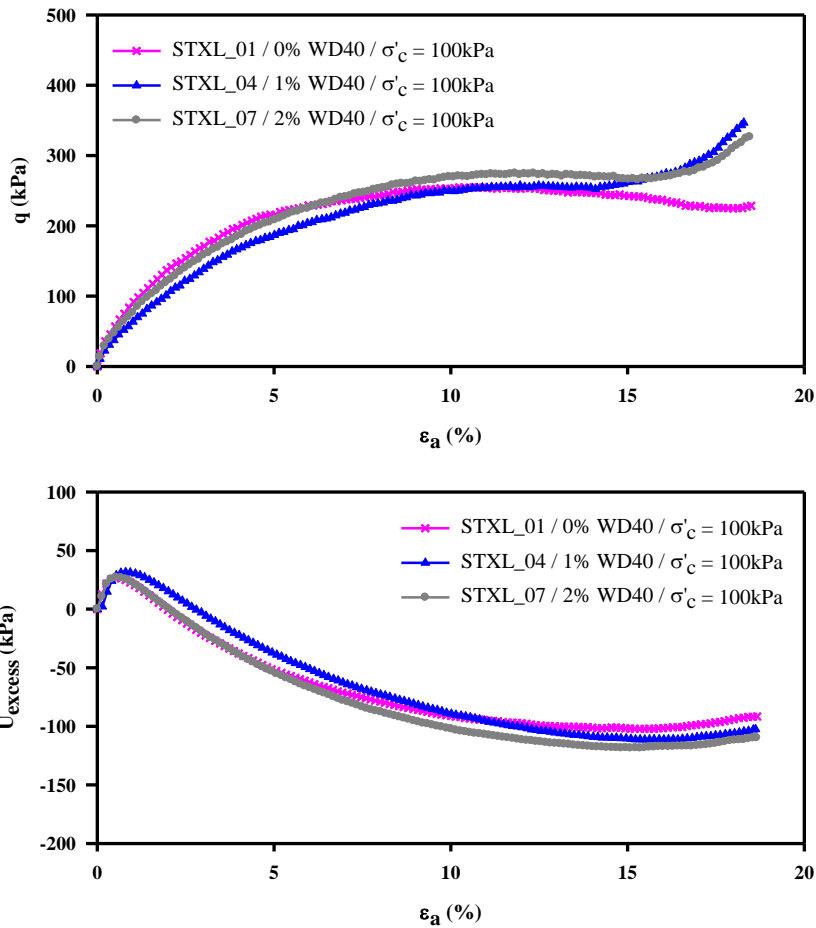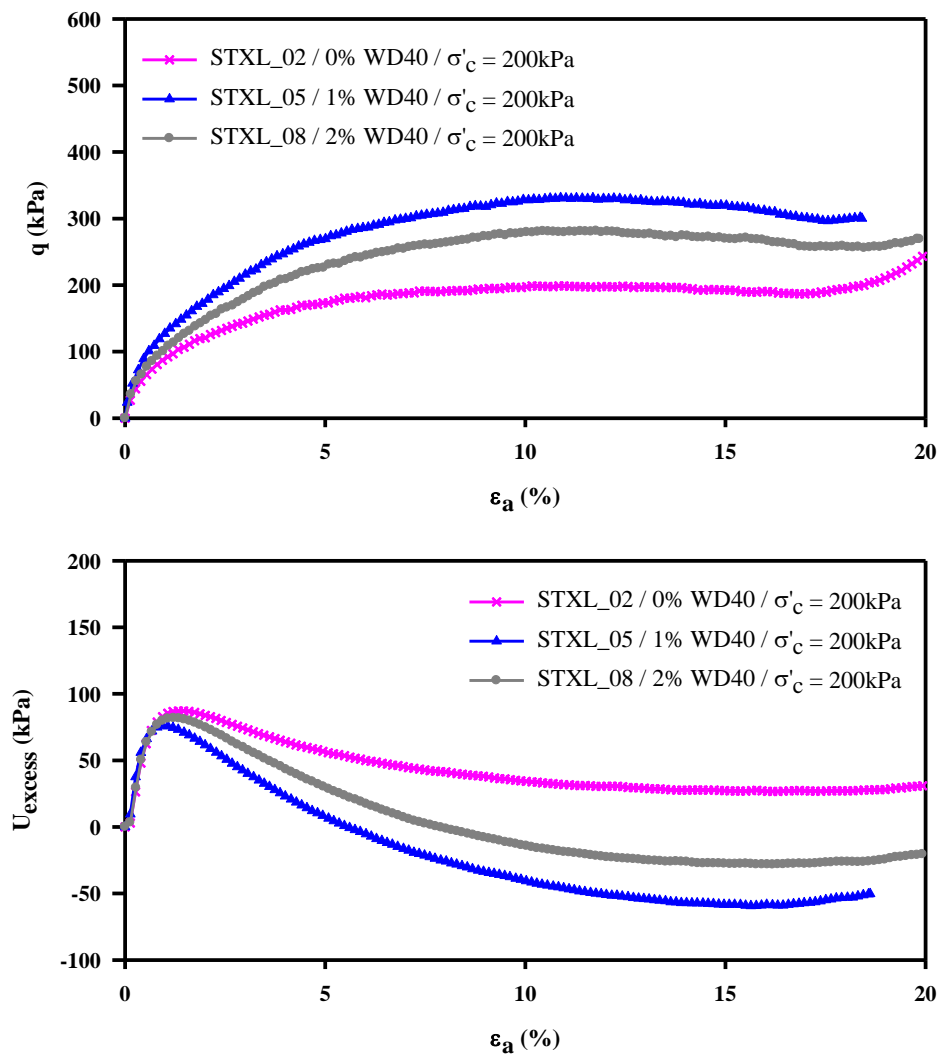**Figure 4.11. Comparison of responses of tests STXL_02, STXL_05 and STXL_08 ($D_R \cong 40\%$)**
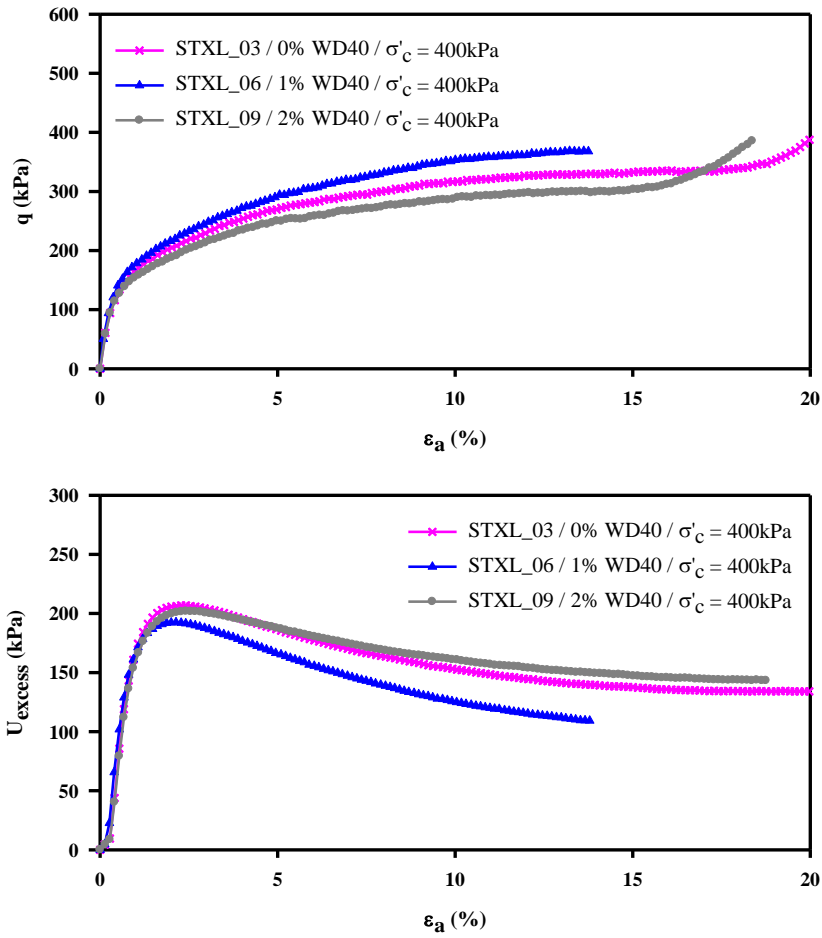
Figure 4.12. Comparison of responses of tests STXL_03, STXL_06 and STXL_09 ($D_R \cong 40\%$)

CHAPTER 5

SUMMARY AND CONCLUSION

5.1. Summary and Conclusion

The scope of this thesis study is defined as to investigate the effect of hydrophobicity on the consolidated undrained shearing response of sands. With this scope, it was intended to contribute to the limited data available in the literature regarding geotechnical properties of hydrophobic sands.

A detailed literature survey was performed on straining response and strength of hydrophilic sands and on the factors affecting their responses. In brief, strength and straining responses of sands are understood to be dependent on the density and stress states of the samples. If tests are continued to large strain levels, regardless of the initial state, all samples reach to the same ultimate state. This ultimate strength state is named as critical state and the behavior of a sample at critical state is defined as continuous shearing under constant loading with no volume change or no change in the excess pore water pressure according to drainage conditions of loading. Dense samples exhibit dilative behavior and loose samples exhibit contractive behavior. An important point that must be addressed is that the terms dense and loose define the position of the initial state of samples relative to the critical state line. Defining samples as dense or loose on the basis of their initial relative density only may result in incorrect predictions of their responses since their stress states were not taken into consideration. Whether the sample is going to exhibit a dilative or contractive behavior is defined by both their density and stress states. Increasing initial density makes sample more dilative and increasing confining stress makes sample less dilative.

To assess the effect of hydrophobicity on the consolidated undrained shearing response of sands, a laboratory triaxial testing program was designed. Testing program consists of 18 consolidated undrained triaxial tests with pore water measurements which were performed on samples having initial relative densities of $D_R \cong 40\%$ and 80% and consolidated to $\sigma_c = 100$ kPa, 200 kPa and 400 kPa.

Before performing the triaxial tests, to specify the index properties of the sand used in the study, soil index tests containing specific gravity (G_S), minimum void ratio (e_{min}) and maximum void ratio (e_{max}) determination and sieve analysis were performed. In order to prepare homogeneous samples, dry pluviation and wet tamping sample preparation techniques were applied and obtained relative densities were compared. Taking the limitations of laboratory environment and triaxial testing equipment into consideration, relatively dense and relatively loose samples were prepared by wet tamping method with different tamping rods and different number of blows. Hydrophobicity of the samples was achieved by adding WD-40 lubricant.

9 of test were performed on relatively dense samples ($D_R \cong 80\%$) and 9 of test were performed on relatively loose samples ($D_R \cong 40\%$). 3 of each 9 samples were prepared as pure (hydrophilic) sands with no lubricant addition and rest were performed on hydrophobic sand with different WD-40 amounts. Individual test results were presented by plotting deviatoric stress vs. axial strain, deviatoric stress vs. mean effective stress, effective vertical stress vs. shear stress, excess pore water pressure vs. axial strain and stress obliquity vs. mean effective stress graphs. For the failure of samples, maximum stress obliquity criteria were applied. For relatively dense samples, axial strains between 2.4% and 4.2% and effective internal friction angles between 38.7° and 40.5° were measured. For relatively loose samples, axial strains between 4.6% and 10.2% and effective internal friction angles between 32.5° and 35.3° were measured.

The observed straining response of relatively dense and loose samples and determined strength parameters were compatible with the literature data. For example, for a certain initial density state, the amount of dilatancy decreased with increasing consolidation pressure as given in Figure 5.1. Moreover, internal friction

angles determined for relatively dense and loose samples are consistent with the data compiled by Andersen and Schjetne (2013) for corresponding confining stress levels as given in Figure 5.2.
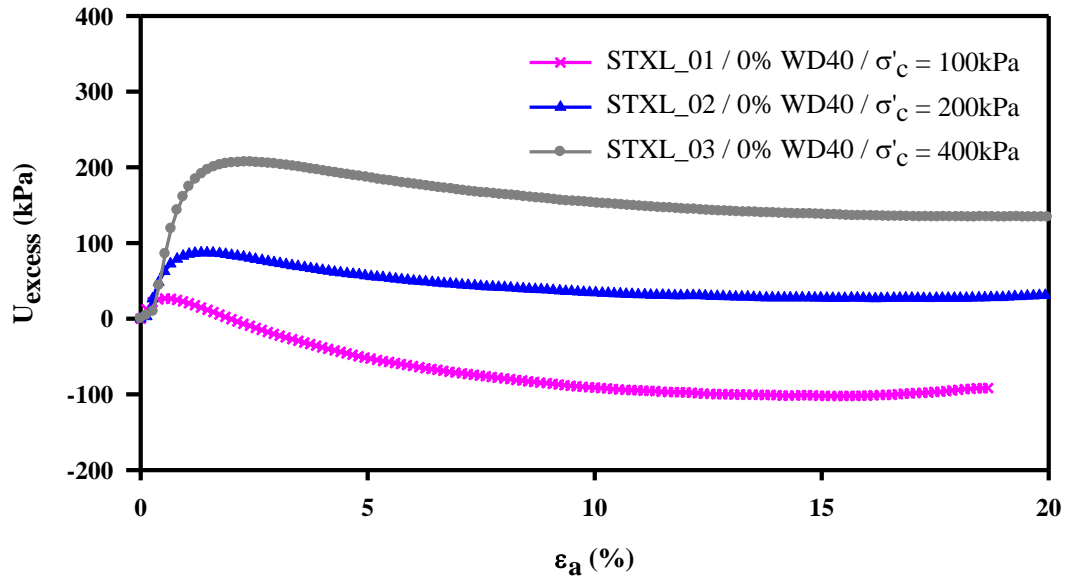
Figure 5.1. Comparison of dilatancy responses of tests STXL_01, STXL_02 and STXL_03 ($D_R \cong 40\%$)
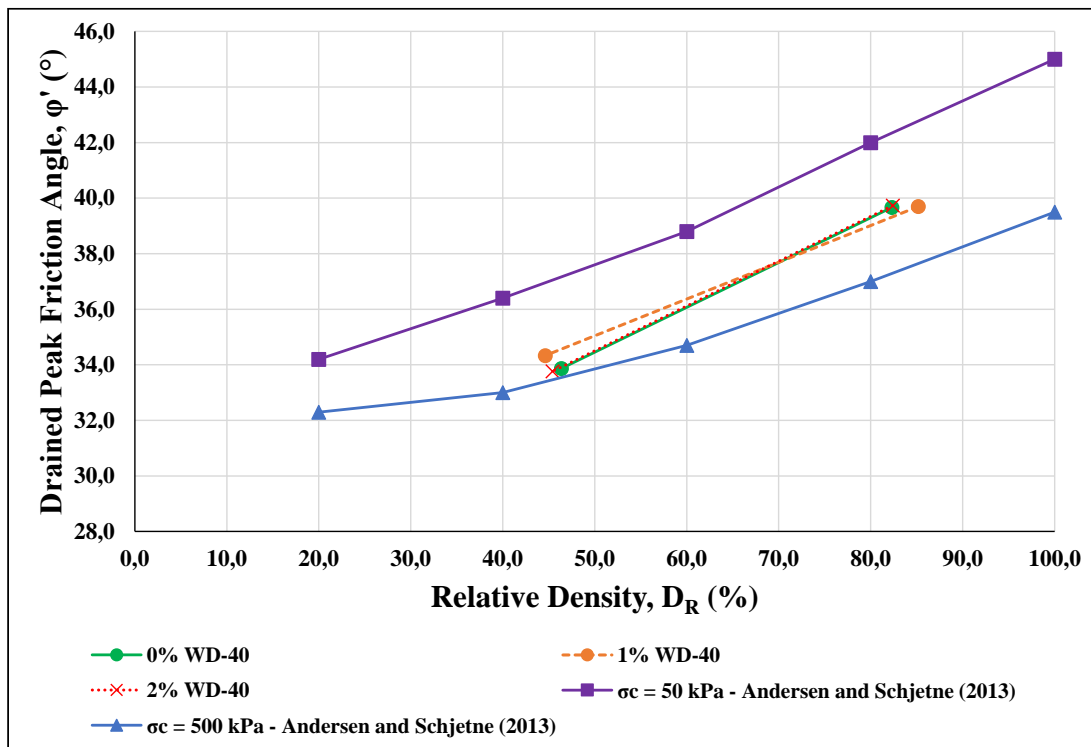
Figure 5.2. Comparison of determined strength with available literature

Whole of relatively dense samples and some of relatively loose samples dilated during shearing which shows that samples were at the dry side of the critical state line at the beginning of shearing. Only relatively loose samples under high confining pressures contracted. This observation underlines the difference between "dense / loose" and "relatively dense / relatively loose" states.

To determine the effect of hydrophobicity on shear strength, Mohr circles and Mohr - Coulomb shear strength envelopes of samples prepared with same amount of WD-40 and consolidated at different pressures were replotted together. Comparison of shear strength envelopes and effective internal friction angles reveal that hydrophobicity has insignificant effect on the strength of relatively dense and relatively loose sand samples under undrained loading conditions. However, this conclusion is only valid for the type and the amount of lubricant used in this study.
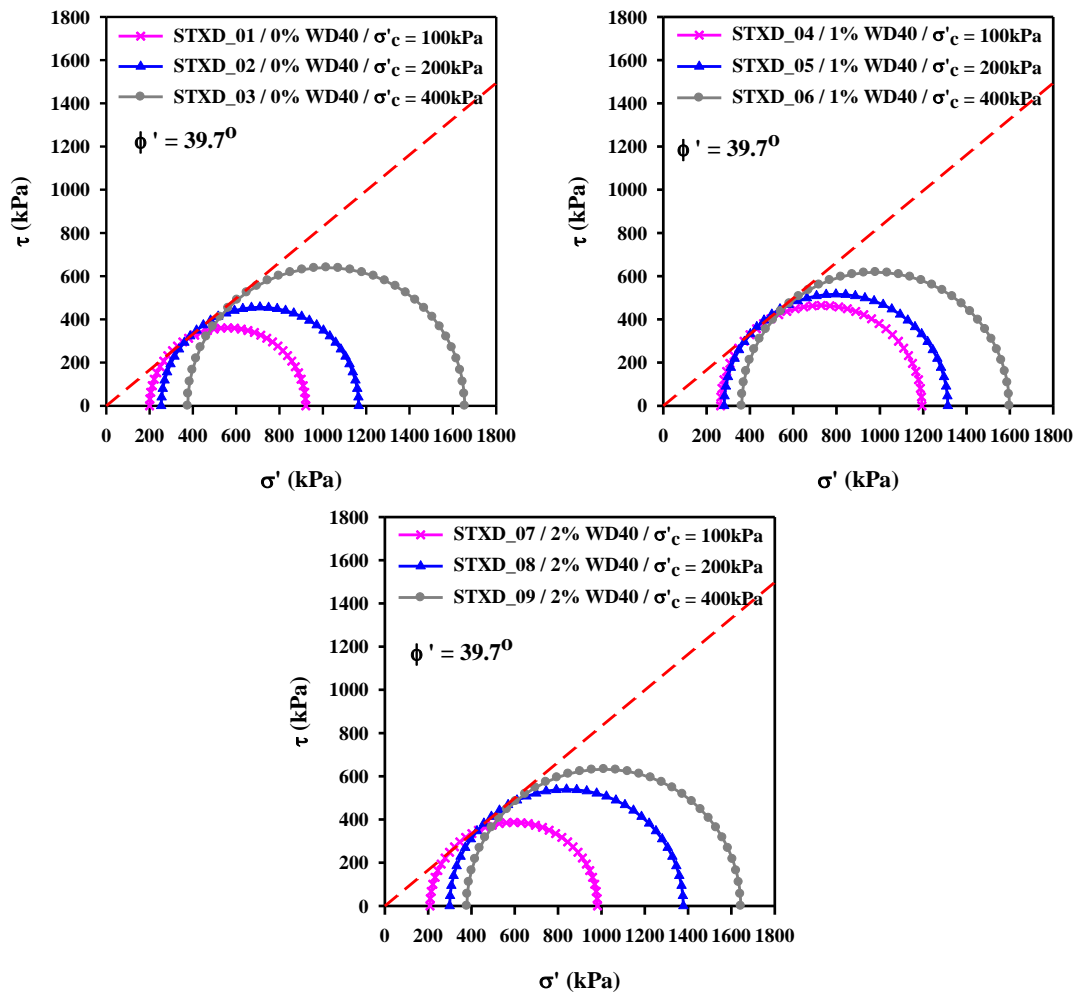
Figure 5.3. Comparison of shear strength envelopes of relatively dense samples
($D_R \cong 80\%$)

To determine the effect of hydrophobicity on the straining response, deviatoric stress vs. axial strain and excess pore water pressure vs. axial strain graphs of samples prepared with different amount of WD-40 and consolidated at the same pressures were replotted together.

Comparison of straining responses of relatively dense samples reveals that tendency to suck water into specimen (dilation) usually increases in the presence of WD-40 amount of 1% and reduces if this amount is increased to 2 %. It can be inferred that hydrophobicity (up to addition of 1% WD-40) increases the dilatancy of sands at

relatively high densities. This effect is more pronounced at low confining pressures (~100kPa) since sample is more dilative, and decreases with increasing confining stress levels.

Comparison of straining responses of relatively loose samples reveals that tendency to suck water into specimen (dilation) usually increases in the presence of WD-40 amount of 1% and reduces if this amount is increased to 2 %. It can be inferred that hydrophobicity (up to addition of 1% WD-40) increases the dilatancy of sands at relatively loose densities.

In the presence of hydrophobic agent, observations like increase in dilatancy and no significant change in shear strength are found consistent with available literature. Reduction in shear strength parameter observed by Kim et al. (2013) and Byun and Lee (2012) in direct shear tests under drained loading conditions was balanced with additional strength due to more dilative behavior of hydrophobic sand samples under undrained loading conditions.
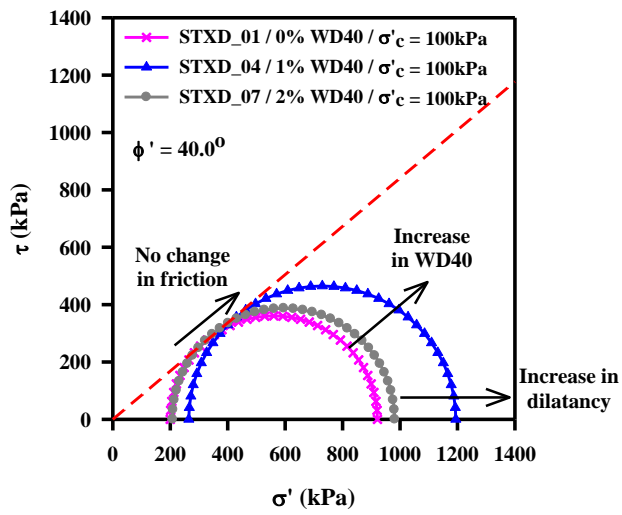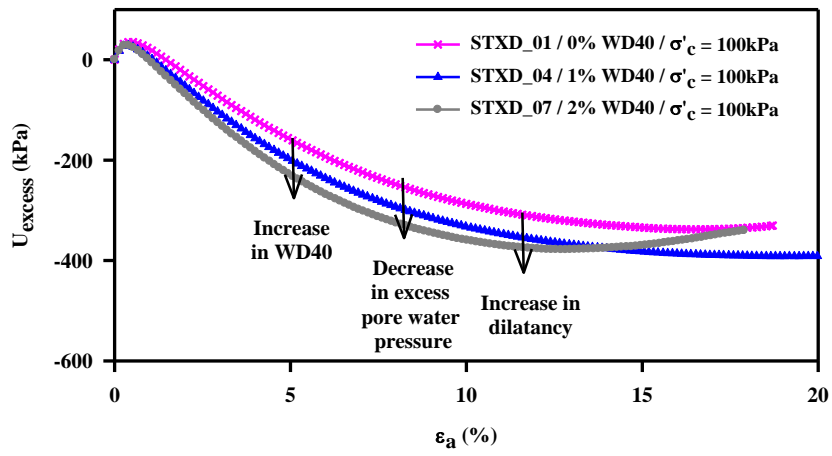
Figure 5.4. Comparison of responses of tests STXD_01, STXD_04 and STXD_07 ($D_R \cong 80\%$)
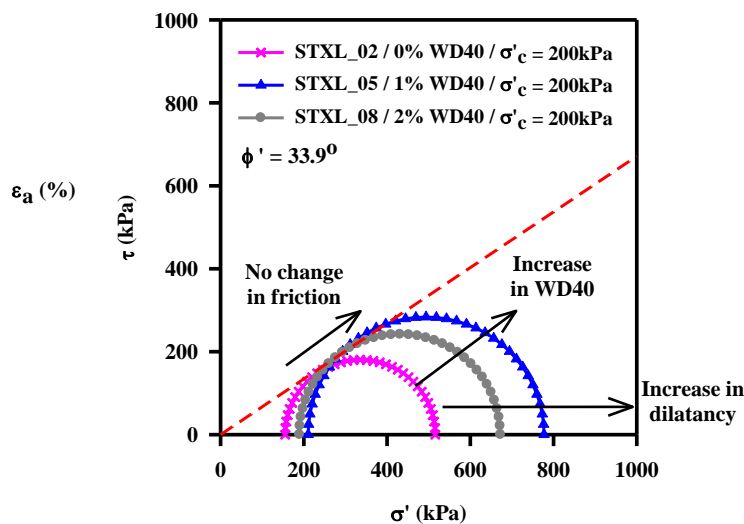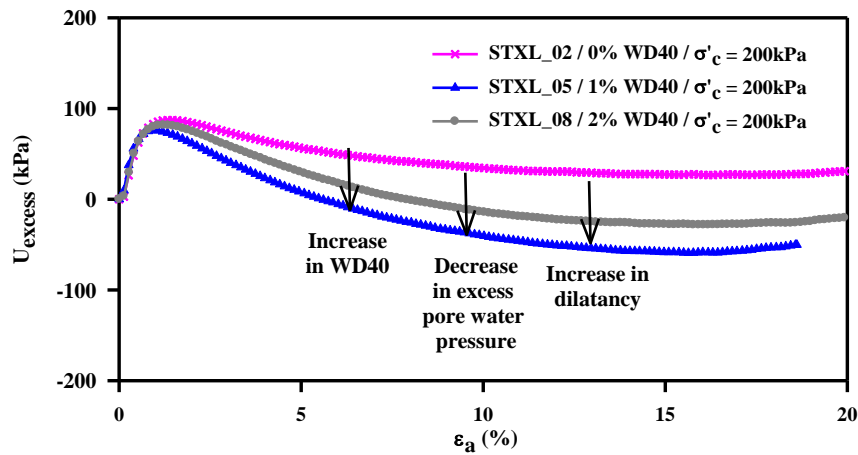
Figure 5.5. Comparison of responses of tests STXL_02, STXD_05 and STXD_08 (D$_R \cong$ 40%)

5.2. Future Studies

In this experimental study, it was observed that hydrophobicity does not have a negative effect on the shear strength of sandy soils under undrained loading conditions. Validation of this finding on a large scale can be achieved by increasing the number of tests with different initial density and stress states. In triaxial tests performed on this study, critical state was not observed due to the limitations of the testing equipment. The absence of triaxial testing conditions after about 12-13%

axial strain of samples makes the behavior at this strain levels unreliable. Therefore, a testing system that allow large deformations can be used in further studies to investigate the effect of hydrophobicity on the critical state strength. Moreover, cyclic tests with similar testing program can be performed to examine the shearing response of hydrophobic sands under cyclic loading.

REFERENCES

Andersen, K. H., & Schjetne, K. (2013). Database of Friction Angles of Sand and Consolidation Characteristics of Sand, Silt, and Clay. *Journal of Geotechnical and Geoenvironmental Engineering*, *139*(7), 1140–1155. https://doi.org/10.1061/(ASCE)GT.1943-5606.0000839

ASTM. (1995). Standard Test Method for Consolidated Undrained Triaxial Compression Test for Cohesive Soils. *ASTM International*, 1–11. https://doi.org/10.1520/D4767-11.2

Astm D6913-04R2009. (2004). Standard Test Methods for Particle-Size Distribution (Gradation) of Soils Using Sieve Analysis. *ASTM International, West Conshohocken, PA, 4*(Reapproved 2009), 1–35. https://doi.org/10.1520/D6913-04R09.2

Bal-, S., & Pycnometer, G. (2014). Standard Test Methods for Specific Gravity of Soil Solids by Water Pycnometer 1. *ASTM Standard Guide*, *4*(May), 1–8. https://doi.org/10.1520/D0854-10.

Bardet, J.-P. (1997). *Experimental Soil Mechanics*. https://doi.org/10.1038/134566b0
Benz, T. (2007). *Small-Strain Stiffness of Soils and its Numerical Consequences*. *University of Stuttgart*.

Bolton, M. D. (1986). The strength and dilatancy of sands. *Géotechnique*, *36*(1), 65–78. https://doi.org/10.1680/geot.1986.36.1.65

Byun, Y., & Lee, J. (2012). Influence of Particle Shape of Hydrophobic Granular Materials on Shear Strength.

Cornforth, D. (2017). Prediction of Drained Strength of Sands from Relative Density Measurements. *Evaluation of Relative Density and Its Role in Geotechnical Projects Involving Cohesionless Soils*, 281-281–23. https://doi.org/10.1520/STP37878S

Hardin, B. O. & Black, W. L. (1969). Closure to: Vibration modulus of normally consolidated clays. *J. Journal of Soil Mechanics and Foundation Division, ASCE, 95*(6), 1531–1537.

Houlsby, G. T. (1991). How the dilatancy of soils affects their behaviour. *Proceedings of the 10th European Conference on Soil Mechanics and Foundation Engineering*. Retrieved from http://www.eng.ox.ac.uk/civil/publications/reports-1/ouel_1888_91.pdf

Juneja, A., & Raghunandan, M. E. (2010). Effect of Sample Preparation on Strength of Sands. *Indian Geotechnical Conference 2010, GEOtrenz*, (1999), 327–330.

Kim, B., Kato, S., & Park, S. S. W. (2013). Characterization of geomechanical and hydraulic properties of non-wettable sands. *Proceedings of the 18th Internation Conference on Soil Mechanics and Geotechnical Engineering*, 361–364.

Lo Presti, D., Pedroni, S., & Crippa, V. (1992). Maximum Dry Density of Cohesionless Soils by Pluviation and by ASTM D 4253-83: A Comparative Study BT - Maximum Dry Density of Cohesionless Soils by Pluviation and by ASTM D 4253-83: A Comparative Study. *Geotechnical Testing Journal*, *15*(2), 180–189. https://doi.org/10.1520/GTJ10239J

Maimon, A., Gross, A., & Arye, G. (2017). Greywater-induced soil hydrophobicity. *Chemosphere*, *184*, 1012–1019. https://doi.org/10.1016/j.chemosphere.2017.06.080
NAVFAC. (1982). Soil Mechanics, DM 7.01, 383. Retrieved from vulcanhammer.net

Paikowsky, S. G., Canniff, M. C., Lesny, K., Kisse, A., Amatya, S., & Muganga, R. (2010). *LRFD Design and Construction of Shallow Foundations for Highway Bridge Structures. NCHRP Report 651* (Vol. 651). https://doi.org/10.17226/14381

Roscoe, K. H., Schofield, A. N., & Wroth, C. P. (1958). On The Yielding of Soils. *Géotechnique*, *8*(1), 22–53. https://doi.org/10.1680/geot.1958.8.1.22

Rowe, P. W. (1962). The Stress-Dilatancy Relation for Static Equilibrium of an Assembly of Particles in Contact. *Proceedings of the Royal Society A: Mathematical, Physical and Engineering Sciences*, *269*(1339), 500–527. https://doi.org/10.1098/rspa.1962.0193

Schmertmann, J. H. (1978). *Guidelines for Cone Penetration test (Performance and Design)*.

Schofield, A. N., & Wroth, C. P. (1968). Critical State Soil Mechanics. *Soil Use and Management*, 228. https://doi.org/10.1111/j.1475-2743.1987.tb00718.x

Sun, X., Liu, Y., Mopidevi, S., Meng, Y., Huang, F., Parisi, J., … Lei, Y. (2014). Super-hydrophobic "smart" sand for buried explosive detection. *Sensors and Actuators, B: Chemical*, *195*, 52–57. https://doi.org/10.1016/j.snb.2013.12.095

Terzaghi, K., Peck, R. B., & Mesri, G. (1996). Soil Mechanics in Engineering Practice. https://doi.org/10.1007/SpringerReference_4898

Tong, P., Barden, L., & Ismail, H. (1969). Plane Strain Deformation of Granular Material at Low and High Pressures. *Géotechnique*, *19*(4), 441–452. https://doi.org/10.1680/geot.1969.19.4.441

Wichtmann, T., & Triantafyllidis, T. (2009). On the correlation of "static" and "dynamic" stiffness moduli of non-cohesive soils. *Bautechnik*, *86*(SUPPL. 1), 28–39. https://doi.org/10.1002/bate.200910039

Wroth, C. P., & Bassett, R. H. (1965). A Stress–Strain Relationship for the Shearing Behaviour of a Sand. *Géotechnique*, *15*(1), 32–56. https://doi.org/10.1680/geot.1965.15.1.32

APPENDIX A

SPECIFIC GRAVITY TEST RESULTS

Table 7. Details of Specific Gravity Tests

Sample No	1	2	3	4
Mass of Battle, W1 (g)	124,603	125,571	122,822	115,092
Mass of Battle + Soil, W2 (g)	220,864	223,839	214,855	211,583
Mass of Battle + Soil + Water, W3 (g)	447,965	447,242	447,998	437,892
Mass of Battle Full of Water Only, W4 (g)	387,790	385,908	390,489	377,535
Mass of Soil, W2 - W1 (g)	96,261	98,268	92,033	96,491
Mass of Water Used, W4 - W1 (g)	263,187	260,337	267,667	262,443
Volume of Soil, (W4 - W1) - (W3 - W2) (ml)	36,086	36,934	34,524	36,134
Specific Gravity of Soil, Gs	2,6675	2,6606	2,6658	2,6704
Average Specific Gravity of Soil, Gs	2,6661			

APPENDIX B

MAXIMUM AND MINIMUM VOID RATIO TEST RESULTS

Table 8. Details of Maximum and Minimum Void Ratio Determination

Inner Diameter of Mould (mm)	151,95
Height of Mould (mm)	116,14
Volume of Mould (ml)	2106,07
Mass of Mould (g)	4540,20
Specific Gravity of Soil	2,6661

Loosest State		
Sample No	1	2
Mass of Soil + Mould (g)	7563,10	7564,10
Mass of Soil (g)	3022,90	3023,90
Volume of Soil Particles (ml)	1133,83	1134,20
Volume of Voids (ml)	972,24	971,87
Maximum Void Ratio, e_{max}	0,8575	0,8569
Average e_{max}	0,8572	

Densest State		
Sample No	1	2
Mass of Soil + Mould (g)	8191,70	8209,50
Mass of Soil (g)	3651,50	3669,30
Volume of Soil Particles (ml)	1369,60	1376,28
Volume of Voids (ml)	736,47	729,79
Minimum Void Ratio, e_{min}	0,5377	0,5303
Average e_{min}	0,5340	

APPENDIX C

SIEVE ANALYSIS TEST RESULTS

Table 9. Details of Sieve Analysis Test

Weight of Dry Sample (g):		824,55		

Sieve Number	Diameter (mm)	Soil Retained (g)	Soil Retained (%)	Soil Passing (%)
#4	4,750	0,00	0,00	100,00
#10	2,000	4,09	0,50	99,50
#30	0,600	267,99	32,50	67,00
#50	0,300	346,59	42,03	24,97
#70	0,212	123,52	14,98	9,99
#100	0,150	57,26	6,94	3,04
#200	0,075	19,40	2,35	0,69
Pan	-	5,70	0,69	0,00
		824,55	**100,0**	

Sieve Analysis Results	
USCS:	SP
% Gravel:	0,00
% Sand:	99,31
% Fines:	0,69
D_{10} (mm):	0,22
D_{30} (mm):	0,33
D_{60} (mm):	0,52
C_u:	2,36
C_c:	2,88

APPENDIX D

CALCULATION DETAILS

Details of calculations performed on the data measured during tests in order to prepare 4 way plots are provided in the CD given beside thesis.